Surface Topography of the Lower Part of Columbia Glacier, Alaska, 1974–1981

U.S. GEOLOGICAL SURVEY PROFESSIONAL PAPER 1258–E

Surface Topography of the Lower Part of Columbia Glacier, Alaska, 1974–1981

By L. A. RASMUSSEN *and* M. F. MEIER

STUDIES OF COLUMBIA GLACIER, ALASKA

U.S. GEOLOGICAL SURVEY PROFESSIONAL PAPER 1258–E

Obtaining surface altitudes on a square grid by applying the method of "optimum interpolation" to irregularly positioned altitudes obtained by photogrammetry.

Revised May 1985

UNITED STATES GOVERNMENT PRINTING OFFICE, WASHINGTON : 1985

DEPARTMENT OF THE INTERIOR

DONALD PAUL HODEL, *Secretary*

U.S. GEOLOGICAL SURVEY

Dallas L. Peck, *Director*

Library of Congress Cataloging in Publication Data

Rasmussen, L. A.
Surface topography of the lower part of Columbia Glacier, Alaska, 1974–81.

(U.S. Geological Survey professional paper ; 1258–E)
Bibliography: p.
Supt. of Docs. no.: I 19.16:1258–E
1. Columbia Glacier (Alaska) I. Meier, Mark Frederick, 1925– . II. Title. III. Series: Geological Survey professional paper ; 1258E.
GB2427.C64R377 1984 551.3'1'097983 84–600191

For sale by the Distribution Branch, U.S. Geological Survey
604 South Pickett Street, Alexandria, VA 22304

CONTENTS

ILLUSTRATIONS

TABLES

SYMBOLS AND ABBREVIATIONS

Symbol	Name	Units (where applicable)
A	Correlation study point at x=5,250 m, y=27,500 m	
a	Coefficient for obtaining norm field from 1974 and 1981 maps	Dimensionless
a	Year.	
α	Coefficient of correlation function	a
B	Correlation study point at x=6,500 m, y=22,000 m.	
b	Coefficient for obtaining norm field from 1974 and 1981 maps	m
β	Coefficient of correlation function	km
C	Correlation study point at x=6,250 m, y=18,500 m.	
D	Correlation study point at x=8,250 m, y=18,500 m.	
d	Horizontal distance	m
E	Correlation study point at x=6,750 m, y=15,000 m.	
E_f	Error in fitting IPP's with $f(x,y)$	m
E_G	Interpolation error estimated by algorithm	m
E'_G	Actual interpolation error with ground-truth sample	m
E''_G	Version of E'_G adjusted for errors in surveying and time discrepancy	m
E_I	Error in digitizing 1974 and 1981 maps	m
E_P	Random error of IPP altitudes	m
E_r	Error in approximating $r^*(\tau,d)$ by $R(\tau,d)$	Dimensionless
E_T	Departure of IPP's from digitization of 1974 and 1981 maps	m
E_w	Part of E_T due to IPP being on wrong side of contour	m
E_2	Error in approximating IPP's by $P(x,y)$	m
E_3	As E_2, but corrected by "nearest three" residual averaging	m
e	Mathematical constant, 2.71828... .	
F	Correlation study point at x=8,750 m, y=15,000 m	
$f(x,y)$	Norm field	m
I	Subscript denoting row of 762.5-meter data grid.	
IPP	Individual photogrammetric point (coordinates determined by vertical aerial photography).	
i	Base of imaginary numbers.	
J	Subscript denoting column of 762.5-meter data grid.	
K_0	Modified Bessel function of the second kind.	
km	Kilometer.	
L	Subscript denoting flight number.	
λ	Fraction of IPP's from same flight as point being interpolated	Dimensionless
m	Number of IPP's common to 1974 and 1981 maps	Dimensionless
m	Meter.	
N	Order of linear system for determining interpolation weights	Dimensionless
n	Sample size, used generically	Dimensionless
$P(x,y)$	Second-degree polynomial	m
p	Coefficient of $P(x,y)$.	
Φ	Fourier transform of correlation function.	
ϕ	Coordinate axis of Φ.	
ψ	Arbitrary rotation angle.	
$R(\tau,d)$	Correlation function	Dimensionless
$r(d,\theta,\tau)$	Correlation between $Z(0,0,t+\tau)$ and $Z(d,\theta,t)$	Dimensionless
$r^*(\tau,d)$	Empirical correlation of IPP departures from $f(x,y)$	Dimensionless
$\overline{r_\theta}(d,\tau)$	Azimuth-averaged $r(d,\theta,\tau)$	Dimensionless
$\overline{r_d}(\theta,\tau)$	Distance-averaged $r(d,\theta,\tau)$	Dimensionless
t	Time coordinate	a
Δt	Time difference of surface surveyed altitude from some t_L	a
τ	Time lag	a
θ	Azimuth (compass direction).	
UTM	Universal Transverse Mercator.	
u	Component of surface velocity in x-direction	ma^{-1}
V	Variance of IPP's about $f(x,y)$	m^2
v	Component of surface velocity in y-direction	ma^{-1}
w	Linear-combination weights for interpolation algorithm	Dimensionless
x	Horizontal coordinate, positive to east	m
ξ	Local coordinate within 200-meter digitization square	200 m
y	Horizontal coordinate, positive to north	m
$\hat{y}$	Coordinate of v-advected IPP	m
Z	Glacier surface altitude above National Geodetic Vertical Datum of 1929, herein referred to as sea level	m
$\overline{Z}$	Average of Z at vertices of 200-meter digitization square	m
Z_{IPP}	Altitude coordinate of an IPP	m
$Z(0,0,t+\tau)$	Altitude of point used in correlation study	m
$Z_L(x_k,y_k)$	IPP altitude for kth point of flight L	m
$Z^*(x,y)$	Altitude estimated by interpolation algorithm	m
$Z'_{L(x,y)}$	Ground-thruth altitude adjusted to flight date t_L	m
$\hat{Z}(x,y)$	Altitude at (x,y) by advecting IPP with v for τ	m
ΔZ	Deviation of IPP from norm field, as used in weights equation	m
ΔZ^*	Value of ΔZ estimated by algorithm	m
$\Delta Z_L(x_k,y_k)$	Deviation of IPP from $f_L(x,y)$	m
δZ	Systematic error in the photogrammetric data	m
ζ	Local coordinate within 200-meter digitization square	200 m
$<>$	Integer function operator; that is, $<x>$ is the integer part of x.	

Note: Use of names of firms or their products in this report does not imply endorsement.

STUDIES OF COLUMBIA GLACIER, ALASKA

SURFACE TOPOGRAPHY OF THE LOWER PART OF COLUMBIA GLACIER, ALASKA, 1974–81

By L. A. RASMUSSEN and M. F. MEIER

ABSTRACT

The method of optimum interpolation is used to get surface altitudes on the nodes of a square grid superimposed over a map of the lowest 18 kilometers of Columbia Glacier, a large, grounded, iceberg-calving glacier near Valdez, Alaska. Vertical aerial photography has been obtained about five times a year since July 1976. For each of 29 flights, the altitude of the glacier surface has been determined photogrammetrically at the locations of prominent surface features. The large amount of data, the noisy character of the topographic data due to the rough surface, and a modeling need to know precisely how the ice surface changes with time require a sophisticted interpolation procedure. The recently developed method of optimum interpolation is used here because it minimizes the interpolation error by developing and using knowledge of the statistical properties of the data. The reduction of these surface altitude and velocity data will lead to the best data set ever generated for a glacier, and that data will be valuable for investigating calving mechanics, for studying glacier dynamics, and particularly for using in modeling the drastic retreat of Columbia Glacier.

Topographic maps of the glacier surface were obtained from flights on July 27, 1974, and September 1, 1981. The first approximation of the topography on the date of a particular intervening flight is taken to be the linear combinaton of the two maps that best fits the photogrammetric data from that flight. The deviations of the individual photogrammetric points about this first approximation are the quantities to which the method of optimum interpolation is actually applied in estimating the altitudes of the grid nodes. Between 116 and 202 photogrammetric points are available from flight to fight.

The statistical properties of the surface topography are described in terms of the correlation between the altitude changes at a point and the changes at some other point. This correlation has a high degree of homogeneity and isotropy, both spatially and temporally, and was little affected by the glacier flow. This remarkable regularity permits the use of a very simple implementation of the optimum interpolation algorithm.

The random error in the photogrammetrically determined altitudes is estimated at 3.5 meters by comparing the individual points with maps made from the same flights. A ground-truth sample of 58 individual and averaged points was used to test the interpolated results for three flights. The asymmetry of these sample deviations about the first-approximation surfaces suggests that there may be a systematic error of about +1.5 meters in the photogrammetrically determined altitudes. The standard error in the altitudes interpolated on the grid nodes is estimated to be 2.5 meters.

INTRODUCTION

Columbia Glacier is a large (67 km long and 1,100 km^2 in area), calving glacier near Valdez, Alaska (fig. 1). Although much of its bed is below sea level, the glacier is grounded everywhere except for some short, floating segments along its margins where it spills into ice-dammed, freshwater lakes. The terminus pushes against a moraine shoal; the top of the shoal is about 20 m below sea level, but a short distance upglacier the bed is about 400 m below sea level.

Recent studies of calving glaciers in Alaska have shown that calving speed is related to water depth at the terminus, and that if a glacier retreats off of a shoal so that its terminus faces deep water, the retreat will become rapid and irreversible (Post, 1975). Columbia Glacier clearly has the potential to make a drastic retreat. This situation is of practical as well as academic interest, because drastic retreat will cause a large increase in iceberg discharge; some icebergs from Columbia Glacier drift into shipping lanes in Valdez Arm (Kollmeyer and others, 1977).

To predict whether Columbia Glacier might begin rapid retreat and, if so, when and by how much the iceberg discharge might increase, the U.S. Geological Survey began an intensive study in 1977 involving aerial photography and ground-based and boat-based fieldwork (Meier and others, 1978). Results of the fieldwork during the 1977–78 principal data year have been

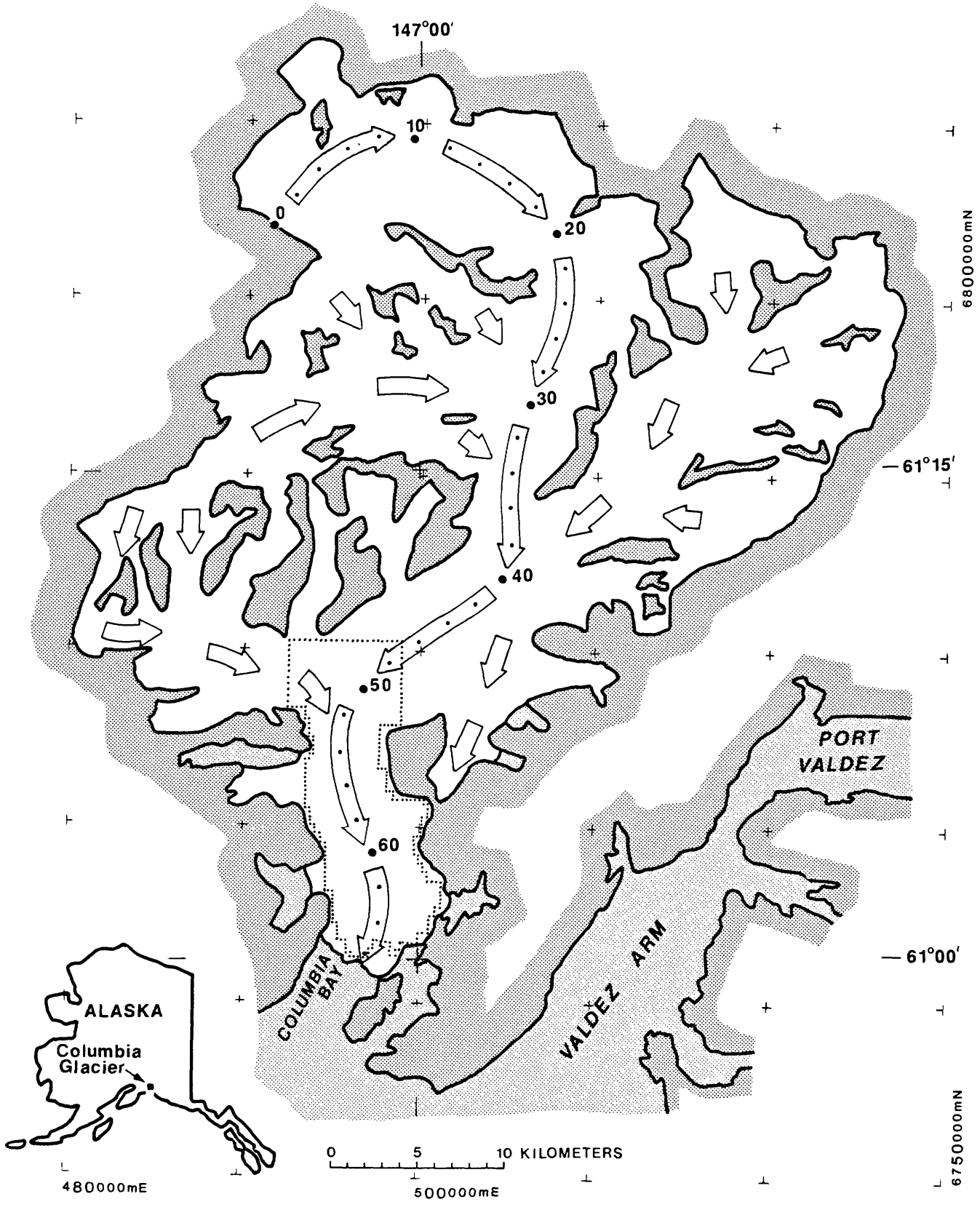

FIGURE 1.—Index map of Columbia Glacier, Alaska. Arrows show direction of flow. Main ice stream is indicated by longer arrows and dots at 2-kilometer intervals along the longitudinal coordinate system. The border of the interpolation domain is dotted.

reported (Mayo and others, 1979; Sikonia and Post, 1980), and a preliminary prediction was issued in June 1980 (Meier and others, 1980). Two postulated formulations of the calving relation were investigated (Brown and others, 1982; Sikonia, 1982). Detailed calculations from three predictive models (Rasmussen and Meier, 1982; Sikonia, 1982; Bindschadler and Rasmussen, 1983) soon followed; they all reinforced the initial expectation of substantial retreat during the mid-1980's, along with an order-of-magnitude increase of the iceberg discharge.

The ground-based and boat-based fieldwork was supplemented by vertical aerial photography done about five times a year since July 1976, usually for the 18-kilometer-long lower part of the glacier only. For each flight, photogrammetric analysis has yielded accurate coordinates of points on the glacier surface (Meier and others, 1984) and, because identifiable surface features can be followed form one flight to the next, average flight-to-flight surface velocities have been determined (Fountain, 1982).

This photogrammetric data set is characteristically different from data sets obtained by traditional field programs, in that the data are numerous (about 7,000 separate point coordinate determinations), the data are irregularly distributed in both time and space, and some important information (such as changes in glacier thickness over time) may be immersed in noise owing to the spatially irregular glacier surface. The data contain only the two vriables, surface altitude and displacement. Numerical modeling of changes in flow and shape of a glacier requires (1) data interpolated on a grid fixed in space, (2) special treatment to obtain the best possible estimate of time changes in that field, and (3) knowledge of the errors and statistical properties of the data set. These modeling requirements, imposed on a nontraditional data set, make it necessary to use a sophisticated data-analysis procedure. Use of this procedure may have broader application, especially as modern methods of data acquisition greatly increase the complexity of data analysis.

The central problem in this analysis procedure is the need to use all relevant information in the interpolation algorithm. Only by doing so can the signal-to-noise ratio be maximized. Large-scale swells and swales in the surface topography tend to persist because they are caused by the underlying bedrock, and this means that the interpolation scheme can be aided if the temporal as well as the spatial dimension is included. Thus, general-purpose contouring programs, which deal with a two-dimensional field only, are not sufficient. Constructing topographic maps by photogrammetry from each set of aerial photographs also ignores the temporal dimension and, in addition, would be prohibitively expensive.

The method of interpolation reported here incorporates both temporal and spatial information. It has the additional advantage of requiring and producing information on the statistical structure of the field. Statistical structure refers to how well the altitude of a certain point correlates with the altitudes of neighboring points, distributed in both space and time, and whether that correlation depends on location (a test of homogeneity) or on direction (a test of isotropy). Defining this statistical correlation function is critical to the method of optimum interpolation and also enables determination of the interpolation error.

The interpolated surface topography, when combined with the surface velocity and other variables on the same grid, will constitute an extraordinarily rich data set for use in time-dependent, two-dimensional models of glacier flow. The data set must be internally consistent with respect both to the continuity equation and to the flow law, and it must be faithful, within the bounds of observational error, to the field data. Because Columbia Glacier is a calving glacier, the data set will be useful for continuing the investigation of the calving mechanism as well as for studying glacier dynamics generally. Because rapid retreat appears to have begun (Meier and others, 1984), the future extension of the data set will include the only detailed, high-quality data on this process in existence.

The report begins with a description of the photogrammetric data in the section "Original Topographic Data": first the inherent altitude error is estimated, and then the temporal and spatial distributions of the data are described. Because the benefit of low interpolation error is gained at the cost of first determining the variable's statistical properties, several preliminary interpolation schemes are introduced in "Statistical Properties of the Surface Topography"; these results are then used to estimate the point-to-point correlation of altitude changes, between points displaced from one another in both space and time, and to determine whether the correlation is homogeneous and isotropic. Described in "First Approximation to the Interpolated Altitudes" are how the 1974 and 1981 topographic maps were used to make norm fields for the times of intervening flights and how deviations of irregularly positioned photogrammetric points were established as the variable actually interpolated; also discussed is obtaining a mathematically proper function for representing the correlation. In "The Interpolation Algorithm," the derivation of optimum interpolation is briefly recapitulated and several of its chief properties are mentioned, the result of applying it to the photogrammetric data is compared, for several tens of points, with altitudes surveyed from the glacier surface, and the exact specification of the algorithm actually used is given.

Finally, in the section titled "Discussion," errors and shortcomings of the results are considered, the elusiveness of defining the surface altitude of a severely fractured and irregular ice mass is mentioned, and speculations are offered on extrapolating the data set.

ACKNOWLEDGMENTS

We are particularly grateful to Alan Thorndike for valuable counsel on the statistical basis of this work, and to him, Craig Lingle, and Uwe Radok for helpful reviews of the manuscript.

ORIGINAL TOPOGRAPHIC DATA

Two topographic maps for the lower reach of the Columbia Glacier surface (indicated by the box in fig. 1) were produced photogrammetrically at 1:50,000 scale and 10-meter contour interval for the flights on July 27, 1974 (fig. 2), and September 1, 1981. For these and the intervening 27 flights, the glacier surface altitude was determined photogrammetrically at numerous irregularly positioned points (table 1). Except for the September 1, 1981, map, which was produced by Air Photo Tech of Anchorage, Alaska, all the processing was performed by the USGS Western Mapping Center at Menlo Park, Calif. The coordinates of the individual points are compiled in Fountain (1982). The 1974 map was smoothed by the photogrammetrist, but the photogrammetrist who made the 1981 map followed contours in and out of crevasses. Figure 3 shows a section, at 1:50,000 scale, of the original September 1, 1981, map.

Both maps were digitized by visually interpolating altitudes on a 200-meter square grid (4 mm at 1:50,000 scale). The uncertainty of how to interpolate between contour lines was used, to a modest degree, to attempt to make the resulting difference field relatively free of spurious small-scale features. The manual contouring of the digitized values for the 1981 map is shown here (fig. 4) because its smoothness, which is comparable with that of the 1974 map, makes 1974 to 1981 changes in the glacier surface easier to discern than using the original 1981 map. The box in figure 4 indicates the section shown in figure 3, and the difference between the 1974 and 1981 maps is shown in figure 5.

The digitizations of the two maps are used as the bases for the ultimate interpolation to the nodes of the square grid. This requires determining the altitudes, at the times of each of the two maps, at the x,y location of any of the (irregularly positioned) photogrammetric points from any of the intervening flights. For interpolating between the nodes of the 200-meter grid, a piecewise planar surface is assumed to pass through the altitudes at the nodes. Every grid cell is subdivided into four triangular regions, each of which has as its vertices the center of the square and two adjacent vertices of the square. The altitude $\overline{Z}$ at the center of the square is taken to be the average of the altitudes at the square's four vertices; this $\overline{Z}$ is also the ordinate at the center of the square of the plane best fitting the points at the four vertices in the least squares sense. For each triangle, the surface is defined to be the plane passing through the altitudes at the triangle vertices. That is, if a local coordinate system is chosen so that the coordinates of the surface at the vertices of the square are $(\xi,\zeta,Z)=(0,0,Z_{00})$, $(1,0,Z_{10})$, $(1,1,Z_{11})$, $(0,1,Z_{01})$, then the surface is interpolated according to

$$Z=\begin{cases} 2\zeta\overline{Z}+(1-\xi-\zeta)Z_{00}+(\xi-\zeta)Z_{10} & (\xi\geq\zeta,\ \xi+\zeta\leq 1) \\ 2(1-\xi)\overline{Z}+(\xi+\zeta-1)Z_{11}+(\xi-\zeta)Z_{10} & (\xi\geq\zeta,\ \xi+\zeta\geq 1) \\ 2(1-\zeta)\overline{Z}+(\xi+\zeta-1)Z_{11}+(\zeta-\xi)Z_{01} & (\xi\leq\zeta,\ \xi+\zeta\geq 1) \\ 2\xi\overline{Z}+(1-\xi-\zeta)Z_{00}+(\zeta-\xi)Z_{01} & (\xi\leq\zeta,\ \xi+\zeta\leq 1) \end{cases}. \quad (1)$$

The interpolation surface is continuous in ordinate but has discontinuity of derivative at the edges of the triangles, both within a square and from square to square. Although it is not relevant to the present analysis, this interpolating surface has a practical advantage over other zero-order-continuity interpolating surfaces, such as the bidimensional linear interpolation: the construction of a normal from an external point is a direct, linear calculation. The result of this interpolation for the July 27, 1974, map is denoted $f_2(x,y)$, and for the September 1, 1981, map, $f_{30}(x,y)$, the numbers 2 and 30 corresponding to the numbers of aerial photographic flights as listed in table 1.

ALTITUDE ERRORS IN INDIVIDUAL PHOTOGRAMMETRIC POINTS

The lower reach is a very rough surface (fig. 3, 6), and this roughness may contribute to the lack of perfect agreement between the maps and the individual photogrammetric points (IPP's) from the same flights. When drawing a contour line on a map, the operator smooths out small-scale roughness and attempts to do so without introducing bias. When picking IPP's for coordinate determination, the operator must see nearby surface topography to form a stereo image; thus, isolated peaks or depressions are not used. However, the local surface seen around an IPP does not necessarily correspond to a mean surface over a larger area. Coordinate determination is accurate to within about 2 m, but it is subject to human error (R. W. Olsen, 1980, oral commun.). Because of the roughness of the actual surface, the representativeness of any particular point is a serious consideration.

For each of the two maps, the distribution of the departures of the IPP altitudes from the digitization of the map was carefully examined, to estimate how much of the discrepancy was due to interpolation error and how

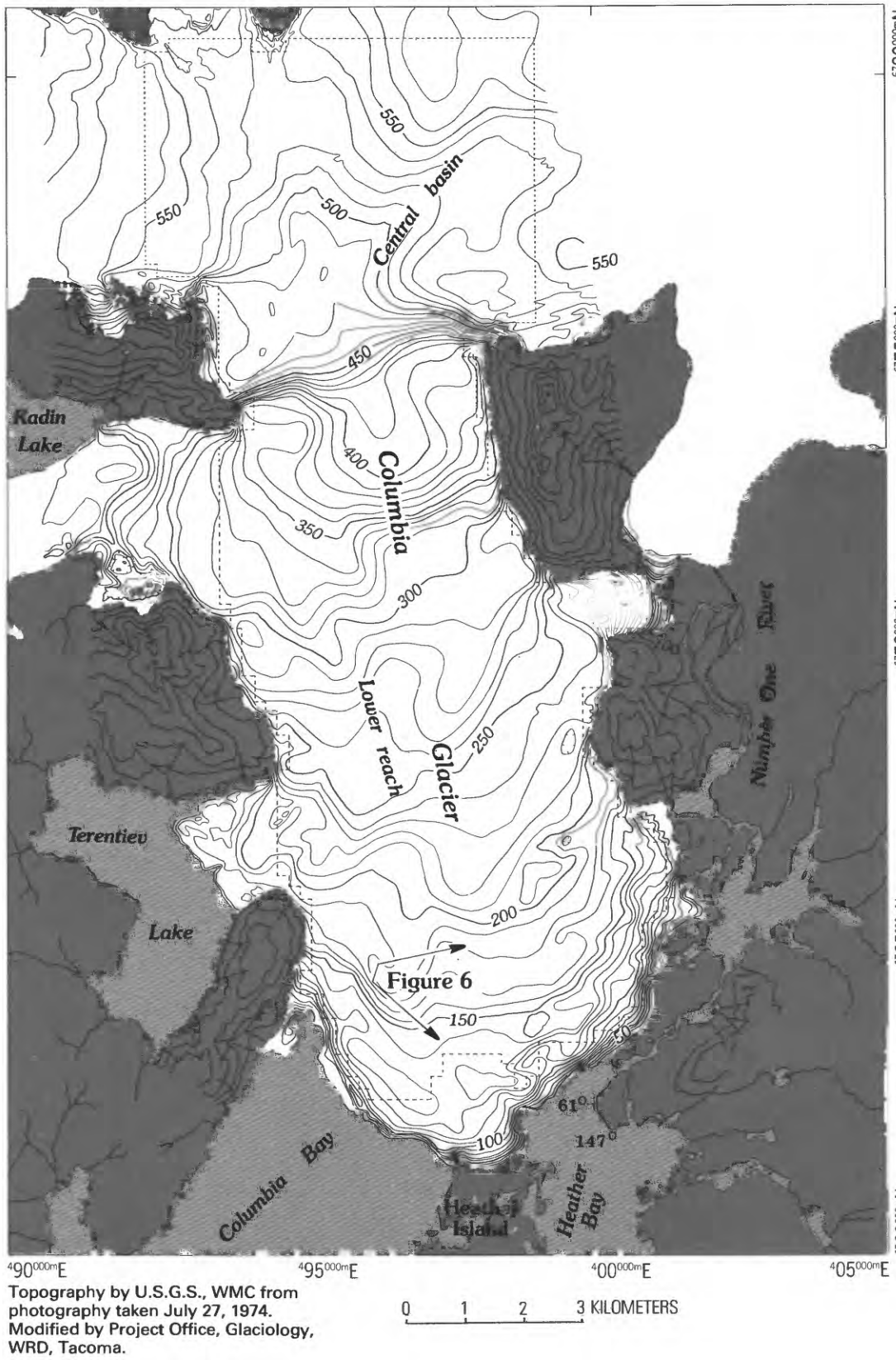

Topography by U.S.G.S., WMC from photography taken July 27, 1974. Modified by Project Office, Glaciology, WRD, Tacoma.

FIGURE 2.—July 27, 1974 (flight 2), surface topography, in meters above sea level, with 10-meter contour interval, prepared photogrammetrically by the U.S. Geological Survey Western Mapping Center at Menlo Park, Calif. Approximate scale is 1:100,000. The border of the interpolation domain is dotted. The field of view of figure 6 is indicated.

TABLE 1.—*Date and coverage of aerial photography*

[Decimal year indicates time of flight; t=1978.000 at 0000 hours on January 1, 1978, and increases by 1/365.2422 for each day thereafter. Coverage designations: a, most of glacier; b, whole glacier; c, lowest 4 km; d, lower reach; e, icefall reach; f, central basin. IPP=individual photogrammetric point]

Flight Number	Date	Decimal year	Flight altitude (m)	Coverage	Total number of IPP's
	1957				
1	July 29	1957.574	9,000	a	266
	1974				
2	July 27	1974.568	7,920	b	551
	1976				
3	July 24	1976.561	5,490	c	137
4	Oct. 1	.750	5,490	c	148
5	Nov. 17	.879	5,490	c	73
	1977				
6	Jan. 19	1977.051	5,490	c	68
7	Mar. 7	.180	5,490	c	64
8	Apr. 23	.309	5,490	c	154
9	June 2	.418	5,490	c	196
10	July 7	.514	7,010	d	222
11	Aug. 29	.659	7,010	d	227
12	Nov. 8	.854	7,010, 8,230	d, f	202
	1978				
13	Feb. 28	1978.160	6,400	d	202
14	April 19	.297	7,010, 7,770	d, e, f	193
15	June 11	.442	7,010, 7,770	d, e, f	272
16	July 30	.576	7,010, 8,530	d, e, f	247
17	Aug. 26	.650	7,010	d	193
18	Nov. 8	.853	5,490	d	193
	1979				
19	Jan. 6	1979.014	6,100	d	169
20	April 12	.277	7,010	d	175
21	Aug. 18	.628	7,010	d	151
22	Oct. 20	.800	7,010	d	162
	1980				
23	Feb. 29	1980.162	7,010	d	146
24	May 12	.361	7,010	d	149
25	July 22	.556	7,010	d	134
26	Sept. 2	.671	7,010	d	130
27	Oct. 30	.830	7,010	d	127
	1981				
28	Mar. 7	1981.180	7,010	d	125
29	June 16	.457	7,010	d	123
30	Sept. 1	.667	7,010	d	123

much was due to inherent error in the IPP altitudes. The results are summarized in table 2. The total departure is defined to be the difference, $E_T=Z_{IPP}(x,y)-f(x,y)$. To investigate the discrepancy that may be due to interpolation error, both in the digitization and in the interpolation within the 200-meter grid, only those points on the wrong side of a contour are considered. That is, if an IPP with altitude Z_{IPP} falls between contours Z and $Z+10$ m, its departure E_W is reckoned as follows, regardless of the position of the point relative to the two contours:

$$E_W=\begin{Bmatrix} Z_{IPP}-Z & (Z_{IPP}<Z) \\ 0 & (Z\le Z_{IPP}\le Z+10) \\ Z_{IPP}-(Z+10) & (Z_{IPP}>Z+10) \end{Bmatrix}. \qquad (2)$$

This is the extreme interpretation of the topography between the contours to give the minimum possible $|E_W|$; for example, $|E_T|$ may be as great as 10 m when $E_W=0$. The mean square total departure $\overline{E_T^2}$ between the IPP altitudes and the digitization of the map is

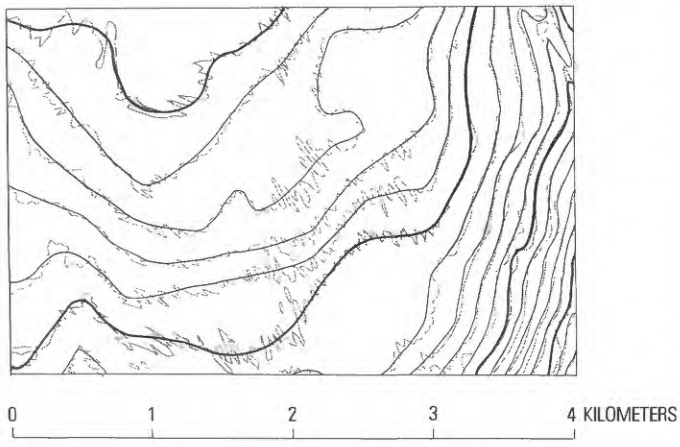

FIGURE 3.—Surface topography of lower part of Columbia Glacier, section of September 1, 1981 (flight 30), map. Surface topography in meters above sea level, with 10-meter contour interval, prepared photogrammetrically by Air Photo Tech of Anchorage, Alaska. Approximate scale is 1:50,000. Shown are original contours (light) and smoothed contours (heavy).

assumed to consist of two parts: that due to the two sources of interpolation error $\overline{E}_I^2$ and that due to the actual departure $\overline{E}_P^2$ of the IPP altitudes from the true surface altitudes. Assuming these two components to be statistically independent,

$$\overline{E}_T^2=\overline{E}_P^2+\overline{E}_I^2 \ . \tag{3}$$

If the excess of the total departure above the wrong-side departure is assumed to be equally divided between interpolation error and further contribution to $\overline{E}_P^2$, then

$$\overline{E}_I^2=\frac{1}{2}(\overline{E}_T^2-\overline{E}_W^2) \ , \tag{4}$$

so that, from equations 3 and 4:

$$\overline{E}_P^2=\frac{1}{2}(\overline{E}_T^2+\overline{E}_W^2) \ . \tag{5}$$

Each map, therefore, affords a separate estimate of E_P, as shown in table 2. An additional assumption underlying this analysis is that an IPP's map position is correct, and that any error it may have is only in its altitude. The sensitivity of the ultimate results to the uncertainty of the actual value of E_P will be investigated in a later section.

SPATIAL DISTRIBUTION OF INDIVIDUAL PHOTOGRAMMETRIC POINTS

If the IPP's are to be used as the source data for interpolating altitudes on the nodes of the square grid, it is important that they give good coverage over the domain of the interpolation. The spatial distribution of the IPP's is examined in two ways. Shown in figure 7 is a partitioning of the studied region into 24 squares, each 2 km on a side. Table 3 gives the percentage distribution of the points, square by square, for flights 2 through 30. Consistent with table 1, the total number of points falling within the 24 squares generally declines with time after flight 9. The nonuniformity of the distribution over the squares follows a pattern with strong persistence; for example, square 21 is relatively densely covered, and square 14 is relatively sparsely covered, for all 22 full-coverage flights (flights 9 through 30). Fortunately, the increase of surface roughness downglacier is accompanied by an increase of IPP density downglacier.

Another indication of the quality of the spatial distribution of the IPP's is how well they sample the 7.1-year (1974–81) altitude-change field (fig. 5), which is considered separately in two sections. The dashed line in figure 7 approximates the position on both maps of the zone of steep slope running the full width of the glacier at the constriction. The two sections are the region common to both map digitizations, as subdivided by the dashed line; they are here termed the central basin (above, 36 km^2) and the lower reach (below, 69 km^2).

Neglecting possible digitization error here, the true average altitude change over the 7.1 years is obtained by subtracting the 200-meter digitizations of the two maps; for the central basis the altitude fell 12.0 m, for the lower reach it fell 27.0 m, and for the combined region it fell 21.8 m. What is taken here to be the true change is determined by about 900 digitization nodes in the central basin and by about 1,700 nodes in the lower reach, a much greater density than the IPP's. Table 4 gives for each full-coverage flight, for each section, the IPP-sampled 7.1-year change as a fraction of the true 7.1-year change; this fraction is used to scale the IPP-sampled altitude change from July 27, 1974, until a particular flight, in order to estimate the true altitude change until that flight. There may be two causes of the apparently better sampling in the lower reach: (1) the five-thirds greater density of points and (2) the greater altitude change there, which must be compared with the estimated error in the IPP altitudes.

The time profile of the altitude change for each section is shown in figure 8; for both sections the change was much greater over the second half of the 7.1-year interval than over the first half. This must be regarded as only a zero-order estimate of the altitude change.

STATISTICAL PROPERTIES OF THE SURFACE TOPOGRAPHY

Knowledge of the statistical structure of a field variable is important to the specification of an algorithm for interpolating among given values of that variable. The

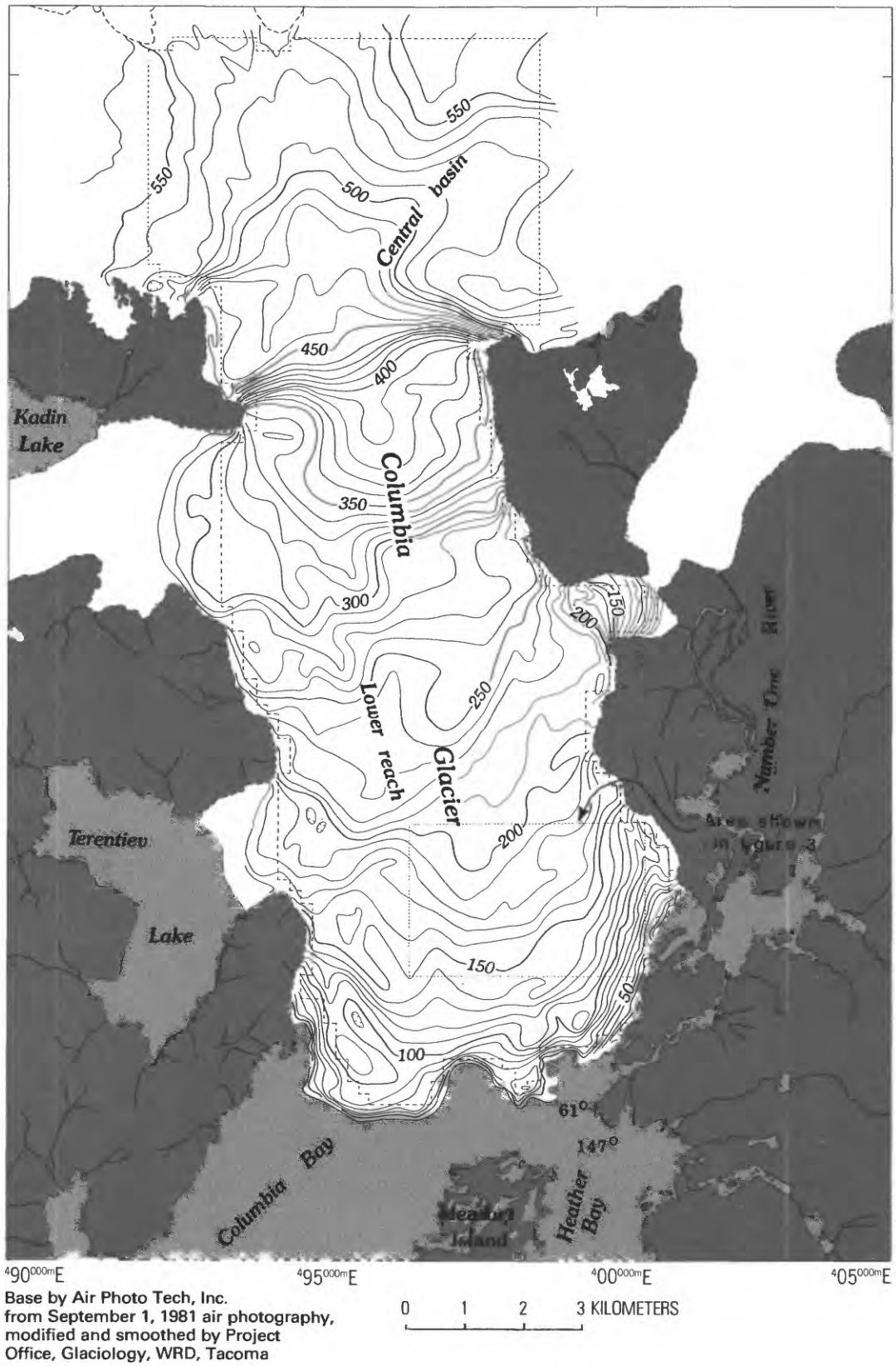

Base by Air Photo Tech, Inc.
from September 1, 1981 air photography,
modified and smoothed by Project
Office, Glaciology, WRD, Tacoma

FIGURE 4.—Smoothed September 1, 1981 (flight 30), surface topography, in meters above sea level, with 10-meter contour interval. The dashed box indicates the section shown as figure 3. Approximate scale is 1:100,000. The border of the interpolation domain is dotted.

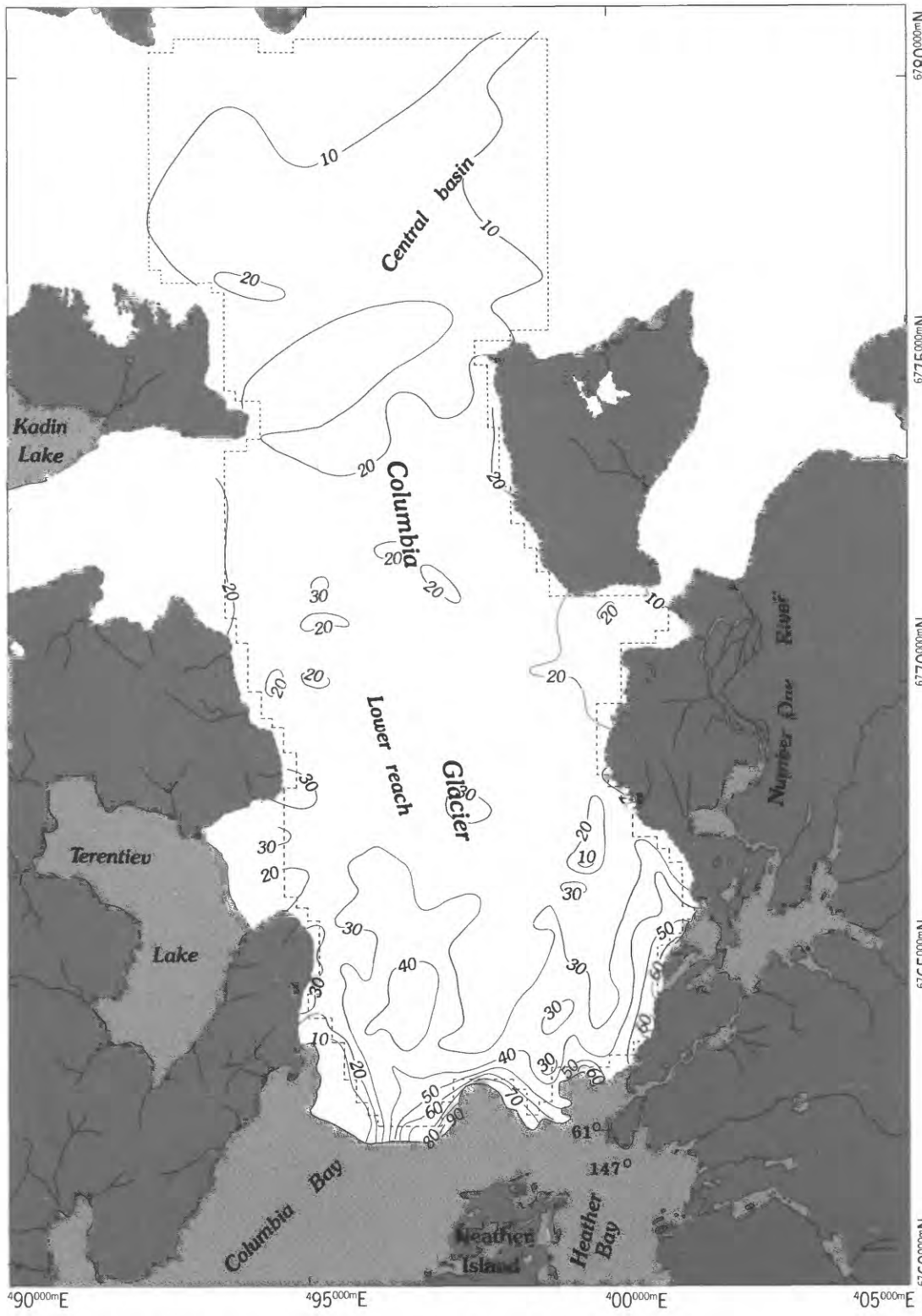

Base by Air Photo Tech, Inc.
from September 1, 1981 air photography,
modified and smoothed by Project
Office, Glaciology, WRD, Tacoma.

FIGURE 5.—Altitude decrease between July 27, 1974, surface topography (fig. 2) and smoothed September 1, 1981, surface topography (fig. 4), with 10-meter contour interval. Approximate scale is 1:100,000. The border of the interpolation domain is dotted.

FIGURE 6.—Photograph taken on October 8, 1975, showing the roughness of the glacier surface. The major crevasse valleys seen here are about 20 m deep and are spaced about 50 m apart. The location of this picture is shown on figure 2. U.S. Geological Survey photograph by L. R. Mayo.

TABLE 2.—*Estimated error distribution of individual photogrammetric point altitudes*

[Errors: Between all n points and map digitization (E_T), between digitization and only points on wrong side of a contour (E_W), due to digitization interpolation (E_I), and between all points and true surface topography (E_p); see eq. 2–5]

	July 27, 1974 (n=216)				September 1, 1981 (n=120)			
	E_T	E_W	E_I	E_p	E_T	E_W	E_I	E_p
Minimum ---------- (m)	−16	−12	--	--	−9	−6	--	--
Mean ---------- (m)	−0.9	−0.1	--	--	0.7	0.4	--	--
Maximum ---------- (m)	30	27	--	--	23	17	--	--
Mean square ---------- (m^2)	16.8	5.3	5.8	11.0	19.4	6.8	6.3	13.1
Root-mean-square -------- (m)	4.1	2.3	2.4	3.3	4.4	2.6	2.5	3.6

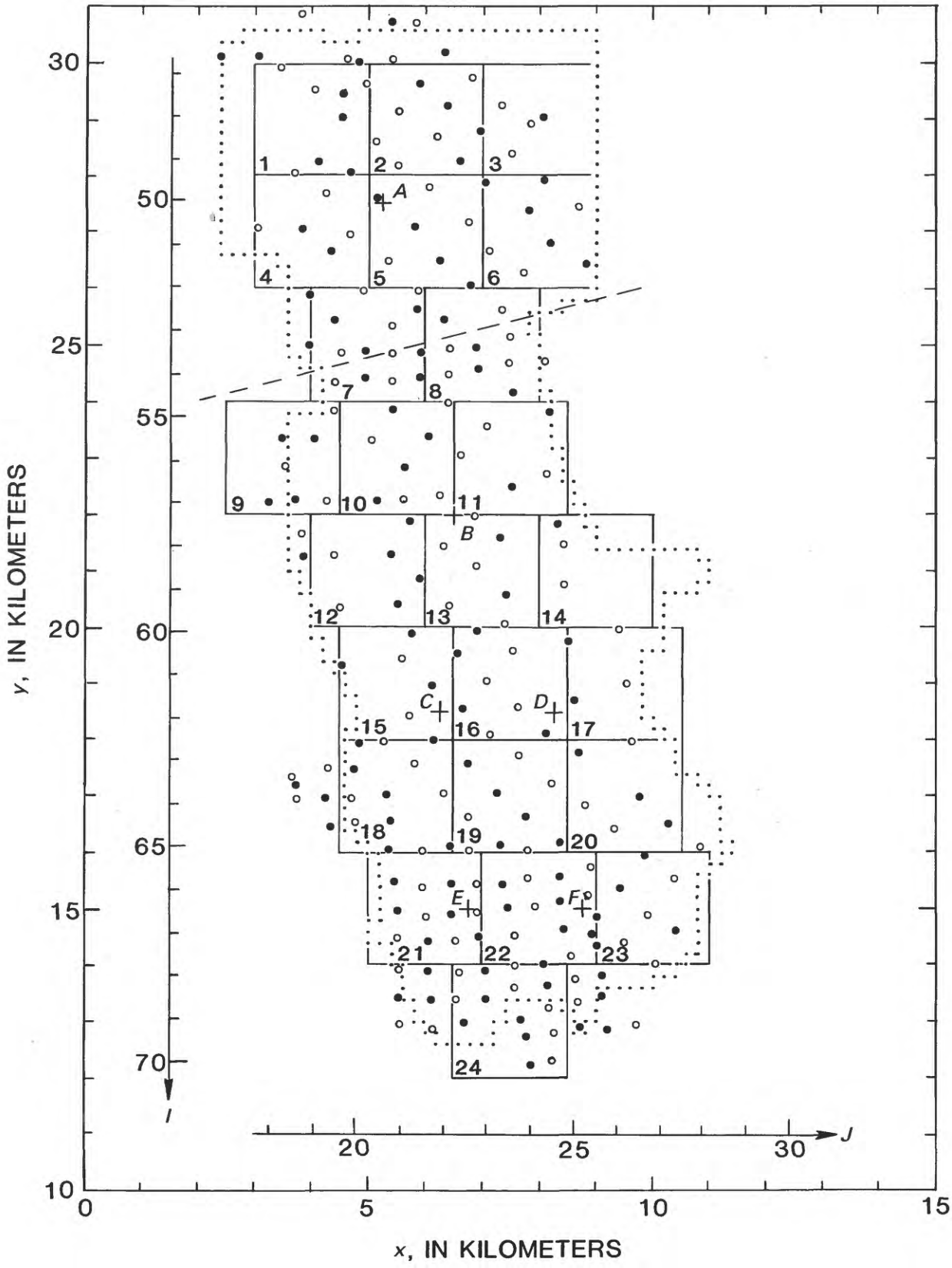

FIGURE 7.—Spatial classification of individual photogrammetric points (IPP's). The twenty-four 2-kilometer squares are the basis for the distribution statistics given in table 3. The six lettered crosses (*A, B, C, D, E, F*) are the study points for investigating the statistical structure of the surface topography. The small circles are the IPP's from flight 11 (at the beginning of the principal data year on August 29, 1977); the solid circles are odd-numbered points, and the open circles are even-numbered points. The dashed line separates the central basin (above) and the lower reach (below). Also shown are some of the rows (*I*) and columns (*J*) of the 762.5-meter data grid. The dotted border shows the region common to the digitizations of the two maps (figs. 2, 4).

TABLE 3.—*Spatial distribution of individual photogrammetric points (IPP's) over the 24 squares shown in figure 4*

[The total refers only to those points falling within one or another of the 24 squares; because of rounding, the sum of the percentages may not be 100. The average percentage value is 4.2]

Flight	Total number of IPP's	Average number per square	Square-by-square distribution of total number of IPP's, in percent																							
			1	2	3	4	5	6	7	8	9	10	11	12	13	14	15	16	17	18	19	20	21	22	23	24
2 ----	205	8.5	1	0	1	2	2	5	4	7	3	5	5	6	4	3	6	5	2	4	5	5	6	5	5	5
3 ----	119	5.0	0	0	0	0	0	0	0	0	0	0	0	0	0	0	8	5	0	15	14	3	21	16	3	13
4 ----	130	5.4	0	0	0	0	0	0	0	0	0	0	0	0	0	0	5	8	1	15	12	6	21	14	3	15
5 ----	56	2.3	0	0	0	0	0	0	0	0	0	0	0	0	0	0	0	0	0	0	14	0	54	14	0	18
6 ----	49	2.0	0	0	0	0	0	0	0	0	0	0	0	0	0	0	0	0	0	0	12	0	33	16	0	39
7 ----	48	2.0	0	0	0	0	0	0	0	0	0	0	0	0	0	0	0	0	0	0	13	0	33	13	0	42
8 ----	108	4.5	0	0	0	0	0	0	0	0	0	0	0	0	0	0	0	0	0	0	6	0	21	6	0	67
9 ----	169	7.0	2	4	2	2	4	1	7	5	2	4	2	4	4	2	3	5	2	6	6	2	8	9	5	9
10 ----	187	7.8	3	5	2	3	4	3	6	5	3	4	3	3	3	2	4	4	2	6	5	3	7	9	4	7
11 ----	192	8.0	4	5	2	3	4	4	7	5	4	3	3	3	4	2	3	4	2	6	5	3	6	7	4	7
12 ----	175	7.3	5	4	2	2	4	4	7	6	4	4	2	3	3	2	2	5	2	6	5	3	7	8	3	7
13 ----	172	7.2	3	5	1	3	5	1	8	6	4	3	3	3	4	2	3	4	2	6	5	3	8	8	4	5
14 ----	161	6.7	2	4	1	4	4	1	6	5	3	5	2	3	4	2	3	5	2	7	4	4	7	8	5	9
15 ----	159	6.6	3	6	1	4	4	1	6	7	4	5	4	3	3	2	3	3	2	5	4	3	6	8	5	8
16 ----	157	6.5	2	6	2	4	5	1	5	6	2	4	4	3	4	2	4	4	3	6	5	3	6	6	4	8
17 ----	168	7.0	3	4	1	4	5	3	5	5	4	5	4	4	4	2	3	4	2	7	5	4	7	7	4	7
18 ----	166	6.9	4	5	1	4	5	2	4	5	4	5	5	4	4	2	4	4	2	7	5	4	7	7	4	5
19 ----	155	6.5	4	7	1	4	5	3	3	5	4	6	4	3	4	2	5	5	2	6	5	4	6	5	3	6
20 ----	157	6.5	4	5	1	4	4	1	4	5	4	6	6	4	5	2	4	4	2	4	4	4	6	6	4	6
21 ----	133	5.5	5	4	0	4	5	1	4	6	3	7	5	4	6	2	4	5	2	8	5	1	6	5	3	8
22 ----	143	6.0	4	5	0	4	5	1	3	6	3	6	6	4	6	1	3	5	3	6	6	4	6	4	4	4
23 ----	129	5.4	2	5	0	4	4	1	4	6	4	6	6	5	5	2	2	6	3	8	6	3	5	5	4	3
24 ----	127	5.3	3	4	0	4	5	1	4	6	3	6	6	6	6	2	3	7	3	6	6	3	6	6	4	3
25 ----	119	5.0	3	3	0	4	4	1	5	4	3	8	7	3	7	2	4	7	2	6	7	3	7	5	3	4
26 ----	118	4.9	2	3	0	4	3	1	4	5	3	8	7	3	8	0	4	6	2	6	8	3	7	5	4	4
27 ----	117	4.9	2	4	0	4	3	1	3	5	3	8	5	3	9	1	4	6	2	6	8	3	7	5	4	3
28 ----	115	4.8	2	4	0	4	3	1	3	5	3	7	4	3	9	1	4	7	2	7	7	3	7	5	3	3
29 ----	110	4.6	2	3	0	5	4	0	3	4	4	5	6	5	7	2	3	7	2	8	7	3	7	6	4	4
30 ----	112	4.7	2	3	0	4	5	0	4	4	4	5	6	4	7	2	3	9	2	8	7	3	6	6	4	3

interpolation method adopted here is that known as "optimum interpolation" (Gandin, 1963). Because the time rate of change of the surface altitude has profound glacier-dynamics implications, through the equation of continuity, the interpolation is conducted not only within the x,y domain but also within the t domain. The salient statistical representation to be obtained is the correlation function, which states how well the altitude at some point correlates with the altitude at some other point; the method of optimum interpolation has these correlations as its coefficients. A further consideration is whether the same function applies regardless of where within the region the two points are and regardless of the relative orientation of the two points. These two properties, respectively, homogeneity and isotropy, are usually associated with the x,y domain, but they also have analogs in the t domain.

A PRELIMINARY INTERPOLATION

Optimum interpolation cannot be applied until after a correlation function is assumed. Because the original data occur irregularly in space and time (table 1, fig. 7), a preliminary interpolation scheme is necessary for investigating the statistical structure of the surface topography, from which the correlation function can be deduced. The scheme devised here uses an isotropic inverse-square-distance interpolation among the residuals from a second-degree polynomial that best fits, in the sense of least squares, all of the IPP's for a particular flight, for either the lower reach or the central basin. That is, first the polynomial

$$P(x,y)=p_1x^2+p_2xy+p_3y^2+p_4x+p_5y+p_6 \qquad (6)$$

minimizing

$$E_2^2=\frac{1}{n}\Sigma[Z(x,y)-P(x,y)]^2 \qquad (7)$$

is formed, where the summation is over all n of the IPP's for that flight for that region. Then, to interpolate the altitude $Z^*(x_0,y_0)$ at some arbitrary point, the residuals at the three nearest points are averaged by weighting each by the reciprocal of the square of the distance from (x_0,y_0):

$$Z^*(x_0,y_0)=P(x_0,y_0)+\frac{\Sigma[Z(x,y)-P(x,y)]\,/\,[(x-x_0)^2+(y-y_0)^2]}{\Sigma 1/[(x-x_0)^2+(y-y_0)^2]}, \qquad (8)$$

where the summations are here over the three points nearest (x_0,y_0).

Two different variations of this scheme were considered. Polynomials of degree one and degree zero were also used, and the averaging of residuals was also done for all points within each of several fixed radii of influence ranging from 500 to 3,000 m. These variations were tested by applying them to those nodes of the 762.5-meter grid for which values could be determined from the digitizations of the two maps. For the "nearest three" averaging rule, the second-degree polynomial agreed better with the digitized values than the first-degree, which agreed better than the zero-degree. For the second-degree polynomial, the "nearest three" averaging rule gave results better than most of, but not all of, the several influence radii tested. The use of a restrictively small radius of influence along with the zero-degree polynomial, on the other hand, often produced very poor results.

Table 5 shows the result of using the "nearest three" rule with the second-degree polynominal for each of the two maps, for the lower reach and for the central basin. Except for the case of the central basin on September 1, 1981, for which 25 interpolations were made from only 21 IPP's whose distribution is highly skewed, the residual-averaging substantially reduced the error.

CORRELATION CALCULATIONS AND COMPARISONS

The statistical structure of the surface topography is investigated by using the correlation between the altitude at some point $(0,0,t+\tau)$ and the altitude at some other point (d,θ,t):

$$r(d,\theta,\tau)=\frac{\Sigma[Z(d,\theta,t)-\overline{Z}(d,\theta,t)][Z(0,0,t+\tau)-\overline{Z}(0,0,t+\tau)]}{\{\Sigma[Z(d,\theta,t)-\overline{Z}(d,\theta,t)]^2\Sigma[Z(0,0,t+\tau)-\overline{Z}(0,0,t+\tau)]^2\}^{1/2}}, \qquad (9)$$

where (d,θ) are polar coordinates in the x,y plane and t is time. Time is defined in terms of decimal years, with $t=1978.000$ at 0000 hours on January 1, 1978, and increases by 1/365.2422 for each day thereafter. The summations are over as many flights as possible, subject to the constraints

$$\left.\begin{array}{l} t\geq 1977.418 \\ t+\tau\leq 1981.667 \end{array}\right\}, \qquad (10)$$

and the bar denotes averaging over those same flights; when $\tau=0$, the sumations are over all 22 flights (flights 9 through 30). Equations 6-8 are used to interpolate the altitudes at each of the six study points *A, B, C, D, E, F* (fig. 7) and at each of 56 points surrounding each study point. The surrounding points consist of all combina-

TABLE 4.—*Estimated average altitude changes from July 27, 1974, until the date of the indicated flight (table 1) for the lower reach and the lower part of the central basin*

[All change values are in meters, and all are negative, indicating a falling surface]

Flight	Number of sample points		Ratio of sampled 7.1-year change to true 7.1-year change		Sampled change from July 27, 1974, until flight date		Scaled change from July 27, 1974, until flight date		Scaled change as fraction of total 7.1-year change	
	Lower reach	Central basin	Lower reach	Central basin	Lower reach	Central basin	Lower reach	Central basin	Lower reach	Central basin
9	135	41	1.05	1.22	3.4	0.9	3.3	.8	.12	.06
10	143	53	1.04	1.16	5.3	0.6	5.1	.5	.19	.04
11	143	57	1.03	1.10	8.9	3.2	8.7	2.9	.32	.24
12	129	53	1.04	1.12	14.5	5.6	14.0	5.0	.52	.42
13	134	47	1.04	1.08	11.7	1.9	11.2	1.8	.42	.15
14	132	37	1.03	1.09	11.6	2.3	11.2	2.1	.41	.18
15	119	42	1.01	1.09	9.7	1.8	9.6	1.6	.35	.14
16	124	40	1.02	1.11	13.2	5.6	13.0	5.0	.48	.42
17	131	41	1.02	1.14	15.2	6.5	14.9	5.7	.55	.48
18	128	46	1.00	1.09	17.4	5.5	17.4	5.0	.64	.42
19	114	42	1.01	1.07	16.4	6.7	16.3	6.2	.60	.52
20	117	42	1.01	1.06	15.0	6.0	14.9	5.6	.55	.47
21	104	33	1.02	1.07	18.5	8.1	18.1	7.6	.67	.64
22	114	35	1.01	1.05	21.3	10.2	21.1	9.7	.78	.81
23	106	26	.99	1.11	21.5	8.3	21.7	7.5	.80	.63
24	107	29	.98	1.05	20.5	9.1	20.8	8.6	.77	.72
25	100	26	.98	1.11	22.6	9.4	23.1	8.5	.85	.71
26	100	24	.98	1.15	25.3	10.8	25.8	9.4	.95	.79
27	99	23	.98	1.15	22.7	11.2	23.2	9.7	.86	.81
28	99	24	1.00	1.23	17.6	9.2	17.5	7.5	.65	.63
29	96	20	1.00	1.23	17.9	12.8	17.9	10.4	.66	.87
30	96	22	.97	1.22	26.3	14.6	27.0	12.0	1.00	1.00

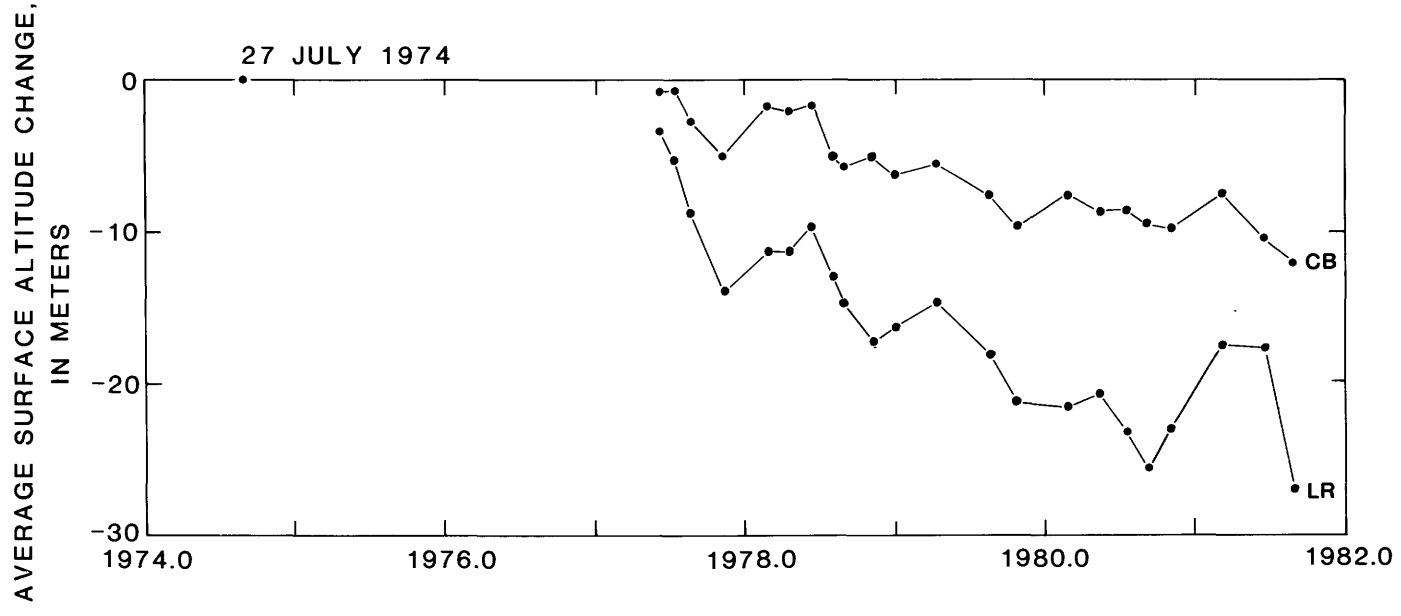

FIGURE 8.—Time profiles of the surface altitude change since July 27, 1974, averaged over the lower reach (LR) and over the central basin (CB).

tions of d=200, 400, ..., 1,400 m and θ=E, NE, N, ... , SE. For each study point and for each time lag τ, the correlation coefficient is averaged over direction for each distance

$$\overline{r_\theta}(d,\tau)=\frac{1}{8}\sum_\theta r(d,\theta,\tau) \tag{11}$$

and is averaged over distance for each direction

$$\overline{r_d}(\theta,\tau)=\frac{1}{7}\sum_d r(d,\theta,\tau)\ . \tag{12}$$

The curves in figure 9 are $\overline{r_\theta}(d,\tau)$ versus d for the six study points and for τ=−1.0, −0.5, 0, 0.5, and 1.0 a. Similarly, the curves in figure 10 are $\overline{r_d}(\theta,\tau)$ versus θ. For each study point, when $\tau\neq 0$, the values of $Z(0,0,t+\tau)$ are interpolated from a hand-drawn curve through the altitudes for each of the 22 flights for that study point; the values of t used in equation 9 are those flight dates that satisfy the associated constraints (relation 10), so that between-flight interpolation need not be conducted for any of the surrounding points. The flights that can be used with τ=−1.0, −0.5, 0, 0.5, and 1.0 a are, respectively, 15-30, 13-30, 9-30, 9-27, and 9-25 (table 1).

The question of spatial homogeneity can be examined by comparing, in either figure 9 or figure 10, the six curves occurring vertically for any one of the five time lags τ. In the case of perfect homogeneity, the curves for the six different study points would be identical. The most substantial departure from this condition is that the curves for E and F for $\tau=\pm 0.5$ a, and the curves for A for all τ, are markedly depressed below the average.

The question of spatial isotropy can be examined by considering the variation with direction within each of the curves of figure 10. In the case of perfect isotropy, each curve would be a horizontal line segment; perfect spatial homogeneity would further require that for any τ the curves would all have the same r-value for all six study points.

The apparent departure from perfect isotropy is not reduced if the flow of the glacier is considered. The open circles in figure 10 represent distance-averaged correlations from equations 9 and 12, but the $Z(d,\theta,t)$ values used in equation 9 are interpolated by equation 8 from altitudes at IPP's that have been allowed to move with the glacier flow from time t until time $t+\tau$. Because the y-component of velocity v is much greater than the x-component (Fountain, 1982), only the former is used in advecting the points; that is,

$$\hat{Z}(x,y)=Z(x,\hat{y})\,, \tag{13}$$

where

$$\hat{y}=y+\int_t^{t+\tau} v[x,y(t)]dt \tag{14}$$

is used instead of $Z(x,y)$ in equation 8. Because $\hat{y}=y$ when $\tau=0$, and because few velocity data are available for the central basin, circles do not accompany the curves in figure 10 either for $\tau=0$ or for study point A.

The question of temporal isotropy can be examined by comparing the curves (for any study point in either figure 9 or figure 10) for τ=−0.5 a and τ=+0.5 a, and for τ=−1.0 a and τ=+1.0 a. There is a high degree of left-right (negative τ, positive τ) symmetry in both figure 9 and figure 10.

Although the ideals of homogeneity and isotropy are not unambiguously demonstrated by the curves of figures 9 and 10, neither is any other pattern of correlation unambiguously demonstrated by them. Possible causes for the discrepancies from the ideals include: the n used in equation 9 is determined by the number of flights satisfying condition (relation 10), which ranges from n=22 for τ=0 down to n=16 for τ=−1.0 a; the $Z(0,0,t+\tau)$ values used in equation 9 were interpolated visually from curves drawn by hand through the $Z(0,0,t_L)$ values at flight dates t_L; correlations at study point A are relatively more strongly contaminated by the altitude errors in the IPP's than are the study points in the lower reach, where the altitude changes are more than twice as great as they are in the central basin. The small number of realizations (that is, 22 or fewer flights, depending on the value of τ)

TABLE 5.—*Result of interpolating at a point using a regional second-degree polynomial corrected by averaging the residuals of the three individual photogrammetric points (IPP's) nearest that point*

	July 27, 1974 (flight 2)		September 1, 1981 (flight 30)	
	Lower reach	Central basin	Lower reach	Central basin
Number of IPP's	176	35	101	21
Number of interpolation points (at nodes of the 762.5-meter data grid)	107	25	103	25
E_2, root-mean-square error at interpolation points using only the second degree polynomial fitted to IPP's (m)	13.3	14.5	12.9	9.8
E_3, root-mean-square error at interpolation points when "nearest three" residual averaging used with second degree polynomial (m)	6.4	11.4	8.1	10.3

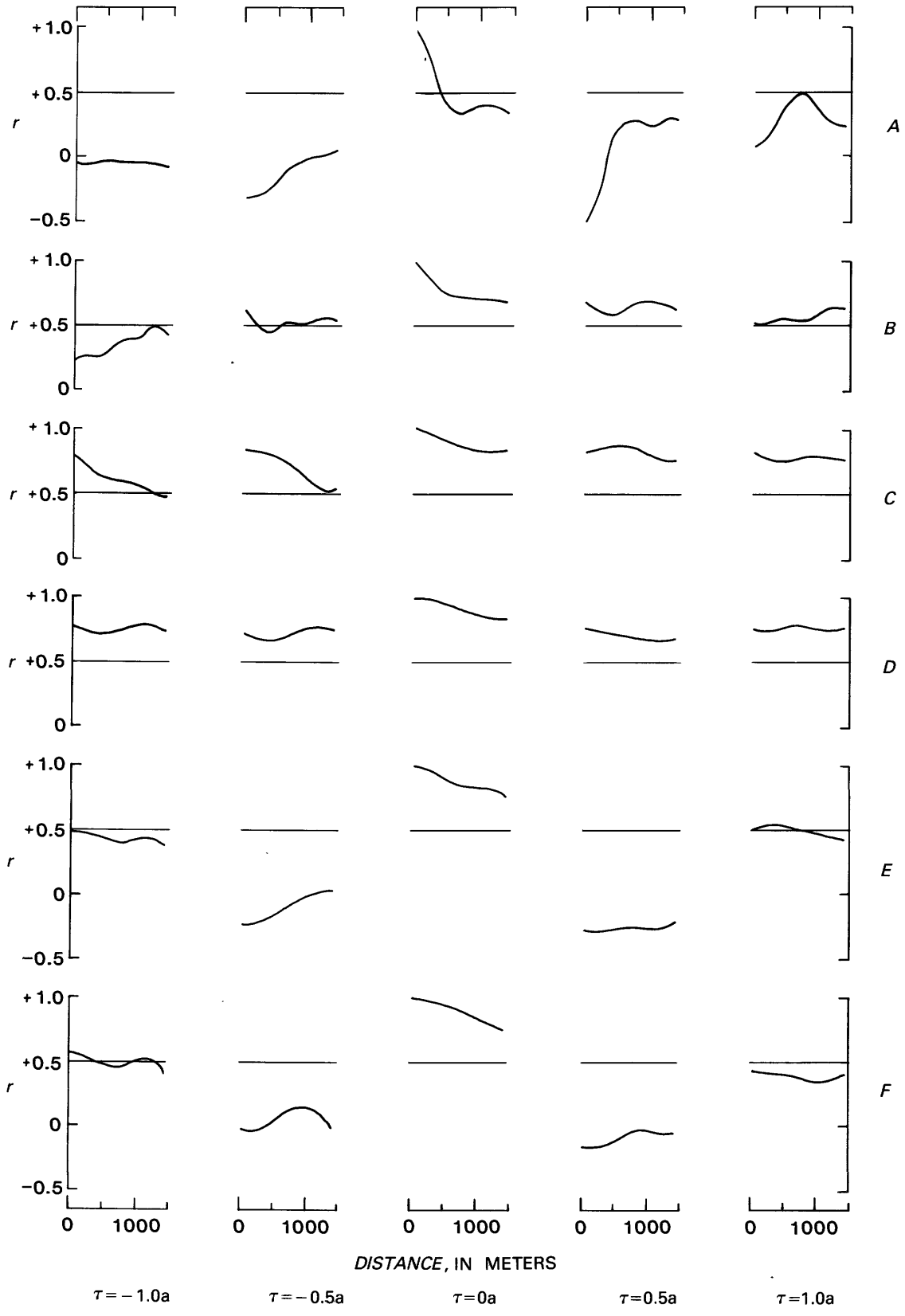

FIGURE 9.—The function $\bar{r}_\theta(d,\tau)$ versus d for each study point (A, ... , F) and for each of the five indicated time lags τ (see eq. 9, 11). Although continuous curves are shown, $\bar{r}_\theta(d,\tau)$ is known only at the eight d-values 0, 200, 400, ...,1,400 m.

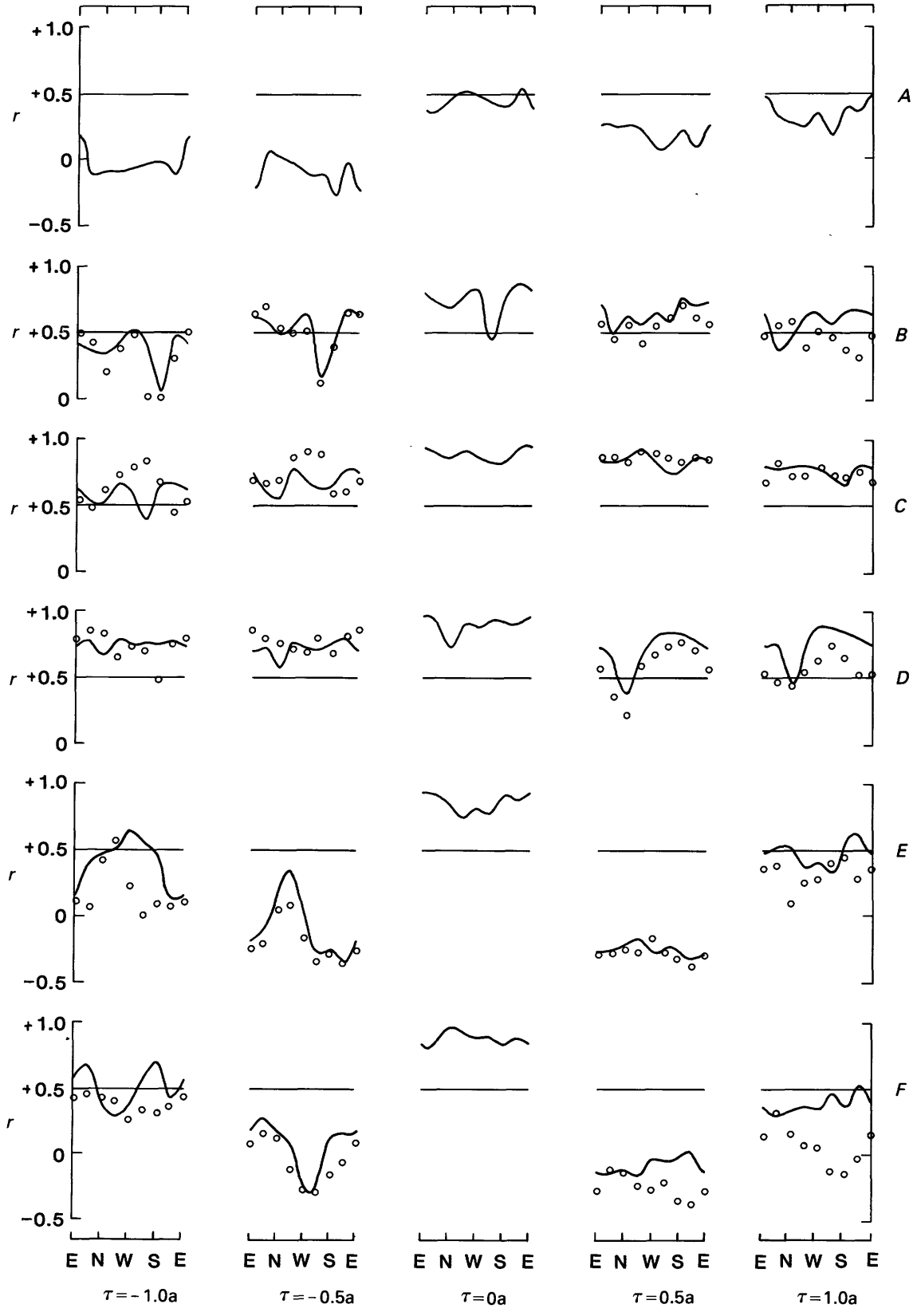

FIGURE 10.—The function $\bar{r}_d(\theta,\tau)$ versus θ for each study point (A, ... , F) and for each of the five indicated time lags τ (see eq. 9, 12); although continuous curves are shown, $\bar{r}_d(\theta,\tau)$ is known only at the eight θ-values E, NE, N, ..., SE. The open circles indicate values obtained by using individual photogrammetric points allowed to move with the glacier flow (eq. 13, 14).

precluded investigation of temporal homogeneity, which is usually termed "stationarity." Because no other pattern is unambiguously demonstrated by the curves of figures 9 and 10, the assumptions of homogeneity and isotropy are made, both spatially and temporally, including the type of isotropy that, surprisingly, permits neglecting the effect of the glacier flow when $\tau \neq 0$.

FIRST APPROXIMATION TO THE INTERPOLATED ALTITUDES

Because optimum interpolation can be applied better to deviations from a norm than to the raw values of the variable themselves (Gandin, 1963, p. 86–92), an interpolation scheme is adopted to provide that norm. The correlation function then expresses the correlation of the deviations from this norm as a function simply, because of the assumptions of homogeneity and isotropy, of the horizontal distance $d=[(x_1-x_2)^2+(y_1-y_2)^2]^{1/2}$ between two points $Z(x_1,y_1,t_1)$ and $Z(x_2,y_2,t_2)$ and of their time difference $\tau=|t_1-t_2|$. As a consequence of adopting this interpolation scheme, two decisions concerning the domain of the interpolation are made: (1) altitudes are interpolated only for the times of the flights, although there is no theoretical bar to interpolating altitudes at any arbitrary time, and (2) a single procedure is applied to the entire combined region of the lower reach and the central basin, thereby avoiding the introduction of a discontinuity between these two regions, but at the risk of increasing the interpolation error.

For each flight, the norm field $f_L(x,y)$ is obtained by taking the altitude change from flight 2 until flight L to be a linear function of the change from flight 2 until flight 30:

$$f_L(x,y)-f_2(x,y)=a_L[f_{30}(x,y)-f_2(x,y)]+b_L$$

or (15)

$$f_L(x,y)=(1-a_L)f_2(x,y)+a_Lf_{30}(x,y)+b_L,$$

in which the coefficients are estimated by minimizing

$$E_f^2=\frac{1}{m_L}\sum_{k=1}^{m_L}[f_L(x_k,y_k)-Z_L(x_k,y_k)]^2 \quad (16)$$

where the sum is over all m_L IPP's for that flight having (x,y) within the domains of the digitizations of the two maps.

A split sample analysis of the m_L points is used to estimate the root-mean-square error in approximating the true topography by the norm field $f_L(x,y)$. The assumption is made that if the m_L points are a good sample of the true topography, subject to their inherent altitude error, then a randomly chosen large subset of them is also a good sample. Two subsets of the points are used, the odd-numbered ones and the even-numbered ones, taking them in the order in which they appear in Fountain (1982). The x,y-distributions of the two subsets are shown in figure 7 for flight 11, which is typical of these distributions for the other flights. First, $(a_L)_{ODD}$ and $(b_L)_{ODD}$ are obtained by using only the odd-numbered points in equations 15 and 16; then $(E_f)_{EVEN}$ is computed by using $(a_L)_{ODD}$ and $(b_L)_{ODD}$ in the application of equation 16 to only the even-numbered points. Second, $(E_f)_{ODD}$ is computed by applying equation 16 to only the odd-numbered points, using $(a_L)_{EVEN}$ and $(b_L)_{EVEN}$ obtained by applying equations 15 and 16 to only the even-numbered points. Third, $(a_L)_{ALL}$ and $(b_L)_{ALL}$ are obtained by using all m_L points in equations 15 and 16; then $(E_f)_{ALL}$ is computed by using those coefficients in the applications of equation 16 to all m_L points. Table 6 gives m_L, all three sets of coefficients, and all three values of E_F. Although flights 3–8 only partially cover the region (table 3), and therefore are not used in constructing the correlation function, they are amenable to the application of equations 15 and 16 and are therefore included in these results.

Another interpretation of E_f is as an indication of the variance of the data's deviations about the norm. Although there is a pronounced spatial distribution of the total altitude change between the times of the two maps (fig. 5), with the magnitude of the change generally decreasing upglacier, a second-degree polynomial (eq. 6) very poorly represents the x,y-distribution of the squares of the deviations from $f_L(x,y)$. The goodness of fit (r^2) of the polynomial is also given in table 6; its low values support the reasonableness of the assumption of spatial homogeneity of the variance.

Because the IPP altitude errors are assumed to be uncorrelated with the altitudes themselves, the variance V of the altitudes about the norm field is estimated as the excess of the average E_f^2 over E_p^2. The split-sample values are averaged because they are independent estimates, in that points used to compute E_f are separate from those used to form the norm-field coefficients, whereas $(E_f)_{ALL}$ is computed from the same points used to form the coefficients. Taking $E_p^2=12$ m^2, the result is also coincidentally $V=12$ m^2, compared with 11 m^2 if the $(E_f)_{ALL}$ were used. The variance is assumed to be constant in time as well as in space, and the flight-to-flight variation of E_f is interpreted to be random-sampling variation. If a separate V were to be associated with each flight, and if each were to be obtained by subtracting $E_p^2=12$ m^2 from E_f^2, then V would vary from flight to flight between extreme values of zero for flight 10 to

TABLE 6.—*The coefficients* a_L *and* b_L *used in equation 15 to interpolate the norm field* f_L (x,y) *for flight* L *from the digitizations of the two maps* f_2 (x, y) *and* f_{30} (x, y)

[The coefficients are estimated from all m_L points (ALL), from only the odd-numbered points (ODD), and from only the even-numbered points (EVEN). The error is estimated by using $(a_L, b_L)_{ODD}$ with only the even-numbered points to give $(E_f)_{EVEN}$, by using $(a_L, b_L)_{EVEN}$ with only the odd-numbered points to give $(E_f)_{ODD}$, and by using $(a_L, b_L)_{ALL}$ with all m_L points to give $(E_f)_{ALL}$. The goodness of fit (Fit) is for a second-degree polynomial $P_2(x,y)$ fit to the squares of the deviations of all m_L points from $f_L(x,y)$]

Flight	m_L	ODD		EVEN		ALL		E_f (m)			Fit
		a_L	b_L	a_L	b_L	a_L	b_L	EVEN	ODD	ALL	
2	202	0.029	−0.2	0.092	1.4	0.063	0.7	4.62	3.41	4.03	0.02
3	118	.470	7.7	.506	8.5	.487	8.1	4.42	3.81	4.11	.21
4	128	.712	8.0	.807	11.0	.767	9.8	4.77	4.62	4.66	.21
5	51	1.007	11.6	.872	10.3	.906	9.9	7.52	8.67	7.58	.32
6	48	0.439	−4.2	.798	7.6	.602	1.2	6.31	8.68	6.80	.34
7	45	.574	1.9	.626	1.7	.598	1.7	4.68	5.38	4.70	.27
8	100	.564	6.2	.478	3.8	.520	5.0	4.92	5.40	5.04	.19
9	176	.455	8.7	.273	4.0	.360	6.2	3.94	4.57	3.95	.12
10	196	.342	4.3	.366	4.9	.353	4.5	3.45	3.04	3.24	.04
11	200	.477	3.8	.435	3.1	.458	3.5	3.60	4.80	4.22	.08
12	182	.706	4.7	.714	5.2	.710	5.0	6.57	6.98	6.77	.28
13	181	.744	8.9	.785	9.7	.763	9.3	6.30	6.77	6.53	.16
14	169	.687	7.5	.774	9.5	.725	8.3	5.82	6.81	6.29	.11
15	161	.616	7.4	.667	7.7	.645	7.6	4.51	4.60	4.47	.02
16	164	.578	2.7	.617	3.4	.594	3.0	4.57	3.73	4.16	.02
17	172	.666	3.0	.604	1.5	.635	2.2	3.87	4.02	3.91	.05
18	174	.939	7.3	.887	6.8	.908	7.0	5.27	4.63	4.90	.10
19	156	.906	7.0	.691	2.7	.801	4.9	5.45	5.43	5.08	.11
20	159	.659	2.7	.634	2.3	.650	2.6	5.24	4.60	4.92	.02
21	137	.547	−2.7	.664	−0.2	.601	−1.6	4.10	4.30	4.07	.07
22	149	.891	2.1	.791	0.6	.846	1.5	3.90	4.37	4.01	.09
23	132	1.012	5.6	1.003	5.3	1.008	5.4	5.17	5.14	5.15	.08
24	136	0.766	0.4	0.843	1.6	0.808	1.1	4.34	4.18	4.19	.05
25	126	.758	−1.9	.855	0.3	.801	−0.9	5.00	4.12	4.53	.01
26	124	.816	−3.3	.999	1.9	.906	−0.7	4.38	4.90	4.44	.01
27	122	.776	−1.7	.778	−2.0	.775	−1.9	4.21	4.05	4.12	.03
28	123	.369	−6.1	.514	−4.0	.425	−5.4	5.89	5.50	5.41	.18
29	116	.349	−8.2	.443	−6.1	.385	−7.5	5.41	4.85	5.09	.12
30	118	.848	−3.1	.895	−2.1	.876	−2.5	4.08	3.41	3.75	.04

34 m^2 for flight 12. Part of the variation of E_f may be caused by variation in E_p, but estimates of that quantity are unavailable for flights 3 through 29. If a variation of equation 15 were used, one that lacked the constant term b_L, then the variance would be 14 m^2 and the deviations about the norm field would have a nonzero mean.

THE CORRELATION FUNCTION

The empirical function $r^*(\tau,d)$ gives the correlation between deviations from the norm field $f_L(x,y)$ at different points and different times. Following from the assumptions of homogeneity and isotropy, the function depends only on the horizontal distance d between the two points and on the time difference τ.

For $\tau=0$, any of the flights can be used with itself to estimate the d-dependence $r^*(0,d)$. For $\tau\neq0$, the time distribution of the flights (table 1) permits investigating $r^*(\tau,d)$ for only selected τ. Table 7 gives the value of r^* obtained, after the fashion of equation 9, by considering all the deviations

$$\Delta Z_L(x_k,y_k)=Z_L(x_k,y_k)-f_L(x_k,y_k) \tag{17}$$

falling within each of seven different τ-intervals and within each of ten different d-intervals. These are calculated directly from the deviations, without being vitiated by the crude interpolation necessary to get the $Z(0,0,t+\tau)$ values between flight dates for computing $r(d,\theta,\tau)$ at the six study points.

The empirical $r^*(\tau,d)$ distribution of table 7 has several prominent characteristics: (1) it indicates a moderately well behaved function of d and τ, (2) it approaches unity as d and τ both go to zero, (3) for all τ, it approaches zero for large d, and (4) for small d, it remains positive for all τ. The x,y,t density of the IPP's is high enough that several points can easily be obtained for interpolation if

TABLE 7.—*Values of the correlation coefficient calculated from the deviations from the norm fields for the indicated time difference (τ) intervals and the indicated horizontal distance (d) intervals*

[The value of the correlation coefficient is shown above, and the numbers of irregularly positioned photogrammetric points falling within the particular τ-interval and d-interval is shown below. The pairs of flights having the particular time difference are also shown. The correlation for $\tau=d=0$ is assumed to be unity]

τ-interval (a)	Flights	d-interval (m)									
		0-40	180-220	380-420	580-620	780-820	980-1,020	1,480-1,520	1,980-2,020	2,480-2,520	2,980-3,020
0	(9,9), (10,10), ...	(1.000)		.622	.574	.413	.380	.238	.139	.043	−.115
	(30,30)	1	8	151	448	479	937	1,060	1,109	1,300	1,301
.241 to .283	(9,11),(13,15),(14,16), (16,18),(19,20),(25,27), (28,29)	.700	.717	.473	.436	.367	.309	.196	.049	.045	−.003
		168	168	95	298	359	541	660	758	760	850
.486 to .534	(11,13),(13,17),(20,22), (21,23),(23,26),(26,28), (28,30)	.409	.401	.396	.302	.208	.219	.173	.108	.014	−.088
		108	66	224	287	273	451	546	711	739	764
.756 to .796	(10,14),(11,15),(12,17), (18,21),(19,22),(22,25), (26,29)	.167	.206	.301	.244	.281	.243	.071	.043	−.001	−.074
		68	113	188	299	379	532	641	773	844	919
.980 to 1.024	(9,15),(11,17),(12,18), (14,20),(17,21),(23,28), (26,30)	.304	.293	.197	.389	.176	.251	.204	.074	−.047	−.075
		55	117	172	298	422	461	701	770	789	822
1.136 to 1.202	(9,16),(10,17),(11,18), (12,19),(15,21),(17,22), (19,23),(21,27)	.417	.624	.346	.402	.293	.268	.135	−.012	−.045	−.082
		61	142	199	393	464	579	848	904	996	1029
1.295 to 1.358	(10,18),(11,19),(14,21), (15,22),(18,23),(19,24), (23,29),(24,30)	.481	.478	.338	.218	.191	.103	.169	.052	−.023	−.030
		34	129	188	326	392	505	665	706	884	877

they are required to be within a d and a τ substantially smaller than the ranges of those variables represented by the empirical data. If the correlation function is known perfectly (Gandin, 1963, p. 70-72), the interpolation error decreases as more and more points are used, albeit more and more slowly. However, the correlation function here is not known perfectly.

Requiring a point to be within $d=1$ km and $\tau=0.39$ a still includes a large number of points, and it also restricts the domain over which $r^*(\tau,d)$ must be approximated functionally to the domain over which the empirical values are themselves better behaved. This domain actually used is twice that large ($d\leq 2$ km and $\tau\leq 0.78$ a), because the method of optimum interpolation requires the correlations between the included points themselves, as well as between the included points and the point where the interpolation is made; for example, two of the included points may each be within a kilometer of the point where the interpolation is made, but they may be 2 km away from each other.

Because the correlation function must have a positive Fourier transform (Gandin, 1963, p. 38-40), the class of functions that can be used for approximating the $r^*(\tau,d)$ data is severely restricted. Two analytical functions that are widely used (Gandin, 1963; Thiebaux, 1975) are the damped cosine and the Gaussian

$$\hat{R}(\tau,d)=e^{-\hat{\alpha}^2\tau^2-\hat{\beta}^2d^2} \quad . \tag{18}$$

The empirical data do not exhibit oscillation of sign, which would imply using the damped cosine. Another function having a positive transform (Oberhettinger, 1973) is

$$R(\tau,d)=\left(\frac{\alpha^2}{\alpha^2+\tau^2}\right)\left(\frac{\beta^2}{\beta^2+d^2}\right) , \tag{19}$$

which approximates the empirical data much better than equation 18 does.

The relative suitabilities of function 18 and function 19 for approximating the $r^*(\tau,d)$ values of table 7 are compared in figure 11. In both, the coefficients are chosen to minimize

$$E_r^2=\frac{1}{30}\sum[R(\tau,d)-r^*(\tau,d)]^2 , \tag{20}$$

in which the summation is over all 30 combinations of $\tau=0$, 0.27, 0.51, and 0.78 a and $d=0$, 0.2, 0.4, 0.6, 0.8, 1.0, 1.5, and 2.0 km except for the two smallest d-values when $\tau=0$. The minimizing coefficients are $\hat{\alpha}=2.79$, $\hat{\beta}=1.11$ in function 18 for $E_r=0.109$, and $\alpha=0.470$, $\beta=0.755$ in function 19 for $E_r=0.069$. Not only are the residuals produced by function 19 smaller than those produced by function 18, but they are also more randomly distributed. Function 18 systematically produced negative residuals for small values of either τ or d and positive residuals for large values; this is true to a lesser degree with function 19 as well.

Although the assumption of spatial homogeneity permits determining r as a function of only the distance d as well as the time difference τ, the Fourier transform

must be of the same dimensionality as that of the space in which the data points exist. The transform

$$\Phi(\phi_1,\phi_2,\phi_3)=\int_{-\infty}^{\infty}\int_{-\infty}^{\infty}\int_{-\infty}^{\infty}\left(\frac{\alpha^2}{\alpha^2+\tau^2}\right)\left(\frac{\beta^2}{\beta^2+x^2+y^2}\right)e^{i(\phi_1\tau+\phi_2 x+\phi_3 y)}dxdyd\tau\ , \quad (21)$$

in which x and y denote the two components of the distance d, may be shown to be positive for all finite, positive values of the coordinates ϕ_1, ϕ_2, and ϕ_3 (appendix A).

THE INTERPOLATION ALGORITHM

Because the present work is a part of a larger effort in investigating the behavior of Columbia Glacier, and of glaciers generally, rather than pursuing questions in data analysis itself, no direct comparison has been made between various interpolation methods. Optimum interpolation is widely used in the objective analysis of meteorological variables. In making an individual interpolation, it tends toward using all of the available data and it provides an estimate of the interpolation error. In analyzing rainfall patterns in south-central France, Creutin and Obled (1982) compared it with several other methods, including the highly similar kriging, and found it to be superior, overall. Although it is called optimum interpolation, it extrapolates as well; that is, it is not restricted to estimating values at points that are in any sense between the given points.

OPTIMUM INTERPOLATION

The interpolated altitude at some point for flight L, $Z_L^*(x,y)$, is obtained by adding the estimated deviation there, ΔZ_0^*, to the norm:

$$Z_L^*(x,y)=f_L(x,y)+\Delta Z_0^*\ . \quad (22)$$

The method of optimum interpolation (Gandin, 1963) is used to obtain ΔZ_0^* as a linear combinatin of the deviations ΔZ_i at N nearby points selected, in general, both from flight L and from other flights close in time to flight L:

$$\Delta Z_0^*=\sum_{i=1}^{N} w_i\Delta Z_i\ . \quad (23)$$

The weights w_i are obtained from a system of simultaneous linear equations that minimizes (and, therefore, gives the method its name) the error:

$$E_G^2=\frac{1}{M}\sum_{k=1}^{M}(\Delta Z_0^*-\Delta Z_0)_k^2\ , \quad (24)$$

in which the summation is over a larger number M of applications of the method at some particular point (x,y), and ΔZ_0 is the true deviation from $f_L(x,y)$ there.

If equation 23 is substituted into equation 24, and if the squaring is performed, then

$$E_G^2=\frac{1}{M}\sum_{k=1}^{M}(\Delta Z_0)_k^2-2\sum_{i=1}^{N}\left[\frac{w_i}{M}\sum_{k=1}^{M}(\Delta Z_i\Delta Z_0)_k\right]+\sum_{i=1}^{N}\sum_{j=1}^{N}\left[\frac{w_iw_j}{M}\sum_{k=1}^{M}(\Delta Z_i\Delta Z_j)_k\right]\ . \quad (25)$$

If ΔZ_i is assumed to have zero mean over large M, and if its variance is taken to be constant, as suggested by table 6, then the first term on the right-hand side of equation 25 is the variance of ΔZ_i, which is denoted V. If equation 25 is divided by V it becomes

$$E_G^2/V=1-2\sum_{i=1}^{N}w_ir_{i0}+\sum_{i=1}^{N}\sum_{j=1}^{N}w_iw_jr_{ij}\ , \quad (26)$$

where r_{ij} is the correlation between ΔZ_i and ΔZ_j, and is calculated from equation 19 using the distance d and time difference τ between the two data points having those deviations. Minimizing E_G with respect to the w_i is accomplished by requiring

$$\partial E_G/\partial w_i=0 \quad (27)$$

for $1\le i\le N$, and solving the resulting linear system, in which the $r_{ii}=1$,

$$\sum_{j=1}^{N}r_{ij}w_j=r_{i0}\ (1\le i\le N) \quad (28)$$

to obtain the w_i. If equations 28 are multiplied by w_i, and if the sum is taken over i, then equation 26 may be simplified to

$$E^2{}_G=\left(1-\sum_{i=1}^{N}w_ir_{i0}\right)V\ . \quad (29)$$

The condition $0\le E_G^2<V$ is always fulfilled if the matrix of equation 28 is positive definite, which is ensured

(Gandin, 1963, p. 39) if the correlation function used to form the r_{ij} has a positive Fourier transform.

The foregoing development is for the simplified special case in which the ΔZ_i are known exactly. Because they are not, being subject to the IPP altitude error given by equation 5, the linear system must be modified (Gandin, 1963, p. 79) to

$$\left(\frac{E_p^2}{V}\right) w_i + \sum_{j=1}^{N} r_{ij} w_i = r_{i0} \quad (1 \le i \le N) \tag{30}$$

for determining the w_i, which are then used in equation 23 to get the interpolant ΔZ_0^* and in equation 29 to get the error estimate E_G. Using equation 30 is predicated on three assumptions regarding the IPP altitude errors: (1) they have zero mean, (2) they are not correlated with the true altitude values, and (3) they are not correlated with each other. The detailed comparison of the IPP's with the two maps, to compute the error E_w of equation 2, revealed no contradiction of these assumptions.

The presence of the error term in equation 30 has two important consequences (Gandin, 1963, p. 80–84). First, it increases the interpolation error E_G. Second, the value of E_p that produces the smallest E_G is its true value; that is, E_G will be increased if a value of E_p is used that is either larger or smaller than its true value.

If the errors at the individual points are indeed uncorrelated, or poorly correlated, the resulting interpolation error E_G can be less than E_p. As the points used tend to be farther away from the interpolation point, and the correlations r_{i0} tend to zero, the weights also tend to zero, and the interpolated value $Z_L^*(x,y)$ tends to the norm $f_L(x,y)$, whether or not the error term is present. However, if the interpolation is conducted among the values of the variables themselves, instead of among the deviations from the norm, this does not occur unless the algorithm is modified in a way that increases the error (Gandin, 1963, p. 89).

SOME INDEPENDENT TEST DATA

An abundance of ground-truth topographic data was obtained for Columbia Glacier by standard surveying methods (Mayo and others, 1979), and the data are useful for investigating the dependence on N, and for other purposes. Unfortunately, the ground-truth altitudes $Z(x,y,t_L+\Delta t)$ are for dates slightly different from the flight dates t_L, and the interpolation model obtains altitudes only for the flight dates. For use in comparing the interpolated values against them, the ground-truth altitudes are adjusted to the nearest flight dates; it is assumed that the time rate of change of the actual altitude at some point (x,y) is equal to the average time rate of change of the norm field there during the time interval between the two flight dates t_L and t_L' that bracket the date $t_L+\Delta t$ of the point to be adjusted. That is, the adjusted value is given by

$$Z'_L(x,y) = Z(x,y,t_L+\Delta t) - \Delta t \frac{f_L(x,y) - f_{L'}(x,y)}{t_L - t_{L'}}, \tag{31}$$

in which $L' = L + \Delta t/|\Delta t|$.

Many surface altitude points given by Mayo and others (1979) are for times close to one or another of the three flights 11, 15, and 17. Because of the practical difficulty created by the extreme roughness of the glacier surface, the observations are skewed spatially; within the combined region, they are concentrated primarily in the central basin and secondarily near the centerline in the lower reach (fig. 12). To relieve the skewness in the sample of observations selected to compare the interpolation algorithm against, central basin points were required to be nearer a flight date than were lower reach points. Another device used for improving the spatial uniformity of the sample was the averaging, of all three space coordinates, of observations lying within about 100 m of one another. To permit investigation of the effect of the number of points N used in the interpolation equations 30, only those ground-truth points were admitted to the sample that had at least 10 points among the IPP's within 1.0 km and 0.39 a. Table 8 gives the distribution, by Z and by Δt, of the 58-point sample selected; the greatest equation 31 adjustment was 0.8 m, and the root-mean-square value was 0.3 m.

The three flight-by-flight sections of the sample are highly similar in the distribution of their departures $Z'_L(x,y) - f_L(x,y)$ from the norm field. The mean departures for the three sections are, respectively, −2.7, −3.7, and −2.3 m; the median departures are −3.1, −4.0, and −2.1 m; and the departures are nearly uncorrelated with the altitude itself, the three r^2 values all being less than 0.04. The mean for the entire sample is −2.8 m, the median is −3.0 m, and 46 of the 58 departures are negative. A systematic discrepancy between the photogrammetric data and the surface-survey data may be the source of the predominant negativeness of the departures.

The error estimate E'_G obtained by comparing the adjusted ground-truth altitudes $Z'_L(x,y)$ and the altitudes $Z^*(x,y)$ interpolated by the algorithm is given by

$$E'_G = \sqrt{\frac{1}{58} \sum [Z_L^*(x,y) - Z'_L(x,y)]^2}, \tag{32}$$

in which the summation is over the 58 points in the ground-truth sample. It is compared in figure 13 with

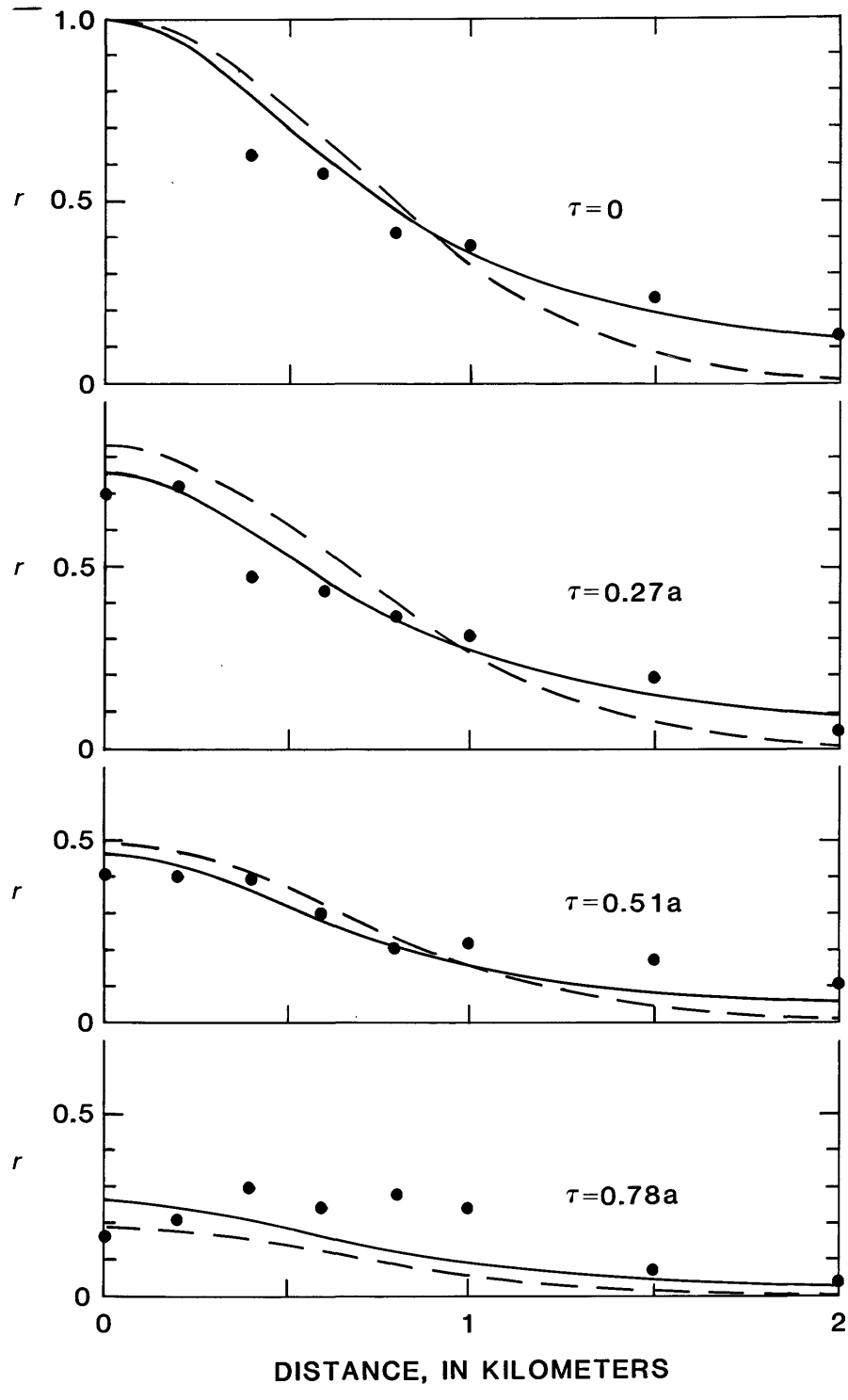

FIGURE 11.—Comparison of best fitting correlation function (eq. 18) with $\hat{\alpha}=2.79$, $\hat{\beta}=1.11$ (dashed line), best fitting correlation function (eq. 19) with $\alpha=0.470$, $\beta=0.755$ (solid line), and empirical $r^*(\tau,d)$ from table 7 (solid circles).

E_G as estimated by the algorithm (eq. 29). Each is shown as a function of N; for any N, the IPP's having the highest correlation with a particular point (x,y,t) through equation 19 are the ones used in estimating $Z^*(x,y,t)$. Because neither the variance V of the IPP's about the norm field nor their random error E_p is known, the sensitivity of both E_G and E'_G to these two quantities is also examined. The actual error E'_G depends only on

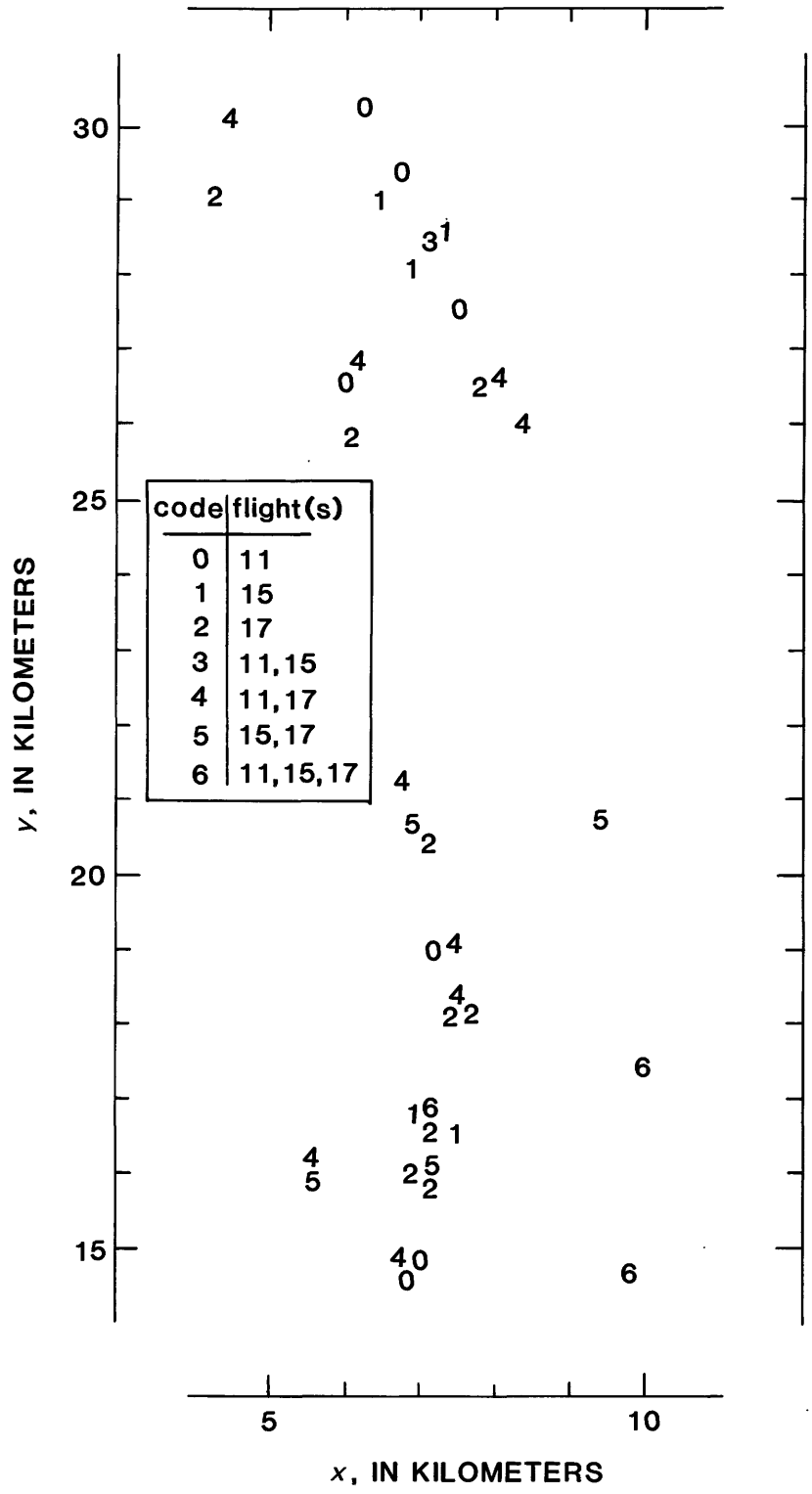

FIGURE 12.—Spatial distribution of individual and averaged points surveyed from the surface.

the ratio E_P^2/V because only that quantity appears in equation 30, from which the interpolating weights w_i are obtained. The estimated error E_G depends on each of them independently, on the ratio in equation 30 and on V alone in equation 29, and is much more sensitive to the values of these algorithm parameters than E'_G is.

In the special case in which the employed correlation function exactly describes the true statistical structure

TABLE 8.—*Distribution of 58-point surface-survey sample*

[The first number in each table entry is the number of single points, and second is the number of averaged points. The time difference between the surface survey and the flight date is Δt, in days]

Flight	Δt	Z-interval (m) 100-199	200-299	300-399	400-499	500-599
11	+4	3,0	--	--	--	--
	−2	--	--	--	--	6,1
	−4	--	1,0	--	2,0	--
	−5	2,0	2,1	--	--	--
	−8	1,0	--	--	--	--
15	−1	--	1,0	--	--	--
	−2	--	1,0	--	--	--
	−3	--	--	--	--	4,0
	−4	2,2	1,2	--	--	--
	−5	0,1	--	--	--	--
17	+8	5,5	4,1	--	--	--
	+7	--	1,2	--	--	--
	+6	--	--	--	1,1	--
	+5	--	--	--	--	2,3

of the variable being interpolated, and the observational error E_p and the variance V are both perfectly known, the interpolation error E_G is a nonincreasing function of the number N of data points used in equations 23 and 28. None of these ideals is fulfilled by the Columbia Glacier photogrammetric data. Belousov and others (1968, p. 92) found that for interpolating the geopotential height of an isobaric surface in the atmosphere, N should be 5 or 6 for dense distributions of points and might be increased "to 7 or 8, but no more" for sparse distributions.

If a systematic error δZ in the photogrammetric data is assumed to contribute to the discrepancy between the two sets of data, and if it were to be subtracted out, then the interpolated values would be adjusted to $Z^*_L(x,y)-\delta Z$, the estimated error E_G would be unaffected, and the sample error would become, for some particular N,

$$[E'_G(\delta Z)]^2=[E'_G(0)]^2+(\delta Z)^2-\frac{2\delta Z}{58}\sum[Z^*_L(x,y)-Z'_L(x,y)] \quad . \quad (33)$$

This adjusted error is shown as a function of N in figure 14 for selected δZ, using $V=E_p^2=12$ m^2.

The $Z'_L(x,y)$ themselves are subject to two sources of error, the surveying itself and the equation 31 adjustment to the flight dates. If the mean square error for these two sources combined is taken to be 1 m^2, then the corrected error, for some N and some δZ, is

$$(E''_G)^2=(E'_G)^2-1 \quad . \quad (34)$$

This is also shown as a function of N in figure 14 for the $\delta Z=0$ case.

THE RESULTS

The optimum interpolation results for flights 3-29 appear in appendix B. The interpolated altitude $Z^*_L(x,y)$ is given to the nearest tenth of a meter, and the estimated error $<E_G>+1$ is given in meters. Although the number of tenths of a meter in $Z^*_L(x,y)$ is not a significant figure, dropping it would lead to an unacceptably large rounding error in forming the average time rate of change of surface altitude between flights, especially for short interflight intervals. Also given in appendix B are the digitization interpolation results for flights 2 and 30, and the estimated digitization error E_I (eq. 4, table 2) is rounded up to the next whole meter: $<E_I>+1=3$ m.

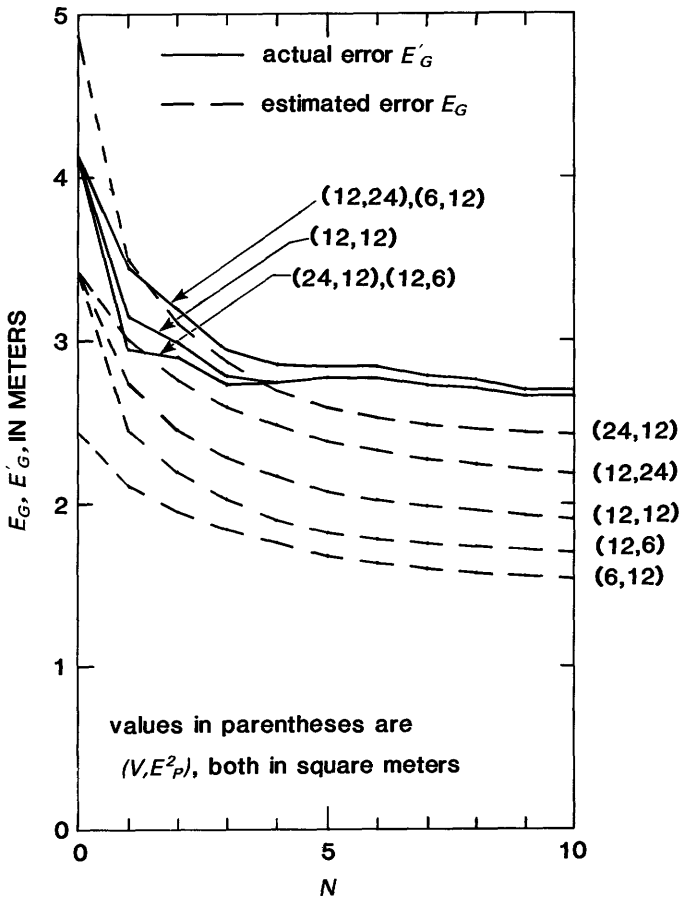

FIGURE 13.—Error E_G estimated by the algorithm (dashed line) and actual error E'_G (solid line) between algorithm results and altitudes surveyed from the glacier surface, as functions of the number N of individual photogrammetric points (IPP's) used for interpolating at any particular point. The sensitivity of these two quantities to the variance V of the IPP's about the norm field and to the inherent IPP altitude error E_p^2 is included for various postulated values for those two parameters. The actual error E'_G depends only on the ratio E_p^2/V because only that quantity appears in equation 30, from which the interpolating weights are obtained. The estimated error E_G depends on each of the two parameters separately, on the ratio in equation 30 and on V alone in equation 29. Although continuous curves are shown for clarity, the quantities exist only for integer N.

Altitudes are interpolated only for the flight dates t_L and only on those nodes (I,J) of the 762.5-meter data grid, on which velocities are given in Fountain (1982), that are common to the domain of the digitizations of the two maps. The (x,y) coordinates of the IPP's are related to these grid coordinates and to the Universal Transverse Mercator (UTM) System according to

$$\begin{pmatrix} I \\ J \end{pmatrix} = \frac{1}{762.5} \begin{vmatrix} 65{,}648-y \\ 10{,}458+x \end{vmatrix} \tag{35}$$

and

$$\begin{pmatrix} x \\ y \end{pmatrix} = \frac{1}{0.9996} \begin{vmatrix} \text{UTM Easting}-490{,}000 \\ \text{UTM Northing}-6{,}750{,}000 \end{vmatrix} . \tag{36}$$

Because the photogrammetric coverage of flights 3-8 was of only the lower part of the lower reach, the correlation study was conducted only for flights 9-30; however, the algorithm based on flights 9-30 was also applied to flights 3-8, but only in the vicinity of the photogrammetric coverage.

Because it is so restricted spatially and temporally, the ground-truth sample probably provides a good estimate of neither the systematic error in the photogrammetric data nor the actual error E_G in the interpolation algorithm. Moreover, the error E_G is only estimated by the algorithm; the correlation function, the variance about the norm, and the random error are all imperfectly known. Of several possible ways of reconciling the apparent difference between E_G and E'_G, increasing the estimate of E_G is probably the safest. The evidence from the ground-truth sample is too weak to justify instituting a systematic δZ adjustment of the photogrammetric data, and it is too strong to ignore. As the uncertainties in the interpolation model tend to cause E_G to be underestimated, and as the scale of errors does not warrant reporting it more precisely than in whole meters, simply rounding up each estimate to the next greater integer number of meters is consistent with both these considerations. The 58-point root-mean-square of these rounded-up values is shown in figure 15 as the curve labeled $< E_G > +1$; for comparison, it shows the E_G curve from figure 13 for $V=E_p^2=12$ m^2, and it shows the E''_G curve from figure 14 for $\delta Z=0$.

All three curves in figure 15 are decreasing functions of N for $0 \le N \le 9$. So also is the fraction $\lambda(N)$ of the N selected interpolating points that are from the same flight as the point being interpolated (fig. 16); it is also obtained from the ground-truth sample, in which flights 9-12 were used for interpolating for flight 11, flights 13-17 for flight 15, and flights 14-19 for flight 17. The advantage of a small $\lambda(N)$ is the heightened flight-to-flight influence on the interpolation; if each flight's data were interpolated independently, the inferred surface topography would have an erratic time variability.

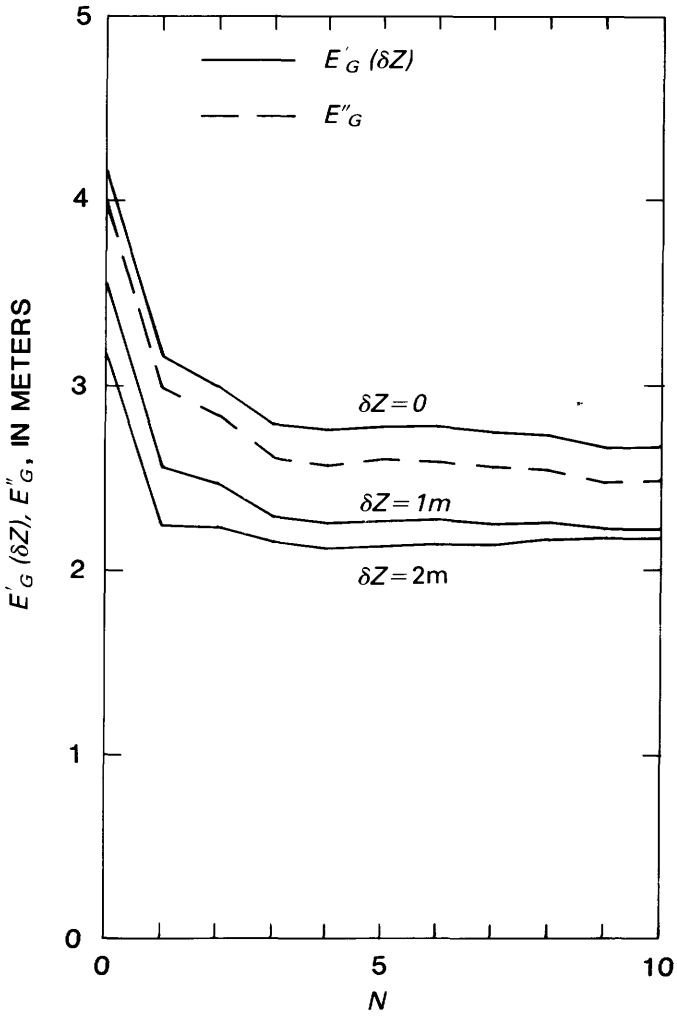

FIGURE 14.—Effect, on actual error E'_G between algorithm results and altitudes surveyed from the surface, of some postulated values of the possible systematic error δZ in the photogrammetry data (solid line). Also shown is the adjusted error E''_G obtained by taking $\delta Z=0$ but assuming a 1-square-meter mean square error for the combined effect of surveying error and error in the equation 31 adjustment to the flight dates (dashed line). Although continuous curves are shown for clarity, the quantities exist only for integer values of the number N of individual photogrammetric points used by the algorithm for interpolating at any particular point.

Finally, the algorithm (eq. 22, 23, 30) is used with both the variance V and mean-square random error E_p^2 taken to be 12 m^2. It is applied to the $N \le 10$ IPP's having the N highest correlations with the point being interpolated, provided they are all within a distance $d \le 1.0$ km and time difference $\tau \le 0.39$ a of that point. Equation 19, with $\alpha=0.470$ a and $\beta=0.755$ km, is used to approximate those correlations, as well as the correlations between the N points themselves. The estimated error E_G is obtained from equation 29 and is reported as

the next greater integer $<E_G>+1$. If no IPP meets the d and τ conditions, then the norm $f_L(x,y)$ is used as the interpolated altitude, and the error is taken to be $<\sqrt{V}>+1=4$ m.

The algorithm-estimated error E_G, through equations 19 and 29, is a decreasing function of the (x,y,t) density of the IPP's. The root-mean-square of the rounded value $<E_G>+1$, when averaged over the 154 interpolated points, rises from about 2.5 m for the early, 190-IPP flights to about 3.1 m for the late, 120-IPP flights. It also rises, secondarily, during periods of long interflight time intervals and falls during periods of short ones. The time-density dependence is weaker than the space-density dependence; when the interflight interval is large, there are still many $\tau=0$ IPP's from the flight of the date for which points are interpolated.

DISCUSSION

No analysis of the interpolated topography is contained in this report. The altitudes are given to one more decimal place (tenths of a meter) than is significant as altitude explicitly. The additional decimal place is included because the data implicitly contain information on the altitude change rate, which has profound dynamic significance. Rounding the interpolated altitudes to the nearest whole meter would seriously degrade this implicit information.

Minor details in each of the two maps may be overrepresented in the interpolations. The actual surface topography $Z(x,y,t)$ may have short-lived, perhaps fast-moving, small-scale features. If so, one of these features present at the time of one or another of the maps will be projected through the time interval, in the same location but with diminishing intensity, to the time of the other map. The norm fields $f_L(x,y)$, which constitute the basis of the interpolation, are linear combinations of the two maps, but the pattern of map-to-map altitude changes (fig. 5) exhibits little congruence between the minor details of the two maps. For any particular flight date, this effect is neutralized, partially, by the interpolation among the IPP deviations from the norm field. Because the results include values interpolated only on the 762.5-meter grid, this overemphasis is tolerable; however, if maps were to be prepared for the intermediate flight dates, or if the interpolation were conducted on a fine grid, the fictional replication of these ephemeral minor details would not be tolerable. The number of points interpolated on the grid nodes is roughly the same as the number of IPP's.

The correlation function $R(\tau,d)$ does not fit the empirical $r^*(\tau,d)$ exactly, and the ideals of homogeneity and isotropy are fulfilled only approximately. These imperfections affect the results, ultimately, as irregularities

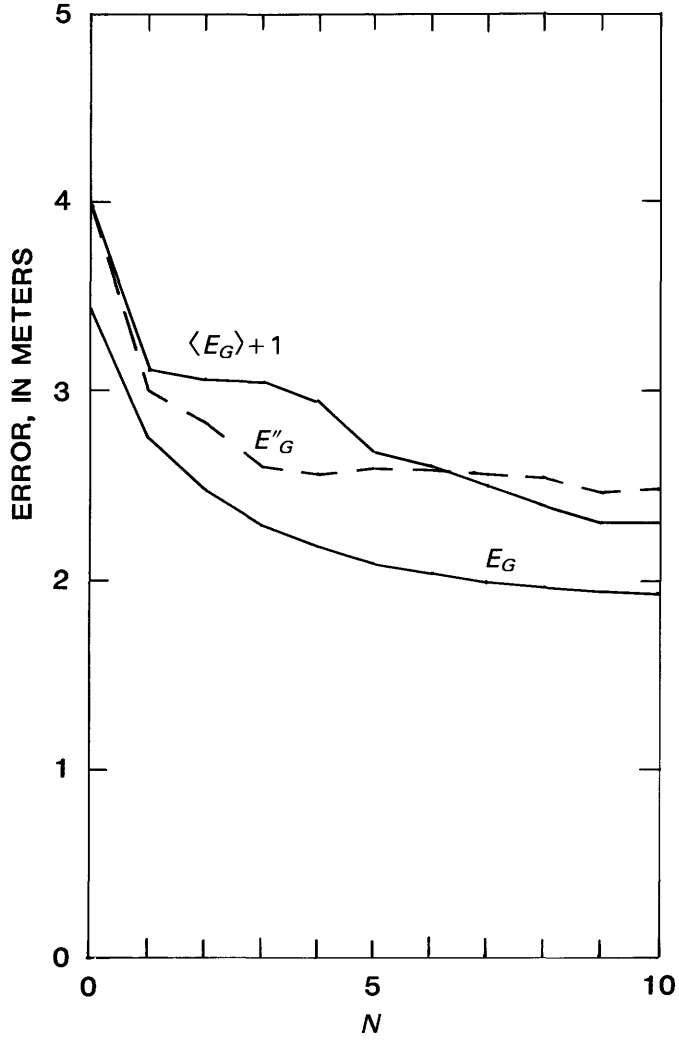

FIGURE 15.—Error E_G estimated by the algorithm using $V=E_p^2=$ 12 m² from figure 13, the error E''_G from figure 14, and the error $\langle E_G\rangle+1$ formed as the root-mean-square of the algorithm-estimated errors for individual points being rounded up to the next whole number of meters. Although continuous curves are shown for clarity, the quantities exist for only integer values of the number N of individual photogrammetric points used by the algorithm for interpolating at any particular point.

in the weights w_i. Generally, unless the data density is very low, slight irregularities in the weights produce only a slight increase in the actual interpolation error (Gandin, 1963, p. 67). The good fit of the norm fields to the IPP's, without any interpolation among the residuals, would itself yield glaciologically usable data; the error for the ground-truth sample was $E'_G=4.15$ m when only the norm field ($N=0$) was used.

Probably the most surprising result is that the radial symmetry of the empirical correlation function is independent of the glacier flow (eq. 13, 14; fig. 10); that is, for finite time lag τ, the correlation is still isotropic. Perhaps the high ratio of seasonal variation to long-term trend (fig. 8) masks the effect of kinematic waves

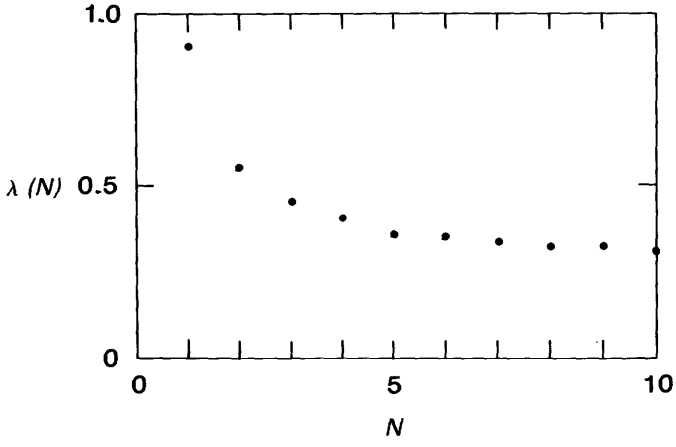

FIGURE 16.—Fraction $\lambda(N)$ of the number N of individual photogrammetric points used for interpolating that are from the same flight as the point being interpolated. These results are from the 58-point sample of individual and averaged points surveyed from the glacier surface.

on the correlation statistics, or perhaps none were present. The space-time variation of surface velocity (Meier and others, 1984) has this same synchronous behavior over the same domain, except for very near the calving terminus.

APPLICATION TO FUTURE WORK

A few conclusions can be drawn regarding design of data-collection programs. If flight-to-flight average velocities are required, the flight frequency is bounded by the persistence of identifiable natural features, such as crevasse patterns or other surface figuring. Because the interpolation error rises gently as the IPP density declines, the volume of photogrammetric processing for any particular flight could probably be reduced, so long as the coverage is complete.

Although altitudes are interpolated here only for the dates of the photo flights, it is not because IPP's must be available for the same time as the time coordinate of the point being interpolated; obtaining the correlation values for equation 30 from equation 19 does not depend on any of the time lags being zero. Instead, it is because the flight dates themselves give a reasonably rich time distributon of values, and because the method of equations 15 and 16 can be used only for the flight dates. However, the time variation (fig. 17) of the coefficients $(a_L, b_L)_{ALL}$ of table 6 is reasonably well behaved, so that norm fields for times between the flight dates could be obtained by performing (yet another) preliminary interpolation to get $a(t)$, $b(t)$ for some arbitrary time.

Moreover, if the photogrammetric processing of flights later than September 1, 1981, is used for producing only IPP's instead of a later map, equations 15 and 16 could obtain norm fields for those flight dates as extrapolation outside the time interval of the two existing maps. As in interpolating between flight dates, the algorithm (eq. 22, 23, 30) would then proceed as usual, once a norm field is obtained. The suitability of such extrapolated norm fields would not have to be established independently; as long as the equation 16 error E^2_f remained reasonably low, the norm field could be confidently accepted as the basis of the interpolation.

Good ground truth is essential to determining absolute altitude. However, if there were a systematic error, constant in x and y, and if the bed topography were inferred from the same data set, then the dynamic variables—velocity, glacier thickness, and surface slope—would be unaffected by this error. For a calving glacier, though, accurate absolute altitudes would be necessary to represent the terminus physics properly.

For use in dynamic models, the altitude errors are probably less significant than the spatial and temporal variations in the crevasse pattern and in the density of the snow and firn layers. In determining the normal stress at a point on the glacier bed, some account must be taken of the compactness and density of the overlying material. Perhaps a mass-equivalent topography could be employed, so that the thickness times a constant modeling density would equal the actual thickness-compactness-density integral. Whereas this topography might properly represent the distribution of the normal stress, along with its gradient, it probably would not properly represent the distribution of the shear stress. However, if this concept is furthered, it may be profitable to consider a "dynamically equivalent topography" to which the flow law, including an explicit representation of longitudinal stress, could be applied exactly by using local derivatives, thus avoiding the need for a slope-averaging artifice. It is not obvious how to do slope averaging in a domain with two horizontal space dimensions, but the exact application of such a flow law has been successful in time-dependent, two-dimensional modeling (Rasmussen and Campbell, 1973) of a synthetic data set.

The altitudes interpolated here are accompanied by an error estimate. If fields of other variables (velocity, bed topography, mass balance, and thickness change) were similarly prepared, it may be possible to construct a data set that is consistent through the dynamic equations, for some reasonable choice of values for the flow-law parameters, and that is faithful, within the error bounds, to the field data. Two partial solutions of this problem have already been achieved: Sikonia (1982, written commun.) obtained a two-dimensional data set that is consistent through the continuity equation, and Bindschadler and Rasmussen (1983) obtained a one-dimensional data set that is consistent through both the continuity equation and the flow law.

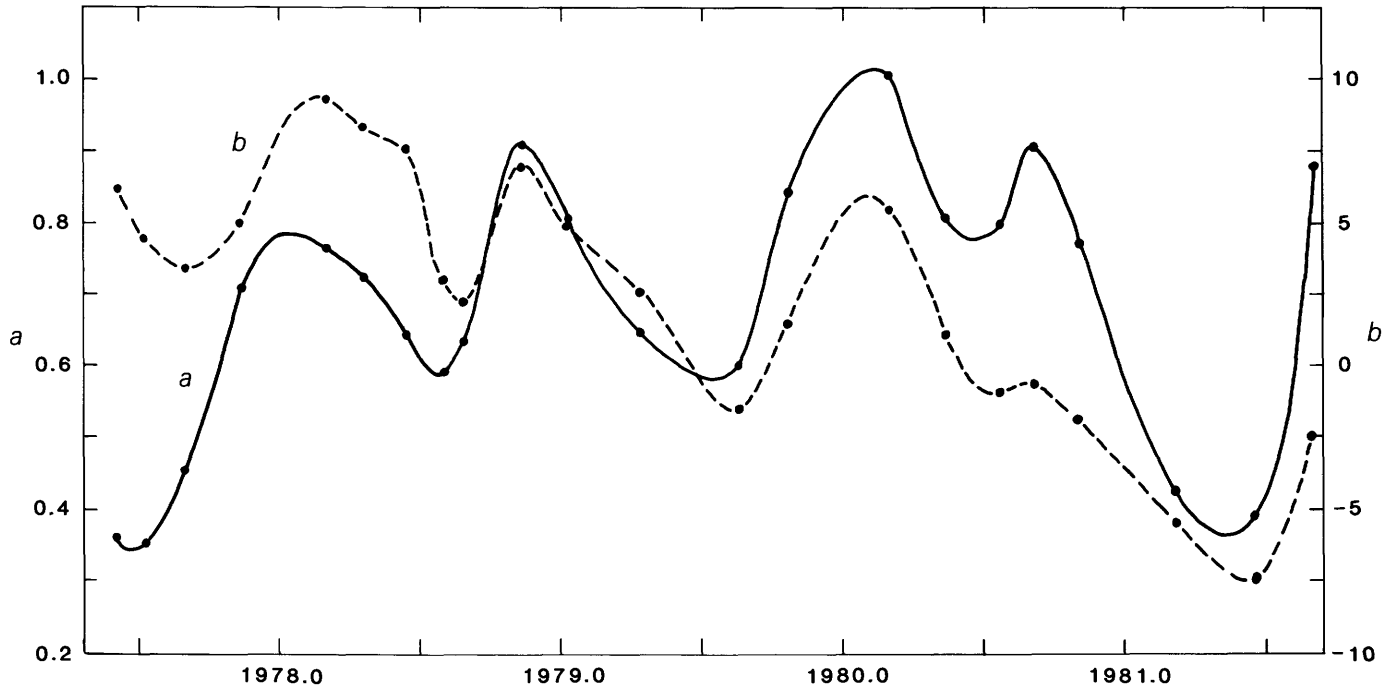

FIGURE 17.—Linear combination coefficients $(a_L, b_L)_{ALL}$ from table 6 for forming the norm fields $f_L(x,y)$. They are connected by smooth curves (solid line for a, dashed line for b) to indicate that the coefficients may be well enough behaved in time to permit interpolating between flight dates, first for the norm field $f(x,y,t)$ and then for surface altitudes $Z^*(x,y,t)$.

REFERENCES CITED

Belousov, S. L., Gandin, L. S., and Mashkovich, S. A., 1968, Computer processing of meteorological data: Leningrad, Hydrometeorological Publishing House. [English translation, Israel Program for Scientific Translations, Jerusalem, 1971.]

Bindschadler, R. A., and Rasmussen, L. A., 1983, Finite difference model predictions of the drastic retreat of Columbia Glacier, Alaska: U.S. Geological Survey Professional Paper 1258-D, 17 p.

Brown, C. S., Meier, M. F., and Post, Austin, 1982, Calving speed of Alaska tidewater glaciers, with application to Columbia Glacier: U.S. Geological Survey Professional Paper 1258-C, 13 p.

Creutin, J. D., and Obled, C., 1982, Objective analysis and mapping techniques for rainfall fields: an objective comparison: Water Resources Research, v. 18, no. 2, p. 413-431.

Dwight, H. B., 1961, Tables of integrals and other mathematical data: New York, Macmillan, 336 p.

Fountain, A. G., 1982, Columbia Glacier photogrammetric altitude and velocity: data set (1957-1981): U.S. Geological Survey Open-File Report 82-756, 225 p.

Gandin, L. S., 1963, The objective analysis of meteorological fields: Leningrad, Hydrometeorological Publishing House. [English translation, Israel Program for Scientific Translations, Jerusalem, 1965.]

Kollmeyer, R. C., Motherway, D. L., Robe, R. Q., Platz, B. W. and Shah, A. M., 1977, A design feasibility study for the containment of icebergs within the waters of columbia Bay, Alaska: U.S. Coast Guard Final Report 128, 135 p.

Mayo, L. R., Trabant, D. C., March, Rod, and Haeberli, Wilfried, 1979, Columbia Glacier stake location, mass balance, glacier surface altitude, and ice radar data, 1978 measurement year: U.S. Geological Survey Open-File Report 79-1168. 72 p.

Meier, M. F., Post, Austin, Brown, C. S., Frank, David, Hodge, S. M., Mayo, L. R., Rasmussen, L. A., Senear, E. A., Sikonia, W. G., Trabant, D. C., and Watts, R. D., 1978, Columbia Glacier progress report—December 1977: U.S. Geological Survey Open-File Report 78-264, 78 p.

Meier, M. F., Rasmussen, L. A., Post, Austin, Brown, C. S., Sikonia, W. G., Bindschadler, R. A., Mayo, L. R., and Trabant, D. C., 1980, Predicted timing of the disintergration of the lower reach of the Columbia Glacier Alaska: U.S. Geological Survey Open-File Report 80-582, 47 p.

Meier, M. F., Rasmussen, L. A., Krimmel, R. M., Olsen, R. W., and Frank, David, 1984, Photogrammetric determination of surface altitude, terminus position, and ice velocity of Columbia Glacier, Alaska: U.S. Geological Survey Professional Paper 1258-F (in press).

Oberhettinger, Fritz, 1973, Fourier transforms of distributions and their inverses: New York, Academic Press, 167 p.

Post, Austin, 1975, Preliminary hydrography and historic terminal changes of Columbia Glacier, Alaska: U.S. Geological Survey Hydrologic Investigations Atlas 599, 3 sheets.

Rasmussen, L. A., and Campbell, W. J., 1973, Comparison of three contemporary flow laws in a three-dimensional, time-dependent glacier model: Journal of Glaciology, v. 12, no. 66, p. 361-373.

Rasmussen, L. A., and Meier, M. F., 1982, Continuity equation model of the drastic retreat of Columbia Glacier, Alaska: U.S. Geological Survey Professional Paper 1258-A, 23 p.

Sikonia, W. G., 1982, Finite-element glacier dynamics model applied to Columbia Glacier, Alaska: U.S. Geological Survey Professional Paper 1258-B, 74 p.

Sikonia, W. G., and Post, Austin, 1980, Columbia Glacier, Alaska: recent ice loss and its relationship to seasonal terminal embayments, thinning, and glacier flow: U.S. Geological Survey Hydrologic Investigations Atlas 619, 3 sheets.

Thiebaux, H. J., 1975, Experiments with correlation representations for objective analysis: Monthly Weather Review, v. 103, p. 617-627.

APPENDIXES A, B

APPENDIX A: FOURIER TRANSFORM OF THE CORRELATION FUNCTION

The Fourier transform,

$$\Phi(\phi_1,\phi_2,\phi_3)=\int_{-\infty}^{\infty}\int_{-\infty}^{\infty}\int_{-\infty}^{\infty}\left(\frac{\alpha^2}{\alpha^2+\tau^2}\right)\left(\frac{\beta^2}{\beta^2+x^2+y^2}\right)e^{i(\phi_1\tau+\phi_2 x+\phi_3 y)}dxdyd\tau\ , \quad \text{(A-1)}$$

is required to be positive for all values $\phi_j>0$ for $j=1, 2, 3$. Because, by using Euler's formula, the exponential may be written as

$$e^{i(\phi_1\tau+\phi_2 x+\phi_3 y)}=[\cos\phi_1\tau+i\sin\phi_1\tau]\,[\cos(\phi_2 x+\phi_3 y)+i\sin(\phi_2 x+\phi_3 y)]\ , \quad \text{(A-2)}$$

and because the coordinates τ, x, and y are independent of each other, equation A-1 may be written

$$\Phi(\phi_1,\phi_2,\phi_3)=\Phi_\alpha(\phi_1)\cdot\Phi_\beta(\phi_2,\phi_3)\ , \quad \text{(A-3)}$$

where

$$\Phi_\alpha(\phi_1)=\alpha^2\int_{-\infty}^{\infty}\frac{\cos\phi_1\tau+i\sin\phi_1\tau}{\alpha^2+\tau^2}\,d\tau \quad \text{(A-4)}$$

and

$$\Phi_\beta(\phi_2,\phi_3)=\beta^2\int_{-\infty}^{\infty}\int_{-\infty}^{\infty}\frac{\cos(\phi_2 x+\phi_3 y)+i\sin(\phi_2 x+\phi_3 y)}{\beta^2+x^2+y^2}\,dxdy. \quad \text{(A-5)}$$

In equation A-4, because the denominator is an even function of τ and $\sin\phi_1\tau$ is an odd function of τ, the imaginary part vanishes; and, because $\cos\phi_1\tau$ is also an even function of τ, the real part is (Dwight, 1961, formula 859.001)

$$\Phi_\alpha(\phi_1)=2\alpha^2\int_0^{\infty}\frac{\cos\phi_1\tau}{\alpha^2+\tau^2}\,d\tau=\pi\alpha e^{-\phi_1\alpha}\ . \quad \text{(A-6)}$$

Similarly, in equation A-5, the imaginary part vanishes, and the real part may be written as

$$\Phi_\beta(\phi_2,\phi_3)=4\beta^2\int_0^{\infty}\int_0^{\infty}\frac{\cos(\phi_2 x+\phi_3 y)}{\beta^2+x^2+y^2}\,dxdy \quad \text{(A-7)}$$

and depends only on the quantity $\phi_{2,3}^2=(\phi_2^2+\phi_3^2)$, which is generalized by setting $\phi_2=\phi_{2,3}\cos\Psi$ and $\phi_3=\phi_{2,3}\sin\Psi$:

$$\Phi_\beta(\phi_2,\phi_3)=4\beta^2\int_0^{\infty}\int_0^{\infty}\frac{\cos[\phi_{2,3}(x\cos\Psi+y\sin\Psi)]}{\beta^2+x^2+y^2}\,dxdy \quad \text{(A-8)}$$

If the substitutions are made,

$$\begin{pmatrix}\bar{x}\\ \bar{y}\end{pmatrix}=\begin{pmatrix}\cos\Psi & \sin\Psi\\ -\sin\Psi & \cos\Psi\end{pmatrix}\begin{pmatrix}x\\ y\end{pmatrix}, \quad \text{(A-9)}$$

from which $\bar{x}^2+\bar{y}^2=x^2+y^2$ and $d\bar{x}d\bar{y}=dxdy$, equation A-8 becomes (Dwight, 1961, formulas 120.01, 859.041):

$$\Phi_\beta(\phi_2,\phi_3)=4\beta^2\int_0^{\infty}\int_0^{\infty}\frac{\cos(\phi_{2,3}\bar{x})}{\beta^2+\bar{x}^2+\bar{y}^2}\,d\bar{y}d\bar{x}$$

$$=4\beta^2\int_0^{\infty}\cos(\phi_{2,3}\bar{x})\left[\frac{1}{\sqrt{\beta^2+\bar{x}^2}}\tan^{-1}\left(\frac{\bar{y}}{\sqrt{\beta^2+\bar{x}^2}}\right)\right]_0^{\infty}d\bar{x}$$

$$=2\pi\beta^2\int_0^{\infty}\frac{\cos(\phi_{2,3}\bar{x})}{\sqrt{\beta^2+\bar{x}^2}}\,d\bar{x}=2\pi\beta^2 K_0(\beta\phi_{2,3})\,, \quad \text{(A-10)}$$

where K_0 is the zero-order modified Bessel function of the second kind, which is a positive function ranging from $+\infty$ for zero argument toward zero for large argument.

Finally, combining equations A-3, A-6, and A-10,

$$\Phi(\phi_1,\phi_2,\phi_3)=2\pi^2\alpha\beta^2 e^{-\phi_1\alpha}K_0(\beta\sqrt{\phi_2^2+\phi_3^2})\ , \quad \text{(A-11)}$$

which is positive for all values of the ϕ_j.

APPENDIX B: COLUMBIA GLACIER SURFACE ALTITUDES

Given in the following grids are results for flights 2 through 30 (table 1). For flights 3 through 29 the altitudes are the results of optimum interpolation, but for flights 2 and 30 they are from the digitizations of the topographic maps for the dates of those two flights. The first figure given is altitude, in meters above sea level (Z_L^* in the case of interpolated altitudes); the figure after the solidus (/) is the estimated error, in meters ($<E_G+1>$ in the case of interpolated altitudes). The column numbers (J) of the 762.5-meter data grid are given across the top of the array of altitudes, and the row numbers (I) are given at the left.

Flight 2, July 27, 1974 (1974.568)

	19	20	21	22	23	24	25	26	27
47	532.2/3	527.4/3	529.3/3	551.5/3	569.8/3	565.6/3	561.7/3	0/0	0/0
48	531.0/3	521.9/3	525.0/3	540.2/3	556.4/3	543.5/3	533.5/3	0/0	0/0
49	529.8/3	512.1/3	511.4/3	525.9/3	526.3/3	524.2/3	527.6/3	0/0	0/0
50	515.5/3	492.6/3	493.5/3	499.9/3	513.6/3	527.1/3	532.7/3	0/0	0/0
51	503.3/3	494.4/3	486.0/3	496.3/3	531.1/3	538.3/3	537.2/3	0/0	0/0
52	481.0/3	485.9/3	480.1/3	483.7/3	495.7/3	522.6/3	533.8/3	0/0	0/0
53	483.6/3	473.5/3	463.6/3	437.1/3	404.3/3	0/0	0/0	0/0	0/0
54	0/0	377.0/3	404.3/3	412.6/3	394.5/3	383.6/3	0/0	0/0	0/0
55	343.1/3	358.9/3	388.2/3	406.8/3	401.7/3	379.0/3	0/0	0/0	0/0
56	341.0/3	360.0/3	376.6/3	385.7/3	374.3/3	343.6/3	0/0	0/0	0/0
57	330.4/3	341.2/3	350.2/3	323.9/3	308.2/3	299.0/3	285.0/3	0/0	0/0
58	322.6/3	334.0/3	333.8/3	322.6/3	300.3/3	296.6/3	292.0/3	0/0	0/0
59	299.7/3	309.3/3	302.5/3	297.0/3	288.0/3	288.2/3	271.7/3	244.6/3	209.0/3
60	278.0/3	288.5/3	293.3/3	271.4/3	270.6/3	282.6/3	256.8/3	249.1/3	231.2/3
61	0/0	256.8/3	267.9/3	258.5/3	271.0/3	273.3/3	246.6/3	234.7/3	0/0
62	0/0	0/0	255.5/3	258.0/3	254.9/3	250.2/3	240.9/3	224.1/3	0/0
63	0/0	210.5/3	235.7/3	249.5/3	237.6/3	236.4/3	232.2/3	216.4/3	188.4/3
64	0/0	202.9/3	218.3/3	209.6/3	212.6/3	226.6/3	215.9/3	197.1/3	173.0/3
65	0/0	0/0	192.3/3	192.8/3	204.5/3	216.8/3	206.2/3	192.9/3	169.9/3
66	0/0	0/0	176.6/3	185.8/3	192.7/3	183.6/3	184.8/3	171.2/3	154.3/3
67	0/0	0/0	139.3/3	181.1/3	178.2/3	167.4/3	170.9/3	165.0/3	122.5/3
68	0/0	0/0	0/0	135.7/3	146.8/3	140.2/3	142.5/3	132.9/3	91.8/3
69	0/0	0/0	0/0	136.7/3	133.5/3	0/0	0/0	0/0	0/0

Flight 3, July 24, 1976 (1976.561)

	19	20	21	22	23	24	25	26	27
61	0/0	253.7/3	263.4/2	254.1/2	267.9/3	270.2/4	243.2/4	232.4/4	0/0
62	0/0	0/0	254.7/2	255.5/2	253.2/2	248.6/2	238.3/3	222.2/4	0/0
63	0/0	207.0/2	234.9/2	248.4/2	233.7/2	232.2/2	229.9/2	216.4/3	186.0/4
64	0/0	204.2/2	217.2/2	205.5/2	209.4/2	224.4/2	215.3/2	198.2/2	172.3/3
65	0/0	0/0	190.3/2	188.7/2	199.4/2	213.3/2	202.4/2	192.6/2	168.2/3
66	0/0	0/0	173.9/2	179.4/2	184.3/2	177.9/2	178.7/2	169.9/2	149.9/4
67	0/0	0/0	128.8/2	172.8/2	168.4/2	161.8/2	159.9/2	159.5/2	118.3/4
68	0/0	0/0	0/0	122.4/2	137.9/2	131.8/2	131.7/2	123.3/2	81.1/4
69	0/0	0/0	0/0	119.1/3	114.2/3	0/0	0/0	0/0	0/0

Flight 4, October 1, 1976 (1976.750)

	19	20	21	22	23	24	25	26	27
61	0/0	248.1/4	257.8/2	248.8/2	262.1/3	263.9/3	237.5/4	227.8/4	0/0
62	0/0	0/0	249.1/2	249.7/2	246.8/2	242.4/2	232.3/3	217.2/3	0/0
63	0/0	202.8/2	229.4/2	242.4/2	228.4/2	226.3/2	223.5/2	210.8/2	180.1/4
64	0/0	201.5/2	211.6/2	198.5/2	205.3/2	219.5/2	209.7/2	192.4/2	166.8/3
65	0/0	0/0	184.4/2	182.0/2	192.9/2	206.7/2	196.5/2	186.3/2	161.8/3
66	0/0	0/0	169.0/2	170.4/2	176.0/2	172.8/2	172.5/2	164.6/2	142.8/4
67	0/0	0/0	124.1/2	164.8/2	156.3/2	156.2/2	153.7/2	154.4/2	112.5/4
68	0/0	0/0	0/0	113.8/2	126.5/2	126.1/2	126.6/2	115.9/2	71.2/4
69	0/0	0/0	0/0	108.0/2	97.7/2	0/0	0/0	0/0	0/0

Flight 5, November 17, 1976 (1976.879)

	19	20	21	22	23	24	25	26	27
64	0/0	199.2/3	207.5/3	194.0/3	203.9/2	217.2/2	205.7/3	188.4/3	163.1/4
65	0/0	0/0	180.1/3	178.1/3	189.3/2	202.0/2	193.0/3	182.0/3	157.5/4
66	0/0	0/0	166.4/2	166.5/2	170.2/2	169.4/2	168.7/3	160.2/3	138.2/4
67	0/0	0/0	122.2/2	159.9/2	150.4/2	153.4/2	150.0/3	151.0/3	108.7/4
68	0/0	0/0	0/0	109.6/2	122.5/2	122.8/2	124.1/2	111.7/3	65.3/4
69	0/0	0/0	0/0	101.7/2	89.0/2	0/0	0/0	0/0	0/0

Flight 6, January 19, 1977 (1977.051)

	19	20	21	22	23	24	25	26	27
64	0/0	197.2/3	208.3/3	195.3/3	202.6/2	216.6/3	203.9/3	188.2/3	163.2/4
65	0/0	0/0	181.1/3	178.1/3	189.1/2	200.9/3	192.7/3	182.4/3	157.1/3
66	0/0	0/0	166.9/3	169.5/3	172.6/2	168.9/3	168.4/3	159.9/3	138.8/3
67	0/0	0/0	124.3/2	163.3/2	153.1/2	153.0/2	152.6/3	150.9/3	107.5/3
68	0/0	0/0	0/0	113.9/2	126.3/2	125.6/2	127.4/2	116.2/3	67.7/4
69	0/0	0/0	0/0	109.2/2	98.9/2	0/0	0/0	0/0	0/0

Flight 7, March 7, 1977 (1977.180)

	19	20	21	22	23	24	25	26	27
64	0/0	197.9/3	207.7/3	193.8/3	202.4/2	216.4/2	203.7/3	189.3/3	164.5/3
65	0/0	0/0	180.2/3	177.0/3	189.0/2	201.6/2	193.9/3	182.3/3	156.7/3
66	0/0	0/0	167.7/3	168.4/3	172.5/2	170.9/3	169.5/3	158.3/3	138.2/3
67	0/0	0/0	124.7/2	163.4/2	154.3/2	154.8/2	153.7/3	150.3/3	106.5/3
68	0/0	0/0	0/0	113.2/2	129.1/2	122.5/2	124.7/2	113.2/3	65.8/3
69	0/0	0/0	0/0	117.9/2	102.8/2	0/0	0/0	0/0	0/0

Flight 8, April 23, 1977 (1977.309)

	19	20	21	22	23	24	25	26	27
64	0/0	203.1/3	213.9/3	198.9/3	205.9/2	220.5/2	208.9/3	195.6/3	170.7/3
65	0/0	0/0	185.2/3	182.5/3	193.4/2	207.8/2	199.0/3	188.4/3	162.1/3
66	0/0	0/0	172.9/2	173.0/2	179.3/2	176.7/2	174.5/3	164.1/3	143.9/3
67	0/0	0/0	130.7/2	169.1/2	162.0/2	160.5/2	160.1/3	155.9/3	111.6/3
68	0/0	0/0	0/0	119.8/2	136.2/2	127.3/2	127.8/2	118.3/3	71.6/3
69	0/0	0/0	0/0	126.5/2	111.8/2	0/0	0/0	0/0	0/0

Flight 9, June 2, 1977 (1977.418)

	19	20	21	22	23	24	25	26	27
47	536.0/3	530.3/2	530.5/2	554.0/2	572.9/2	568.0/3	565.0/4	0/0	0/0
48	533.5/3	525.0/3	525.0/2	541.1/2	559.5/2	544.7/3	535.4/3	0/0	0/0
49	531.7/2	513.2/2	510.5/2	526.6/2	528.1/3	527.4/3	531.0/3	0/0	0/0
50	514.7/2	490.8/3	490.5/3	499.9/3	515.0/3	529.8/3	535.9/3	0/0	0/0
51	500.6/3	491.7/3	482.8/3	494.3/2	532.8/3	540.7/3	538.7/3	0/0	0/0
52	477.2/3	484.2/2	477.4/2	480.9/3	494.6/2	524.5/3	537.6/3	0/0	0/0
53	484.9/2	473.8/2	462.9/2	434.5/2	406.3/2	0/0	0/0	0/0	0/0
54	0/0	379.2/2	405.4/2	410.6/2	394.1/3	381.3/3	0/0	0/0	0/0
55	340.4/3	359.4/3	390.1/2	406.9/2	398.8/2	375.2/3	0/0	0/0	0/0
56	335.9/3	357.1/3	376.6/2	384.2/3	373.4/3	344.4/3	0/0	0/0	0/0
57	327.4/2	340.9/3	350.9/2	322.0/3	306.2/3	298.3/3	283.2/3	0/0	0/0
58	325.1/2	337.1/3	334.1/2	319.7/2	298.4/2	296.4/3	289.2/3	0/0	0/0
59	300.0/3	310.7/3	302.0/2	294.6/2	284.4/3	286.6/3	270.6/3	246.1/4	210.1/4
60	279.8/3	289.7/3	291.0/3	268.1/2	266.5/3	278.8/3	253.6/2	251.0/2	233.3/4
61	0/0	258.1/3	265.7/3	256.2/2	267.5/2	270.8/3	242.9/3	235.9/3	0/0
62	0/0	0/0	255.7/2	256.7/2	253.4/2	247.6/2	237.7/3	225.2/3	0/0
63	0/0	212.0/2	237.8/2	247.8/2	234.4/2	233.0/2	229.4/2	218.7/3	190.5/3
64	0/0	207.3/2	220.1/2	205.1/3	210.2/2	225.2/2	214.2/2	201.3/3	176.5/3
65	0/0	0/0	191.6/2	188.7/2	199.1/2	213.7/2	204.4/2	194.5/3	167.8/3
66	0/0	0/0	178.1/2	179.2/2	187.0/2	182.0/2	179.8/2	169.8/2	150.3/2
67	0/0	0/0	138.7/2	175.7/2	170.2/2	166.2/2	166.8/2	161.7/2	117.2/2
68	0/0	0/0	0/0	124.8/2	142.0/2	133.9/2	134.0/2	126.0/3	79.3/3
69	0/0	0/0	0/0	134.1/2	122.3/2	0/0	0/0	0/0	0/0

Flight 10, July 7, 1977 (1977.514)

	19	20	21	22	23	24	25	26	27
47	534.9/3	529.1/2	529.3/2	552.9/2	571.5/2	566.4/3	563.2/4	0/0	0/0
48	531.7/3	523.8/2	523.7/2	539.6/2	557.7/2	542.8/2	533.5/3	0/0	0/0
49	530.7/2	512.2/2	509.2/2	525.0/2	526.0/2	525.6/3	529.4/3	0/0	0/0
50	513.3/2	489.2/3	488.7/2	498.0/3	512.8/3	528.0/2	534.1/2	0/0	0/0
51	499.1/2	490.2/2	481.1/3	492.7/2	530.6/2	539.1/3	537.1/3	0/0	0/0
52	475.7/2	482.6/2	475.5/2	479.2/2	493.5/2	523.0/3	536.1/3	0/0	0/0
53	483.4/2	472.5/2	461.3/2	433.3/2	404.7/2	0/0	0/0	0/0	0/0
54	0/0	377.7/2	403.5/2	408.8/2	393.3/2	379.9/3	0/0	0/0	0/0
55	339.3/3	358.7/2	389.2/2	405.5/2	397.7/2	373.9/3	0/0	0/0	0/0
56	334.4/3	355.6/3	375.6/2	382.3/2	372.7/3	342.9/3	0/0	0/0	0/0
57	325.6/2	338.7/3	349.8/2	320.2/2	304.4/2	296.8/3	282.0/3	0/0	0/0
58	324.3/2	336.1/3	332.3/2	317.5/2	296.5/2	294.9/3	287.7/2	0/0	0/0
59	298.9/3	309.4/3	300.2/2	292.5/2	282.3/2	284.9/3	269.2/3	244.7/3	208.6/4
60	278.5/3	288.6/3	289.5/2	266.5/2	264.7/2	277.0/3	251.9/2	249.5/2	231.8/4
61	0/0	256.9/3	264.2/3	254.9/2	265.4/2	269.4/3	241.6/3	234.5/2	0/0
62	0/0	0/0	254.2/2	255.4/2	252.0/2	246.1/2	236.7/2	223.9/3	0/0
63	0/0	210.7/2	236.5/2	246.3/2	232.8/2	231.5/2	228.4/2	217.8/3	189.4/3
64	0/0	205.8/2	218.8/2	203.7/2	208.1/2	223.3/2	212.5/2	200.3/2	175.5/3
65	0/0	0/0	190.4/2	187.2/2	196.9/2	211.7/2	202.4/2	193.3/2	166.8/2
66	0/0	0/0	176.8/2	177.7/2	185.0/2	180.2/2	178.2/2	168.7/2	149.2/2
67	0/0	0/0	139.0/2	173.3/2	169.1/2	164.6/2	165.8/2	160.6/2	115.7/2
68	0/0	0/0	0/0	124.5/2	139.6/2	133.1/2	132.3/2	125.7/3	78.0/3
69	0/0	0/0	0/0	130.7/2	120.7/2	0/0	0/0	0/0	0/0

Flight 11, August 29, 1977 (1977.659)

	19	20	21	22	23	24	25	26	27
47	533.2/3	527.2/2	528.0/2	551.3/2	569.4/3	563.9/3	561.8/4	0/0	0/0
48	529.3/3	521.7/2	522.1/2	537.5/2	555.0/2	539.8/2	531.5/3	0/0	0/0
49	528.9/2	510.4/2	507.8/2	522.2/2	523.0/2	523.0/3	527.3/3	0/0	0/0
50	511.5/2	486.9/2	486.7/3	495.3/3	509.6/3	524.8/2	531.7/2	0/0	0/0
51	497.1/2	487.6/2	478.9/2	489.8/2	527.9/2	536.3/3	534.6/3	0/0	0/0
52	473.4/2	480.1/2	472.8/2	476.5/2	490.1/2	520.0/3	534.2/3	0/0	0/0
53	481.0/2	469.3/2	458.3/2	431.1/2	403.6/2	0/0	0/0	0/0	0/0
54	0/0	375.5/2	400.8/2	406.5/2	391.6/2	377.0/3	0/0	0/0	0/0
55	336.9/3	356.3/3	386.4/2	402.7/2	395.4/2	371.2/3	0/0	0/0	0/0
56	331.2/3	352.4/3	372.6/2	378.7/2	369.8/3	340.0/3	0/0	0/0	0/0
57	322.5/2	336.4/3	346.9/2	316.8/2	300.8/2	293.6/3	278.7/3	0/0	0/0
58	321.8/2	332.0/3	327.2/2	313.6/2	293.0/2	291.7/3	284.3/2	0/0	0/0
59	295.9/3	306.6/3	296.1/2	287.7/2	278.6/2	281.6/3	265.9/3	241.9/3	205.6/4
60	275.4/3	285.8/3	285.9/3	262.2/2	261.3/2	272.7/3	248.6/2	246.1/2	229.0/4
61	0/0	253.2/3	260.8/3	251.8/2	261.6/2	265.1/3	238.5/3	231.1/3	0/0
62	0/0	0/0	250.6/2	252.3/2	247.8/2	242.5/2	233.6/2	221.0/3	0/0
63	0/0	208.2/2	233.2/2	242.2/2	229.1/2	228.0/2	224.8/2	214.6/3	185.8/3
64	0/0	202.9/2	214.8/2	199.4/2	204.6/2	218.3/2	209.3/2	196.7/3	172.2/3
65	0/0	0/0	186.5/2	182.5/2	190.4/2	205.4/2	197.7/2	189.5/2	164.1/2
66	0/0	0/0	173.7/2	172.0/2	178.0/2	175.4/2	173.0/2	165.6/2	146.0/2
67	0/0	0/0	136.4/2	166.6/2	161.5/2	158.5/2	160.1/2	156.9/2	113.3/2
68	0/0	0/0	0/0	119.7/2	132.8/2	128.2/2	128.3/2	121.9/2	73.5/3
69	0/0	0/0	0/0	114.0/2	104.3/2	0/0	0/0	0/0	0/0

Flight 12, November 8, 1977 (1977.854)

	19	20	21	22	23	24	25	26	27
47	531.7/3	525.4/2	526.9/3	549.9/3	567.5/3	561.9/4	562.2/4	0/0	0/0
48	527.1/3	519.4/2	520.9/2	535.5/2	552.1/2	536.7/2	530.6/3	0/0	0/0
49	528.0/2	508.8/2	506.2/2	519.6/2	520.4/3	521.3/3	525.4/3	0/0	0/0
50	510.0/2	485.6/3	485.8/3	493.2/3	507.1/3	522.9/2	530.4/3	0/0	0/0
51	495.8/3	486.1/2	477.7/2	487.0/3	525.6/2	533.4/3	532.3/3	0/0	0/0
52	471.4/2	478.0/2	470.4/3	474.7/2	486.3/2	517.2/3	533.7/3	0/0	0/0
53	479.5/2	464.0/3	455.0/2	428.7/2	401.9/2	0/0	0/0	0/0	0/0
54	0/0	374.1/2	398.8/2	406.3/2	391.3/2	374.6/3	0/0	0/0	0/0
55	335.3/3	357.1/3	385.8/2	401.9/2	393.3/2	368.0/3	0/0	0/0	0/0
56	329.4/3	352.5/3	369.9/2	376.3/2	367.7/3	337.2/3	0/0	0/0	0/0
57	320.1/2	334.5/3	343.7/2	314.9/2	297.2/3	289.0/3	275.2/3	0/0	0/0
58	318.1/2	327.3/3	320.4/2	309.7/2	290.5/2	288.3/3	280.2/2	0/0	0/0
59	291.3/3	301.6/3	291.8/2	281.9/2	274.2/2	277.6/3	262.6/3	238.8/4	202.3/4
60	271.3/3	281.3/3	281.5/3	257.5/2	256.6/2	267.7/3	244.9/3	241.9/3	226.0/4
61	0/0	247.9/3	256.7/3	247.3/2	256.5/2	259.2/3	234.2/3	226.5/3	0/0
62	0/0	0/0	245.0/2	248.1/3	242.5/2	237.4/2	229.6/3	216.3/3	0/0
63	0/0	204.9/2	229.2/2	238.1/2	223.5/2	222.0/2	218.8/2	209.6/3	180.6/3
64	0/0	200.9/2	210.6/2	193.7/2	199.8/2	211.9/2	203.6/2	191.5/3	167.6/3
65	0/0	0/0	182.1/2	174.9/2	182.9/2	195.2/2	191.7/2	183.6/2	160.7/3
66	0/0	0/0	169.0/2	161.9/2	166.6/2	166.6/2	166.8/2	160.3/2	142.7/3
67	0/0	0/0	129.0/2	154.1/2	147.3/2	148.5/2	150.1/2	151.6/2	110.8/2
68	0/0	0/0	0/0	108.4/2	120.3/2	119.6/2	119.4/2	115.1/3	66.7/3
69	0/0	0/0	0/0	100.6/2	86.7/2	0/0	0/0	0/0	0/0

Flight 13, February 28, 1978 (1978.160)

	19	20	21	22	23	24	25	26	27
47	534.6/3	528.5/2	529.4/2	551.5/2	569.9/3	565.1/4	566.7/4	0/0	0/0
48	529.8/3	522.6/2	524.3/2	538.4/2	554.7/2	539.7/3	534.3/4	0/0	0/0
49	531.6/2	511.4/2	508.8/2	521.6/2	523.5/3	524.2/3	528.4/4	0/0	0/0
50	513.4/2	489.0/2	489.0/2	495.4/3	510.4/3	526.4/3	534.1/3	0/0	0/0
51	499.5/2	491.3/2	482.6/3	491.3/3	529.9/3	537.5/3	535.8/3	0/0	0/0
52	474.9/2	483.1/3	477.3/2	479.3/2	491.5/3	522.2/3	538.1/4	0/0	0/0
53	484.1/2	468.3/2	459.6/2	433.5/2	405.2/2	0/0	0/0	0/0	0/0
54	0/0	379.2/2	404.2/2	412.1/2	396.8/2	379.2/3	0/0	0/0	0/0
55	342.5/3	364.5/3	391.5/2	408.7/2	399.0/3	372.7/3	0/0	0/0	0/0
56	336.1/3	358.7/3	376.4/3	383.1/2	373.0/3	341.7/3	0/0	0/0	0/0
57	325.1/2	340.7/3	348.1/2	321.1/2	301.5/2	292.3/3	279.3/3	0/0	0/0
58	319.5/2	331.2/3	325.0/2	314.1/3	295.2/2	291.1/3	283.5/2	0/0	0/0
59	292.2/3	304.0/3	294.7/2	283.0/2	276.3/2	280.2/3	266.1/2	242.0/3	205.6/4
60	273.0/3	282.6/3	283.6/2	258.2/2	258.4/2	270.1/3	248.9/3	245.0/2	229.4/4
61	0/0	249.5/3	258.8/3	249.3/2	258.5/2	260.5/3	236.9/3	228.6/3	0/0
62	0/0	0/0	246.5/3	248.8/2	243.0/2	237.3/3	231.9/2	218.7/3	0/0
63	0/0	207.5/2	230.7/2	241.0/2	225.0/2	223.1/2	219.7/2	210.9/3	182.6/3
64	0/0	204.8/2	214.4/2	196.4/2	200.2/2	212.3/2	203.6/2	192.2/3	169.9/2
65	0/0	0/0	185.1/2	177.2/2	183.5/2	196.2/2	191.3/3	183.7/2	164.4/3
66	0/0	0/0	170.0/2	162.8/2	167.3/2	166.0/2	165.6/2	163.1/2	146.1/2
67	0/0	0/0	128.7/2	154.6/2	149.2/2	148.8/2	148.6/2	154.1/2	115.8/2
68	0/0	0/0	0/0	108.2/2	125.3/3	118.6/2	117.8/2	118.7/2	70.7/3
69	0/0	0/0	0/0	104.1/2	95.6/2	0/0	0/0	0/0	0/0

Flight 14, April 19, 1978 (1978.297)

	19	20	21	22	23	24	25	26	27
47	534.4/3	528.3/2	528.7/2	551.1/2	569.5/3	565.0/4	565.9/4	0/0	0/0
48	529.2/3	522.6/2	523.8/2	538.0/2	554.7/2	539.7/3	534.0/4	0/0	0/0
49	530.9/2	510.4/2	507.9/2	521.3/2	522.9/3	523.0/3	527.7/4	0/0	0/0
50	512.7/2	488.1/2	488.7/2	494.2/3	509.4/3	525.5/3	533.6/4	0/0	0/0
51	499.3/2	490.8/2	481.9/3	491.3/3	530.2/3	537.4/3	535.8/3	0/0	0/0
52	474.3/2	483.2/3	477.7/2	479.0/2	491.2/3	523.9/3	538.4/3	0/0	0/0
53	484.5/2	467.9/2	459.6/3	432.8/2	403.5/2	0/0	0/0	0/0	0/0
54	0/0	378.0/2	403.6/2	411.7/2	397.1/2	379.3/3	0/0	0/0	0/0
55	342.1/3	362.8/2	390.9/2	408.3/2	397.5/3	372.7/3	0/0	0/0	0/0
56	336.0/3	358.8/2	376.5/3	382.3/2	372.4/2	341.4/3	0/0	0/0	0/0
57	324.8/2	340.3/3	348.2/2	321.0/2	300.7/2	292.2/3	279.5/3	0/0	0/0
58	318.7/2	330.3/3	327.1/2	314.2/2	294.5/2	290.7/3	283.6/2	0/0	0/0
59	291.0/3	302.3/3	293.9/2	282.7/2	275.6/2	278.9/3	265.8/2	241.9/3	205.5/4
60	272.8/3	282.6/3	283.0/2	257.1/2	257.3/2	270.7/2	248.8/3	245.4/2	229.4/4
61	0/0	249.2/3	258.3/3	248.9/2	258.3/2	260.4/2	236.7/3	228.2/3	0/0
62	0/0	0/0	245.0/3	247.8/2	242.2/2	236.1/3	231.1/2	218.1/3	0/0
63	0/0	205.8/2	229.0/2	241.3/2	224.4/2	222.4/2	218.7/2	210.2/3	182.3/3
64	0/0	204.7/2	214.2/2	196.2/2	199.0/2	213.4/2	202.2/2	191.3/3	169.6/2
65	0/0	0/0	184.6/2	177.5/2	184.6/2	198.3/2	191.3/3	182.5/2	163.7/3
66	0/0	0/0	168.1/2	164.7/2	169.6/2	166.8/2	167.0/2	163.5/2	146.5/2
67	0/0	0/0	128.2/2	157.6/2	151.5/2	151.1/2	149.6/2	153.4/2	115.2/2
68	0/0	0/0	0/0	109.1/2	128.7/2	119.4/2	119.7/2	119.4/2	71.1/3
69	0/0	0/0	0/0	109.0/2	100.6/2	0/0	0/0	0/0	0/0

Flight 15, June 11, 1978 (1978.442)

	19	20	21	22	23	24	25	26	27
47	534.6/3	528.6/2	529.1/2	551.8/2	569.9/3	565.4/4	565.6/4	0/0	0/0
48	529.5/3	522.3/2	524.0/2	538.7/2	555.6/2	540.3/3	534.0/4	0/0	0/0
49	531.2/2	510.8/2	508.4/2	522.3/2	523.8/3	523.0/3	527.8/4	0/0	0/0
50	513.3/2	489.1/2	490.0/2	494.7/2	509.7/3	525.5/3	533.7/4	0/0	0/0
51	500.2/2	491.2/2	481.4/2	492.3/3	530.1/3	538.3/3	536.5/3	0/0	0/0
52	475.8/2	484.1/3	478.4/2	478.4/2	492.1/2	526.0/2	538.8/3	0/0	0/0
53	486.1/2	470.7/2	461.1/3	432.8/2	403.8/2	0/0	0/0	0/0	0/0
54	0/0	376.6/2	403.5/2	410.9/2	397.9/2	380.7/3	0/0	0/0	0/0
55	341.4/3	361.5/2	389.1/2	407.4/2	395.7/3	373.2/3	0/0	0/0	0/0
56	337.3/3	359.7/3	377.5/2	381.7/2	372.4/2	342.6/3	0/0	0/0	0/0
57	325.8/2	340.5/3	349.0/2	320.6/2	300.9/2	294.0/3	281.1/3	0/0	0/0
58	319.5/2	330.6/3	329.2/2	315.4/2	294.9/2	291.1/3	285.6/2	0/0	0/0
59	291.4/3	302.2/3	294.1/2	283.8/2	276.1/2	279.6/3	267.3/2	242.8/3	206.4/4
60	273.9/3	284.3/3	283.8/2	258.7/2	258.5/2	272.9/2	250.5/3	246.8/2	230.2/4
61	0/0	250.1/2	259.4/3	250.3/2	261.3/2	262.0/2	238.2/2	229.5/2	0/0
62	0/0	0/0	245.8/3	248.7/2	243.6/2	237.5/3	232.1/2	218.8/3	0/0
63	0/0	205.5/2	228.2/2	242.5/2	226.1/2	223.9/2	219.7/2	211.3/3	183.6/3
64	0/0	204.8/2	214.7/2	197.6/2	200.8/2	215.8/2	203.4/2	191.3/3	170.7/2
65	0/0	0/0	185.0/2	179.4/2	187.6/2	201.7/2	193.3/2	182.8/2	164.8/3
66	0/0	0/0	168.3/2	168.3/2	175.1/2	170.5/2	170.5/2	164.7/2	147.2/2
67	0/0	0/0	130.2/2	163.3/2	157.2/2	154.9/2	154.0/2	154.5/2	116.3/2
68	0/0	0/0	0/0	112.8/2	132.3/2	122.8/2	121.8/2	121.7/2	73.3/2
69	0/0	0/0	0/0	113.9/2	105.4/2	0/0	0/0	0/0	0/0

Flight 16, July 30, 1978 (1978.576)

	19	20	21	22	23	24	25	26	27
47	530.7/3	524.9/2	525.6/2	548.7/2	566.2/3	562.1/4	561.3/4	0/0	0/0
48	526.0/3	518.8/2	520.2/2	534.9/2	551.7/2	536.7/3	530.1/4	0/0	0/0
49	527.9/2	507.8/3	505.4/2	519.1/2	519.5/2	518.0/3	523.6/4	0/0	0/0
50	510.6/2	485.8/2	487.0/2	490.7/2	504.9/3	520.7/3	529.4/4	0/0	0/0
51	497.7/2	487.3/2	477.7/2	488.3/2	524.5/3	534.4/3	533.5/3	0/0	0/0
52	472.8/2	480.7/3	474.0/2	474.1/2	486.7/2	523.5/2	535.8/3	0/0	0/0
53	483.6/2	468.3/2	456.6/3	428.9/2	399.6/2	0/0	0/0	0/0	0/0
54	0/0	371.3/2	398.8/2	405.9/2	392.2/2	377.2/3	0/0	0/0	0/0
55	336.4/3	355.3/2	383.3/2	402.0/2	391.6/2	369.9/3	0/0	0/0	0/0
56	334.6/3	355.3/3	373.2/2	376.8/2	366.5/2	338.0/3	0/0	0/0	0/0
57	322.7/2	337.0/3	343.9/2	315.8/2	297.1/2	291.0/3	277.8/3	0/0	0/0
58	316.0/2	326.7/3	326.2/2	312.3/2	290.6/2	287.0/3	282.6/2	0/0	0/0
59	288.6/3	298.7/3	290.3/2	281.2/2	272.9/2	276.0/3	263.9/2	239.2/3	202.8/4
60	270.8/3	281.5/3	280.1/2	255.2/2	256.1/2	270.2/2	247.5/3	243.5/2	226.5/4
61	0/0	246.8/2	255.6/3	247.7/2	258.0/2	259.0/2	234.6/2	225.9/2	0/0
62	0/0	0/0	241.9/3	245.5/2	240.8/2	233.7/3	227.9/3	215.2/3	0/0
63	0/0	201.9/2	223.5/2	238.8/2	223.2/2	221.1/2	216.7/3	207.6/3	180.2/3
64	0/0	201.2/2	210.8/2	194.3/2	198.8/2	212.8/2	200.4/2	187.7/3	167.1/2
65	0/0	0/0	181.2/2	176.5/2	184.8/2	199.4/2	190.7/2	179.0/2	160.5/2
66	0/0	0/0	165.3/2	165.0/2	172.7/2	167.3/2	167.6/2	161.1/2	143.5/2
67	0/0	0/0	127.4/2	164.0/2	156.1/2	152.8/2	151.9/2	151.4/2	111.6/2
68	0/0	0/0	0/0	111.9/2	129.2/2	121.4/2	123.8/2	119.3/2	70.8/2
69	0/0	0/0	0/0	114.7/2	104.6/2	0/0	0/0	0/0	0/0

Flight 17, August 26, 1978 (1978.650)

	19	20	21	22	23	24	25	26	27
47	529.8/3	523.8/2	524.9/2	547.8/2	565.0/3	560.9/4	560.3/4	0/0	0/0
48	525.1/3	517.8/2	519.1/2	533.5/2	550.2/2	535.1/3	528.9/4	0/0	0/0
49	527.1/3	507.5/3	504.4/2	517.2/2	517.6/2	516.5/3	522.4/4	0/0	0/0
50	510.4/2	485.5/2	486.1/2	489.2/2	503.1/3	519.0/3	528.0/4	0/0	0/0
51	496.8/2	485.9/2	476.5/2	486.8/2	523.2/3	532.7/2	532.2/3	0/0	0/0
52	471.5/2	479.1/3	472.1/2	472.1/3	484.8/2	522.1/2	534.8/3	0/0	0/0
53	482.4/2	466.5/2	455.2/3	427.6/2	398.2/2	0/0	0/0	0/0	0/0
54	0/0	368.6/2	396.8/2	403.7/2	389.5/2	375.5/3	0/0	0/0	0/0
55	334.4/3	352.6/2	380.9/2	399.5/2	389.3/2	368.1/3	0/0	0/0	0/0
56	333.2/3	353.5/3	370.1/2	374.6/2	364.1/2	335.9/3	0/0	0/0	0/0
57	321.4/2	335.1/3	341.6/2	313.3/2	295.1/2	288.9/3	275.9/3	0/0	0/0
58	314.4/2	325.4/3	324.3/2	310.7/2	288.8/2	285.3/3	280.6/2	0/0	0/0
59	287.3/3	297.2/3	289.4/2	279.7/2	271.3/2	273.6/3	262.2/3	237.6/3	201.2/4
60	269.6/3	280.7/3	278.5/3	253.2/2	254.3/2	268.4/2	246.1/3	241.9/2	225.1/4
61	0/0	245.4/2	254.1/3	246.1/2	256.2/2	257.2/2	232.8/2	223.9/2	0/0
62	0/0	0/0	240.3/3	244.0/2	239.3/2	231.6/2	225.7/3	213.0/3	0/0
63	0/0	200.4/2	221.7/2	237.1/2	221.4/2	219.3/2	214.6/3	206.3/3	178.1/3
64	0/0	199.8/2	208.4/2	192.6/2	197.6/2	211.3/2	199.0/2	185.6/3	165.3/2
65	0/0	0/0	179.7/2	174.6/2	182.9/2	197.0/2	188.7/2	177.1/2	158.7/2
66	0/0	0/0	163.9/2	162.5/2	170.1/2	165.6/2	165.7/2	159.1/2	141.2/2
67	0/0	0/0	126.0/2	161.7/2	154.0/2	150.3/2	149.6/2	149.7/2	109.6/2
68	0/0	0/0	0/0	108.9/2	126.1/2	119.7/2	122.1/2	117.2/2	68.3/2
69	0/0	0/0	0/0	113.6/2	100.6/2	0/0	0/0	0/0	0/0

Flight 18, November 8, 1978 (1978.853)

	19	20	21	22	23	24	25	26	27
47	533.3/2	525.9/2	527.4/3	550.6/3	567.6/4	562.7/4	563.7/4	0/0	0/0
48	527.1/3	520.5/2	521.7/2	535.2/2	550.8/3	536.1/3	531.4/4	0/0	0/0
49	529.4/3	510.0/3	505.3/2	518.9/2	518.7/2	518.0/3	524.5/4	0/0	0/0
50	513.2/2	487.4/2	486.5/2	489.6/2	504.0/2	519.8/3	530.0/4	0/0	0/0
51	498.5/2	485.9/2	476.8/2	486.2/2	523.7/3	533.1/2	533.5/4	0/0	0/0
52	471.7/2	478.3/3	470.7/2	472.2/3	484.5/2	521.6/3	537.7/3	0/0	0/0
53	482.8/3	463.7/2	453.8/3	426.7/2	399.5/2	0/0	0/0	0/0	0/0
54	0/0	367.3/3	394.5/2	402.3/2	387.2/3	374.1/3	0/0	0/0	0/0
55	332.6/3	352.4/2	379.8/2	399.0/2	386.9/2	365.5/3	0/0	0/0	0/0
56	332.3/3	351.6/3	367.3/2	371.0/2	361.8/2	333.2/3	0/0	0/0	0/0
57	320.8/2	334.3/3	340.4/3	311.2/2	293.4/2	286.6/3	273.1/3	0/0	0/0
58	314.0/3	324.7/3	321.6/2	308.8/2	287.7/2	284.6/3	277.3/2	0/0	0/0
59	286.6/3	299.9/3	290.4/3	278.8/2	270.6/2	271.8/3	260.6/3	237.5/3	201.0/4
60	269.6/3	280.6/3	277.0/3	250.9/2	252.2/2	265.9/3	244.7/3	240.6/2	225.2/4
61	0/0	244.3/3	252.4/3	243.7/2	253.5/2	255.3/2	230.4/2	222.1/3	0/0
62	0/0	0/0	239.1/3	243.8/2	237.5/2	228.9/2	221.8/3	210.2/3	0/0
63	0/0	201.7/2	221.4/2	235.0/2	219.2/2	216.2/2	211.8/3	203.6/3	175.3/3
64	0/0	201.9/2	207.3/2	188.1/2	196.1/2	209.0/2	197.5/2	183.8/3	163.1/2
65	0/0	0/0	177.3/2	171.2/2	179.4/2	193.0/2	186.1/2	175.2/2	156.1/3
66	0/0	0/0	163.8/2	156.1/2	162.7/2	163.3/2	161.5/3	155.7/2	137.4/3
67	0/0	0/0	124.2/2	153.3/2	145.4/2	145.1/2	143.0/2	147.4/2	106.8/3
68	0/0	0/0	0/0	103.7/2	118.4/2	113.9/2	115.0/3	111.6/2	62.5/3
69	0/0	0/0	0/0	111.3/2	88.5/2	0/0	0/0	0/0	0/0

Flight 19, January 6, 1979 (1979.014)

	19	20	21	22	23	24	25	26	27
47	531.1/2	524.1/2	526.1/3	548.7/3	566.0/4	561.8/4	562.1/4	0/0	0/0
48	525.9/3	518.5/2	520.3/2	534.5/2	549.9/3	535.5/3	530.2/4	0/0	0/0
49	527.8/3	508.0/3	503.8/2	518.1/2	518.4/2	517.3/3	523.6/4	0/0	0/0
50	511.4/3	485.8/2	484.4/2	489.0/2	504.1/3	519.5/3	528.9/4	0/0	0/0
51	497.2/2	484.9/2	476.2/2	485.8/3	523.5/2	532.2/3	533.3/4	0/0	0/0
52	471.2/3	478.1/3	469.7/2	473.5/3	486.6/3	521.5/3	537.6/3	0/0	0/0
53	482.8/3	465.6/3	455.6/2	427.5/2	399.1/3	0/0	0/0	0/0	0/0
54	0/0	370.2/3	395.8/3	402.8/2	387.6/3	374.6/3	0/0	0/0	0/0
55	334.2/3	353.6/2	380.8/2	399.9/2	389.1/2	366.9/2	0/0	0/0	0/0
56	333.4/3	352.2/3	365.7/2	372.2/2	363.2/3	333.1/3	0/0	0/0	0/0
57	321.0/2	334.6/3	340.7/3	311.4/2	293.2/3	286.3/3	273.3/3	0/0	0/0
58	314.1/3	325.5/3	321.4/2	308.6/3	287.5/2	284.3/3	277.1/2	0/0	0/0
59	288.0/3	301.0/3	291.3/3	279.2/2	271.1/2	271.6/3	259.6/3	236.7/3	200.7/4
60	269.9/3	281.1/3	278.3/3	251.0/2	251.6/2	265.7/3	244.6/3	240.3/2	224.6/4
61	0/0	245.1/3	253.5/3	241.8/2	253.7/2	256.2/2	230.5/3	222.0/3	0/0
62	0/0	0/0	240.8/3	243.9/2	237.9/2	229.8/2	221.5/3	210.5/3	0/0
63	0/0	202.8/2	223.9/2	235.7/2	219.8/2	216.7/2	212.1/3	203.4/3	175.6/3
64	0/0	202.1/3	208.8/2	189.3/2	196.6/2	209.2/2	198.4/2	184.1/3	163.6/2
65	0/0	0/0	179.3/2	172.3/2	180.3/2	193.2/2	186.9/2	176.2/2	156.8/3
66	0/0	0/0	165.1/2	158.5/2	164.8/2	164.1/3	162.0/3	156.1/2	138.1/3
67	0/0	0/0	126.0/2	154.0/2	147.6/2	145.3/2	143.1/2	147.5/3	107.1/3
68	0/0	0/0	0/0	107.4/2	120.1/2	114.4/2	116.1/3	113.8/2	65.0/3
69	0/0	0/0	0/0	115.9/2	93.2/2	0/0	0/0	0/0	0/0

Flight 20, April 12, 1979 (1979.277)

	19	20	21	22	23	24	25	26	27
47	529.3/2	523.2/2	524.7/3	547.3/2	565.3/3	561.1/4	560.6/4	0/0	0/0
48	524.7/3	517.1/3	519.7/2	534.2/2	550.1/3	536.7/4	530.7/4	0/0	0/0
49	525.9/3	506.2/3	503.3/3	518.4/3	519.2/3	518.3/3	523.6/4	0/0	0/0
50	510.1/3	484.7/2	483.6/2	489.9/2	505.2/3	520.3/3	529.3/4	0/0	0/0
51	496.6/2	485.0/3	477.0/2	486.5/3	525.2/3	533.2/3	533.3/4	0/0	0/0
52	472.7/3	478.5/3	470.6/3	474.2/3	487.5/3	520.4/3	536.3/3	0/0	0/0
53	483.7/3	467.6/3	457.3/2	428.6/3	399.5/3	0/0	0/0	0/0	0/0
54	0/0	372.4/3	399.3/3	405.1/2	389.1/3	375.8/2	0/0	0/0	0/0
55	334.8/3	354.1/2	384.1/2	401.3/2	393.1/2	369.3/3	0/0	0/0	0/0
56	333.2/3	351.6/3	365.7/2	373.7/2	364.8/3	334.1/3	0/0	0/0	0/0
57	321.0/3	334.7/3	341.7/3	312.7/3	293.9/3	285.1/3	273.4/3	0/0	0/0
58	314.0/3	325.7/3	322.2/3	308.3/3	287.8/2	284.4/3	277.4/2	0/0	0/0
59	289.1/3	301.3/3	291.4/3	279.5/2	271.1/3	271.3/3	258.4/3	235.9/3	200.7/4
60	269.8/3	280.6/3	278.4/3	250.4/2	251.5/2	264.7/3	243.8/3	240.2/3	224.4/4
61	0/0	245.6/3	253.3/3	241.4/2	253.9/2	256.6/2	230.4/3	222.8/3	0/0
62	0/0	0/0	241.3/3	244.4/2	238.8/2	232.2/2	222.8/3	211.0/3	0/0
63	0/0	202.4/2	225.4/3	236.4/2	220.5/2	218.1/3	213.7/3	204.1/3	176.6/3
64	0/0	200.2/3	208.9/3	191.6/2	197.1/2	210.8/2	199.9/3	184.4/3	163.6/3
65	0/0	0/0	179.0/3	174.1/3	182.4/3	196.7/3	189.3/3	177.4/3	157.2/3
66	0/0	0/0	165.0/2	162.3/2	169.4/2	166.8/3	164.4/3	156.0/2	137.6/3
67	0/0	0/0	128.0/2	158.9/2	154.1/3	150.5/3	146.5/2	147.3/3	106.5/3
68	0/0	0/0	0/0	115.3/2	128.3/2	119.0/2	116.9/3	114.0/3	67.4/3
69	0/0	0/0	0/0	123.6/2	104.2/2	0/0	0/0	0/0	0/0

Flight 21, August 18, 1979 (1979.628)

	19	20	21	22	23	24	25	26	27
47	526.5/2	519.6/2	521.1/3	543.6/3	561.9/4	557.4/4	556.6/4	0/0	0/0
48	522.9/3	515.0/3	516.7/2	530.8/2	546.4/3	533.8/4	526.8/4	0/0	0/0
49	522.8/3	504.5/3	501.5/3	515.0/3	515.5/3	516.0/4	520.5/4	0/0	0/0
50	508.0/3	483.2/3	481.9/2	487.9/2	502.8/4	518.1/4	525.5/4	0/0	0/0
51	494.3/2	483.2/3	474.1/2	483.6/3	522.2/3	530.3/3	530.1/4	0/0	0/0
52	469.7/3	475.3/2	467.0/3	470.5/3	483.0/3	516.2/3	532.8/3	0/0	0/0
53	479.0/3	461.4/3	451.1/3	422.6/3	393.3/2	0/0	0/0	0/0	0/0
54	0/0	367.1/2	392.8/2	399.3/2	383.6/2	371.7/2	0/0	0/0	0/0
55	332.8/3	351.4/2	379.5/2	395.8/2	388.1/3	366.3/3	0/0	0/0	0/0
56	330.8/3	349.0/3	362.4/2	367.4/2	359.4/2	329.9/3	0/0	0/0	0/0
57	318.2/3	332.1/3	340.1/2	309.6/3	291.3/3	280.7/3	268.8/3	0/0	0/0
58	310.7/3	323.8/3	319.7/3	304.4/2	284.4/2	281.0/3	274.4/2	0/0	0/0
59	285.6/3	297.2/3	287.4/2	276.7/3	270.0/3	269.2/3	254.4/3	232.3/3	196.9/4
60	265.7/4	276.2/3	274.9/3	249.4/2	250.1/2	260.8/3	239.7/3	236.8/2	221.0/4
61	0/0	241.5/3	249.4/3	238.6/2	252.0/2	254.1/2	227.7/3	220.2/3	0/0
62	0/0	0/0	237.6/3	241.5/2	236.8/2	231.6/2	221.4/3	207.5/3	0/0
63	0/0	196.8/2	221.6/3	233.1/2	217.4/2	216.4/2	212.8/3	200.0/3	171.5/3
64	0/0	194.2/3	204.6/2	189.8/2	194.7/2	208.0/3	198.5/3	182.3/3	159.3/3
65	0/0	0/0	174.3/2	171.1/3	179.9/2	194.8/3	187.4/3	175.8/3	153.5/3
66	0/0	0/0	159.6/2	159.2/2	167.4/3	164.4/3	163.4/2	153.6/3	133.5/3
67	0/0	0/0	123.5/2	158.0/2	155.4/3	150.2/3	145.8/2	144.7/3	101.5/3
68	0/0	0/0	0/0	113.4/2	129.0/2	119.7/2	114.6/2	109.0/3	64.4/3
69	0/0	0/0	0/0	118.7/2	104.3/2	0/0	0/0	0/0	0/0

Flight 22, October 20, 1979 (1979.800)

	19	20	21	22	23	24	25	26	27
47	527.7/3	519.9/2	521.1/3	544.0/3	562.8/4	557.9/4	558.5/4	0/0	0/0
48	522.3/3	515.3/3	517.3/2	531.2/3	546.8/4	534.4/4	528.0/4	0/0	0/0
49	523.0/3	504.8/3	502.1/3	515.1/3	515.9/3	518.1/4	521.4/4	0/0	0/0
50	507.9/3	483.5/3	481.8/2	487.5/2	503.1/4	518.8/4	526.4/4	0/0	0/0
51	493.9/2	481.7/3	473.2/2	482.4/3	522.3/4	530.3/3	529.9/4	0/0	0/0
52	467.9/3	473.6/2	465.4/3	468.6/3	479.4/3	514.2/3	534.0/3	0/0	0/0
53	477.7/3	455.6/3	447.0/3	420.7/3	393.1/2	0/0	0/0	0/0	0/0
54	0/0	363.9/2	390.2/2	397.2/2	381.5/2	369.3/2	0/0	0/0	0/0
55	330.5/3	349.6/3	377.0/3	393.7/2	385.3/3	363.3/2	0/0	0/0	0/0
56	329.1/3	346.6/3	360.4/2	364.8/2	357.3/2	328.9/3	0/0	0/0	0/0
57	316.2/3	329.9/3	337.5/2	307.8/3	289.8/3	278.1/3	265.1/3	0/0	0/0
58	309.1/3	322.4/3	318.2/3	301.8/2	283.1/2	279.5/3	271.5/2	0/0	0/0
59	282.6/3	295.7/3	286.1/3	273.7/3	267.6/3	266.9/3	252.5/3	231.3/3	195.3/4
60	263.7/4	274.0/3	272.6/3	247.2/2	247.9/2	257.8/3	237.7/3	235.2/2	220.2/4
61	0/0	238.6/3	246.2/3	236.3/2	249.4/2	251.1/3	225.7/3	218.6/3	0/0
62	0/0	0/0	233.4/3	239.0/2	234.4/2	229.1/2	218.4/3	204.7/3	0/0
63	0/0	194.8/2	219.0/3	230.1/2	213.8/2	213.2/2	209.8/3	197.1/3	167.7/3
64	0/0	194.0/3	201.7/2	185.1/3	192.3/2	204.8/3	195.4/3	180.1/3	156.3/3
65	0/0	0/0	170.6/2	167.0/3	175.4/2	191.2/3	184.7/2	172.9/3	149.7/3
66	0/0	0/0	156.4/2	153.1/2	160.2/3	160.5/3	159.8/2	150.8/3	130.0/2
67	0/0	0/0	118.3/2	149.9/2	147.0/3	144.0/3	141.7/3	141.9/3	99.1/3
68	0/0	0/0	0/0	104.9/2	121.5/2	115.0/2	106.6/2	101.8/3	57.1/3
69	0/0	0/0	0/0	110.8/3	91.6/2	0/0	0/0	0/0	0/0

Flight 23, February 29, 1980 (1980.162)

	19	20	21	22	23	24	25	26	27
47	530.4/3	522.5/2	524.3/3	546.9/3	566.0/4	560.0/4	561.5/4	0/0	0/0
48	523.6/3	516.5/3	519.2/3	534.4/3	551.2/3	537.0/4	530.6/4	0/0	0/0
49	524.3/3	505.6/3	503.3/3	516.9/3	518.8/3	520.6/4	523.8/4	0/0	0/0
50	509.1/3	484.6/3	482.5/2	489.0/2	504.7/4	520.9/4	528.9/4	0/0	0/0
51	495.7/2	483.4/3	475.0/3	484.2/3	525.2/4	532.5/3	531.9/4	0/0	0/0
52	468.5/3	473.9/3	466.9/2	470.9/3	481.7/3	516.3/3	537.3/3	0/0	0/0
53	478.4/3	454.0/3	447.9/3	423.6/2	396.9/2	0/0	0/0	0/0	0/0
54	0/0	363.7/3	390.8/3	399.8/3	382.2/2	369.8/2	0/0	0/0	0/0
55	330.2/3	348.9/3	376.9/3	395.9/3	386.9/3	363.9/2	0/0	0/0	0/0
56	328.3/2	346.1/2	361.0/2	366.0/2	360.2/2	330.6/3	0/0	0/0	0/0
57	316.0/3	328.1/3	334.7/2	305.8/2	289.0/3	278.6/3	264.3/3	0/0	0/0
58	310.0/3	322.8/3	318.8/3	302.9/3	284.1/2	280.3/3	272.3/2	0/0	0/0
59	282.1/3	297.5/3	290.1/3	273.8/2	267.2/3	267.7/3	254.9/3	233.1/3	196.4/4
60	264.0/4	274.0/3	274.4/3	247.6/2	246.7/2	259.7/2	240.0/3	236.2/2	221.6/4
61	0/0	239.4/3	245.5/3	234.1/2	248.9/2	251.4/3	226.2/3	220.2/3	0/0
62	0/0	0/0	230.7/3	236.0/2	232.9/2	227.5/2	217.9/3	206.5/3	0/0
63	0/0	196.8/2	218.7/3	228.3/2	212.5/2	211.6/2	208.1/3	198.4/3	169.3/3
64	0/0	196.4/3	202.2/3	182.1/2	190.0/2	202.9/3	193.9/3	180.0/3	157.5/3
65	0/0	0/0	170.6/2	165.3/2	173.6/2	189.3/3	182.7/3	170.7/2	149.1/3
66	0/0	0/0	157.0/2	151.4/3	157.3/2	159.6/3	157.0/2	149.6/3	130.4/3
67	0/0	0/0	116.2/2	146.0/3	142.6/3	141.7/3	139.1/2	142.0/3	100.5/3
68	0/0	0/0	0/0	103.3/2	120.7/3	112.1/3	102.0/2	101.5/3	58.5/3
69	0/0	0/0	0/0	110.6/2	87.3/3	0/0	0/0	0/0	0/0

Flight 24, May 12, 1980 (1980.361)

	19	20	21	22	23	24	25	26	27
47	528.2/3	521.4/2	523.1/3	546.2/3	564.5/4	557.9/4	558.3/4	0/0	0/0
48	522.6/3	514.8/3	517.6/3	534.5/3	551.4/3	535.7/4	527.9/4	0/0	0/0
49	522.1/3	503.6/3	501.6/2	515.1/2	517.9/3	518.1/4	521.3/4	0/0	0/0
50	506.9/2	483.7/3	481.9/2	487.8/2	503.1/4	518.9/4	526.4/4	0/0	0/0
51	494.4/2	483.0/2	474.4/3	484.8/3	524.5/3	531.9/3	530.4/4	0/0	0/0
52	467.7/3	473.4/3	466.7/2	472.1/3	483.1/3	516.0/3	533.9/3	0/0	0/0
53	477.4/3	455.0/3	448.2/3	423.6/3	395.7/3	0/0	0/0	0/0	0/0
54	0/0	361.9/3	390.3/3	400.0/3	381.1/2	369.6/2	0/0	0/0	0/0
55	328.6/3	346.5/2	375.7/3	395.4/2	387.4/2	363.4/2	0/0	0/0	0/0
56	326.2/2	344.9/2	361.6/2	369.0/2	361.8/2	329.7/3	0/0	0/0	0/0
57	315.3/3	326.2/3	332.4/2	302.7/2	286.1/2	278.0/3	264.6/3	0/0	0/0
58	309.3/3	322.1/3	319.7/2	303.4/3	282.8/2	280.1/3	273.0/2	0/0	0/0
59	282.0/3	296.7/3	290.6/3	274.2/2	267.2/2	268.0/2	254.9/3	232.3/3	195.6/4
60	263.2/4	272.9/3	275.3/3	247.7/2	247.1/2	261.7/2	239.9/3	235.2/2	220.1/4
61	0/0	240.0/3	245.9/3	233.9/2	249.0/2	253.1/3	226.8/3	219.6/3	0/0
62	0/0	0/0	231.6/3	234.6/2	232.8/2	227.8/2	219.1/3	207.5/3	0/0
63	0/0	197.6/2	219.1/3	230.9/2	214.0/2	213.0/2	209.8/3	199.7/3	170.8/3
64	0/0	194.8/3	201.8/3	183.9/2	190.7/2	203.9/2	194.4/3	180.1/3	157.7/3
65	0/0	0/0	170.8/2	166.0/2	176.6/2	191.7/3	183.2/3	171.0/2	149.9/3
66	0/0	0/0	158.3/2	155.7/3	162.3/2	161.8/2	157.9/2	149.9/3	131.9/3
67	0/0	0/0	116.6/2	151.0/2	148.8/3	146.1/2	142.0/2	143.3/3	102.4/3
68	0/0	0/0	0/0	109.1/2	126.1/2	117.6/3	108.1/2	105.7/2	65.3/3
69	0/0	0/0	0/0	115.9/2	96.2/3	0/0	0/0	0/0	0/0

Flight 25, July 22, 1980 (1980.556)

	19	20	21	22	23	24	25	26	27
47	527.2/3	520.8/2	522.2/3	545.4/3	563.1/4	556.0/4	556.3/4	0/0	0/0
48	521.7/3	514.4/3	517.0/3	533.9/2	550.3/3	534.2/4	525.9/4	0/0	0/0
49	520.7/3	502.4/3	500.5/2	513.2/2	516.7/3	516.1/4	519.4/4	0/0	0/0
50	505.3/2	482.0/3	481.9/2	486.4/2	501.4/4	517.0/4	524.4/4	0/0	0/0
51	492.7/2	481.5/2	473.9/3	483.8/3	523.6/3	530.3/3	527.9/4	0/0	0/0
52	465.8/3	472.3/3	465.5/3	471.6/3	483.0/3	514.2/3	530.9/3	0/0	0/0
53	476.5/3	454.0/3	446.8/3	422.7/3	393.4/3	0/0	0/0	0/0	0/0
54	0/0	360.6/3	388.4/3	398.6/2	379.2/2	367.4/2	0/0	0/0	0/0
55	324.5/3	342.4/2	373.3/2	393.7/2	384.6/2	360.5/2	0/0	0/0	0/0
56	322.4/2	342.4/2	359.8/2	367.6/3	359.4/2	327.0/2	0/0	0/0	0/0
57	312.2/3	323.8/3	329.9/2	302.0/2	282.5/2	275.8/3	262.5/3	0/0	0/0
58	306.8/3	319.3/3	316.8/2	302.1/3	280.1/2	277.5/2	270.1/3	0/0	0/0
59	279.4/3	294.2/3	289.9/3	272.1/3	265.5/2	265.1/2	252.0/3	229.7/3	193.7/4
60	261.0/4	270.8/2	273.6/3	246.7/2	245.9/2	259.2/2	236.8/3	231.8/2	217.6/3
61	0/0	238.0/2	244.8/3	232.5/2	247.6/2	251.2/3	224.5/3	216.5/3	0/0
62	0/0	0/0	230.7/3	232.5/2	230.8/2	225.7/2	216.8/3	204.8/3	0/0
63	0/0	196.1/2	217.6/3	228.4/2	213.0/2	211.0/2	207.1/3	196.8/3	168.3/3
64	0/0	191.8/3	197.7/2	181.4/2	189.9/2	202.8/2	192.7/3	177.8/3	155.0/3
65	0/0	0/0	166.7/2	162.9/2	175.0/2	190.4/3	182.0/3	168.4/2	146.5/3
66	0/0	0/0	155.9/2	154.4/3	163.2/2	162.7/2	157.1/2	147.7/3	128.7/3
67	0/0	0/0	113.4/2	152.2/2	150.7/3	148.1/3	141.1/2	140.3/3	98.8/3
68	0/0	0/0	0/0	111.2/2	126.2/2	119.3/2	109.4/2	102.5/2	64.3/3
69	0/0	0/0	0/0	115.4/3	95.2/3	0/0	0/0	0/0	0/0

Flight 26, September 2, 1980 (1980.671)

	19	20	21	22	23	24	25	26	27
47	527.1/3	520.5/2	521.7/3	544.9/3	562.4/4	555.0/4	556.0/4	0/0	0/0
48	520.9/3	514.1/3	516.9/3	532.8/2	549.3/3	533.1/4	525.3/4	0/0	0/0
49	520.1/3	501.7/3	499.9/2	512.8/3	516.1/3	515.4/4	518.6/4	0/0	0/0
50	504.3/2	481.0/3	481.5/2	485.4/2	500.4/4	516.0/4	523.7/4	0/0	0/0
51	491.2/2	480.1/2	472.9/2	482.5/3	522.7/3	529.3/3	526.1/4	0/0	0/0
52	464.1/3	471.2/3	464.1/3	470.2/3	481.2/3	512.3/3	529.0/4	0/0	0/0
53	475.1/3	451.8/3	444.7/3	421.2/3	393.8/3	0/0	0/0	0/0	0/0
54	0/0	357.6/3	386.5/3	397.2/2	377.8/2	365.2/2	0/0	0/0	0/0
55	321.1/3	340.2/2	372.2/2	392.3/2	381.8/2	357.9/2	0/0	0/0	0/0
56	319.9/2	339.7/2	357.6/2	365.1/3	356.2/2	323.9/2	0/0	0/0	0/0
57	309.5/3	321.8/3	327.3/2	300.9/2	282.2/2	273.1/3	259.9/3	0/0	0/0
58	304.1/4	315.9/3	314.3/2	299.9/2	277.6/2	274.9/2	266.5/3	0/0	0/0
59	276.4/3	292.0/3	287.3/3	269.9/3	263.2/2	262.5/2	249.4/3	227.7/3	191.8/4
60	259.0/4	268.8/2	271.7/3	244.6/2	243.5/2	255.8/3	233.5/3	229.3/2	215.9/3
61	0/0	235.4/2	242.9/3	231.5/2	245.5/2	248.2/2	221.6/3	213.8/3	0/0
62	0/0	0/0	229.0/3	230.8/2	228.6/2	223.2/2	214.2/3	201.8/3	0/0
63	0/0	193.7/2	215.8/3	226.4/2	210.8/2	208.2/2	204.0/3	193.8/3	165.2/3
64	0/0	190.0/3	194.0/2	177.8/2	187.8/2	200.2/2	190.4/3	174.9/3	152.1/3
65	0/0	0/0	162.6/2	159.3/2	171.7/2	187.4/3	179.6/3	165.0/2	143.3/3
66	0/0	0/0	152.6/2	150.9/3	159.4/2	160.5/2	154.6/2	144.2/3	124.3/3
67	0/0	0/0	110.6/2	148.9/2	147.2/2	145.9/3	137.7/2	136.9/3	95.2/3
68	0/0	0/0	0/0	108.1/3	123.1/2	117.3/2	106.6/2	97.6/2	59.4/3
69	0/0	0/0	0/0	112.0/3	89.6/3	0/0	0/0	0/0	0/0

Flight 27, October 30, 1980 (1980.830)

	19	20	21	22	23	24	25	26	27
47	527.2/3	520.8/2	521.7/3	544.8/3	562.0/4	555.2/4	555.4/4	0/0	0/0
48	521.9/3	514.8/3	517.4/3	532.9/2	549.1/3	533.3/4	525.2/4	0/0	0/0
49	520.3/3	501.5/3	499.9/2	512.9/3	516.8/3	515.3/4	518.6/4	0/0	0/0
50	504.6/2	481.3/3	481.8/2	485.9/2	501.1/4	516.3/4	523.7/4	0/0	0/0
51	490.8/3	481.0/2	474.0/2	483.0/3	523.3/4	529.6/4	525.3/4	0/0	0/0
52	465.0/3	472.5/3	466.3/3	472.3/3	484.0/3	512.9/3	526.1/4	0/0	0/0
53	476.0/3	454.5/3	447.5/3	423.7/3	395.8/3	0/0	0/0	0/0	0/0
54	0/0	358.8/3	389.2/3	399.5/3	380.1/2	366.6/2	0/0	0/0	0/0
55	322.2/3	341.3/2	373.8/2	394.4/3	384.1/2	359.2/2	0/0	0/0	0/0
56	321.3/2	341.3/3	359.2/3	367.0/3	357.8/3	324.3/2	0/0	0/0	0/0
57	310.6/3	323.1/3	329.5/2	302.9/3	286.0/2	276.1/3	261.4/3	0/0	0/0
58	304.5/4	316.5/3	316.2/2	302.5/2	279.1/2	275.7/3	267.5/3	0/0	0/0
59	278.3/4	293.6/3	289.2/3	272.8/3	265.1/2	264.0/3	250.3/3	228.6/4	193.0/4
60	260.7/4	270.9/2	274.1/3	247.0/2	246.6/3	257.5/3	234.9/3	230.4/2	216.5/4
61	0/0	237.1/3	246.0/3	234.8/2	248.3/2	250.5/2	223.1/3	214.4/3	0/0
62	0/0	0/0	232.5/3	233.8/2	231.3/2	225.6/2	216.3/3	202.7/3	0/0
63	0/0	194.9/2	217.9/3	228.8/2	213.1/2	211.1/3	205.8/3	194.4/3	166.3/3
64	0/0	190.5/3	195.3/3	181.7/2	189.6/2	202.0/2	192.7/3	176.1/3	153.5/3
65	0/0	0/0	165.2/3	162.0/2	174.8/2	191.1/3	183.1/3	167.6/2	145.8/3
66	0/0	0/0	155.0/2	153.2/3	163.2/2	163.5/2	158.7/2	146.6/3	126.8/3
67	0/0	0/0	112.9/2	152.5/2	151.3/3	147.3/3	141.3/3	139.5/3	98.6/3
68	0/0	0/0	0/0	110.4/3	127.2/3	121.5/2	112.3/3	100.5/2	62.9/3
69	0/0	0/0	0/0	116.6/3	96.1/3	0/0	0/0	0/0	0/0

Flight 28, March 7, 1981 (1981.180)

	19	20	21	22	23	24	25	26	27
47	523.7/3	516.9/2	521.1/3	543.4/3	560.6/4	555.6/4	553.7/4	0/0	0/0
48	520.9/3	512.5/3	517.7/3	533.9/3	548.6/3	532.8/4	524.5/4	0/0	0/0
49	519.8/4	501.3/3	500.6/3	516.9/3	518.1/3	514.9/4	518.3/4	0/0	0/0
50	505.0/3	481.7/3	481.6/3	488.6/3	502.8/4	516.8/4	523.3/4	0/0	0/0
51	490.7/3	483.8/2	475.7/2	484.8/3	522.6/4	530.0/4	526.4/4	0/0	0/0
52	467.7/3	476.2/3	469.6/3	474.0/3	486.6/3	514.4/3	525.1/4	0/0	0/0
53	476.5/3	462.3/3	453.2/3	428.1/3	398.4/3	0/0	0/0	0/0	0/0
54	0/0	365.0/3	394.9/3	403.9/3	384.3/3	371.0/2	0/0	0/0	0/0
55	326.1/3	345.0/3	378.9/3	398.8/3	389.4/2	363.7/3	0/0	0/0	0/0
56	324.3/2	345.0/3	364.6/3	373.7/3	360.8/3	327.3/3	0/0	0/0	0/0
57	315.2/3	327.3/3	333.8/2	306.5/3	290.5/3	280.8/3	265.9/3	0/0	0/0
58	309.3/4	320.9/3	320.4/2	307.8/2	284.9/2	280.1/3	272.9/3	0/0	0/0
59	284.2/4	297.9/3	292.7/2	280.6/3	270.1/2	269.5/3	255.3/4	231.6/4	196.2/4
60	264.4/4	274.6/3	279.5/3	253.1/3	252.2/3	264.1/3	239.3/3	233.8/3	218.7/4
61	0/0	240.0/3	251.4/3	240.8/3	254.5/2	255.0/2	227.7/3	218.3/3	0/0
62	0/0	0/0	237.7/3	239.0/3	236.6/2	231.1/3	221.6/3	207.8/4	0/0
63	0/0	197.3/2	221.0/3	233.4/2	217.8/2	216.1/3	211.4/3	198.7/3	172.2/3
64	0/0	190.4/3	198.2/3	186.7/2	192.4/2	208.3/2	198.6/3	181.6/3	158.5/3
65	0/0	0/0	171.9/3	168.3/2	182.5/3	199.9/3	191.0/3	175.8/2	152.8/3
66	0/0	0/0	162.0/2	162.4/3	175.1/3	171.7/3	169.0/3	154.4/3	134.4/3
67	0/0	0/0	120.8/2	161.0/3	162.8/2	155.0/3	152.0/3	146.5/3	104.0/3
68	0/0	0/0	0/0	120.1/3	136.4/3	129.4/3	121.6/3	109.1/3	72.0/3
69	0/0	0/0	0/0	127.9/2	114.7/3	0/0	0/0	0/0	0/0

Flight 29, June 16, 1981 (1981.457)

	19	20	21	22	23	24	25	26	27
47	519.0/3	510.7/2	517.0/3	540.9/3	558.6/4	553.9/4	551.8/4	0/0	0/0
48	518.1/3	508.6/3	516.2/3	531.9/3	546.6/4	531.3/4	522.7/4	0/0	0/0
49	518.1/4	500.1/3	500.3/3	516.7/3	516.5/3	513.2/4	516.5/4	0/0	0/0
50	503.2/3	480.6/3	480.8/2	488.4/3	502.0/4	515.2/4	521.6/4	0/0	0/0
51	489.6/3	483.2/3	474.5/2	483.8/3	519.8/4	527.4/4	524.8/4	0/0	0/0
52	467.2/3	475.6/3	468.4/3	471.3/3	480.9/3	509.3/3	523.3/4	0/0	0/0
53	473.4/3	462.2/3	453.4/3	427.0/3	395.6/3	0/0	0/0	0/0	0/0
54	0/0	365.1/3	395.0/3	403.2/3	385.1/3	371.3/2	0/0	0/0	0/0
55	326.8/3	345.6/3	378.4/3	398.0/3	390.0/2	363.3/3	0/0	0/0	0/0
56	324.9/2	346.0/2	363.2/3	372.5/3	360.8/3	325.9/3	0/0	0/0	0/0
57	315.8/3	328.5/2	332.9/3	304.9/3	289.3/3	280.6/3	266.0/3	0/0	0/0
58	308.5/4	320.7/3	318.6/2	306.6/2	284.9/2	281.2/3	273.0/3	0/0	0/0
59	283.2/4	294.9/3	289.6/2	280.6/3	270.1/2	270.8/3	255.6/3	230.5/4	194.9/4
60	262.7/4	272.1/3	277.1/3	254.3/3	252.6/2	266.2/2	241.1/3	233.8/3	217.7/4
61	0/0	237.8/3	250.8/3	242.3/2	255.3/2	256.2/3	228.3/3	218.6/3	0/0
62	0/0	0/0	236.6/3	240.0/3	238.0/2	231.5/3	221.3/3	207.5/3	0/0
63	0/0	195.6/2	219.4/3	232.9/2	218.8/2	217.0/2	212.0/3	198.6/3	171.6/3
64	0/0	188.9/3	197.6/3	187.4/2	193.3/2	208.6/2	198.1/3	179.6/3	156.0/3
65	0/0	0/0	171.8/3	168.2/2	182.4/2	199.0/2	188.3/3	171.4/3	149.4/3
66	0/0	0/0	160.8/2	160.8/2	172.7/2	168.6/3	165.8/3	150.2/3	131.2/3
67	0/0	0/0	119.7/2	159.7/3	160.0/2	151.8/2	150.1/2	144.4/3	101.4/3
68	0/0	0/0	0/0	115.8/2	133.8/3	124.3/3	118.6/3	108.8/3	72.5/3
69	0/0	0/0	0/0	124.9/3	114.1/3	0/0	0/0	0/0	0/0

Flight 30, September 1, 1981 (1981.667)

	19	20	21	22	23	24	25	26	27
47	524.2/3	517.0/3	518.8/3	541.0/3	559.0/3	553.5/3	554.3/3	0/0	0/0
48	517.9/3	511.4/3	515.1/3	528.5/3	544.1/3	530.1/3	523.7/3	0/0	0/0
49	518.0/3	500.4/3	500.1/3	513.9/3	514.5/3	513.8/3	517.1/3	0/0	0/0
50	502.5/3	479.3/3	480.5/3	486.6/3	500.9/3	514.5/3	522.2/3	0/0	0/0
51	488.7/3	478.1/3	471.2/3	479.6/3	517.6/3	524.7/3	523.4/3	0/0	0/0
52	463.1/3	468.9/3	461.3/3	463.5/3	473.4/3	506.0/3	524.8/3	0/0	0/0
53	468.0/3	448.3/3	441.6/3	416.4/3	389.6/3	0/0	0/0	0/0	0/0
54	0/0	354.3/3	383.3/3	393.3/3	376.3/3	363.6/3	0/0	0/0	0/0
55	319.4/3	339.6/3	369.5/3	387.3/3	377.1/3	355.3/3	0/0	0/0	0/0
56	317.4/3	337.9/3	354.8/3	361.2/3	351.3/3	321.9/3	0/0	0/0	0/0
57	307.6/3	320.8/3	329.3/3	305.2/3	287.4/3	275.1/3	260.8/3	0/0	0/0
58	301.7/3	311.4/3	309.2/3	301.2/3	280.8/3	275.9/3	266.6/3	0/0	0/0
59	275.5/3	288.0/3	281.8/3	272.0/3	265.4/3	265.7/3	250.0/3	226.5/3	190.8/3
60	257.3/3	266.9/3	269.8/3	247.5/3	247.6/3	256.6/3	233.6/3	228.4/3	214.4/3
61	0/0	232.5/3	243.5/3	235.7/3	247.7/3	248.1/3	221.7/3	213.0/3	0/0
62	0/0	0/0	229.0/3	234.9/3	230.8/3	224.8/3	214.9/3	200.8/3	0/0
63	0/0	187.6/3	211.1/3	224.3/3	211.6/3	210.1/3	205.7/3	193.3/3	163.4/3
64	0/0	186.0/3	191.9/3	179.0/3	189.8/3	203.3/3	192.3/3	174.2/3	149.9/3
65	0/0	0/0	163.9/3	163.2/3	174.7/3	190.0/3	182.2/3	166.8/3	143.6/3
66	0/0	0/0	151.4/3	151.6/3	158.0/3	160.5/3	158.2/3	145.0/3	124.8/3
67	0/0	0/0	112.7/3	145.9/3	142.5/3	143.8/3	141.0/3	137.4/3	95.8/3
68	0/0	0/0	0/0	101.9/3	116.4/3	111.0/3	106.1/3	95.6/3	52.8/3
69	0/0	0/0	0/0	104.5/3	84.7/3	0/0	0/0	0/0	0/0